SAHC

The structural intervention of St. Torcato Church: documentation and analysis of the strengthening works

Michele Puliga

Portugal | 2014

ADVANCED MASTERS IN STRUCTURAL ANALYSIS
OF MONUMENTS AND HISTORICAL CONSTRUCTIONS

Master's Thesis

Michele Puliga

The structural intervention of St. Torcato Church: documentation and analysis of the strengthening works

University of Minho

Czech university of Prague

Education and Culture

Erasmus Mundus

ADVANCED MASTERS IN STRUCTURAL ANALYSIS
OF MONUMENTS AND HISTORICAL CONSTRUCTIONS

Master's Thesis

Michele Puliga

The structural intervention of St. Torcato Church: documentation and analysis of the strengthening works

This Masters Course has been funded with support from the European Commission. This publication reflects the views only of the author, and the Commission cannot be held responsible for any use which may be made of the information contained therein.

Portugal | 2014

DECLARATION

Name: Michele Puliga

Email: micpul@hotmail.com

Title of the

Msc Dissertation: The structural intervention of St. Torcato Church: documentation and analysis of the strengthening works

Supervisor(s): Luís F. Ramos

Year: 2014

I hereby declare that all information in this document has been obtained and presented in accordance with academic rules and ethical conduct. I also declare that, as required by these rules and conduct, I have fully cited and referenced all material and results that are not original to this work.

I hereby declare that the MSc Consortium responsible for the Advanced Masters in Structural Analysis of Monuments and Historical Constructions is allowed to store and make available electronically the present MSc Dissertation.

University: Universidade do Minho

Date: July 14, 2014

Signature: _____

AKNOWLEDGMENTS

I would like to thank the European Union for the scholarship provided that gave me the opportunity to be a part of the Advanced Masters in Structural Analysis of Monuments and Historical Construction (SAHC) program.

I would like to thank Prof. Ramos for giving me a chance to work on this incredible project and for his trust and belief in my abilities. This research strongly relied on his expertise, and I have thoroughly enjoyed tackling many challenging problems under his mentorship. His enthusiasm and interest in my work, as well as his vision made this project possible.

I am forever indebted to Prof. Petr Kabele and Prof. David Biggs, for sharing their wealth of knowledge and expertise and for introducing me to the wonderful possibilities of the finite element method. It has been a privilege and an honor to have had a chance to conduct same research of a real case study in Prague.

I would like to express my gratitude to all other professors and staff at the České vysoké učení technické v Praze for their tireless effort to make our stay in Prague productive and memorable.

My participation in this program was made possible through the hard work and dedication of the MSc Secretariat, in particular Ms. Ana Fonseca and Mrs. Alexandra Kurfurstova. I am very appreciative of their patience and support throughout my enrollment in the program. Their work behind the scenes has made this experience possible.

I am grateful to my friends and colleagues from Prague for their friendship, help and encouragement. I feel very lucky to have been able to participate in this program and to have met a wonderful group that I can now call my friends. I would like to especially thank my friends in Guimarães for their constant support and encouragement.

I cannot overstate the debt of gratitude I owe to my family for their continued support through many difficult times and for their belief in my abilities and my dreams. Their sacrifice, love and unwavering resolve have made this work a reality.

ABSTRACT

The church of São Torcato represents a masterpiece of the carving skills of Minho craftsmen. However, the arise of several structural anomalies of medium and high intensity, identified since 1976, prompted the beginning of a careful examination of the building that is still ongoing. The aim of this thesis is the retracing of the subsequent investigation steps that were able to identify the causes of the problems, the discussion on the strengthening works planned on the building and the relative assessment of the eventual harm induced by the intervention.

The steps that have been followed for this discussion had started from the historical framework of the church construction, in order to understand how such phases could have trigged the damage phenomena. Subsequently, all the monitoring systems and surveys have been listed in order to understand the logical steps that have been followed to estimate the causes of such problems. The relative strengthening program has been discussed and cross-checked in all its aspect in order to evaluate a possible enhancement on the design. A minor design has been carried out as response of a new demand of the institution involved in the conservation of the building: the replacement of the crosses on top of both spires. Finally, the data of the static monitoring system placed on the tower since 2009 was analyzed and confronted to the actual situation, in order to evaluate the presence of interference with the structure induced by the executive works.

From the analysis of the previous investigations it was possible to build a complete picture of the mechanical characteristics of the church and the causes which trigged the existent damage phenomena. Furthermore, it was possible to understand the level of activity of the damage and the effectiveness of the system of interventions that was designed in order to face the problems of the church. A cross-check on such interventions confirmed its reliability and enhanced as much as possible its defective parts. The analysis of the cross was satisfying except for one of the mathematical models, which should be improved after specific studies of the roof element.

The future tasks will have to take into account the effective development of the intervention works and the comparison with both static and dynamic monitoring data. It is also necessary to perform more specific computational analysis regarding the mechanical behavior of the building considering cracked models and FEM that contemplate both settlement and thermal condition at the same time. Furthermore, several direct tests should be carried on the intervention wastes (such as coring samples) in order to evaluate the reliability of the non-destructive tests performed on the structure.

RESUMO

O Santuário de São Torcato representa a obra-prima em cantaria granito de toda a região do Minho. Todavia, devido à existência de um conjunto de anomalias estruturais de severidade moderada a severa foi necessário realizar um estudo de inspeção e diagnostico, que culminou na elaboração de um projeto de reforço, cujos trabalhos para a estabilização das fundações das torres estão precisamente em curso.

O objetivo da presente dissertação é de registar e analisar as diferentes fases de investigação que permitiram a identificação das anomalias e as suas causas, o acompanhamento da obra em curso, incluindo a validação e controlo da intervenção em curso através da monitorização estrutural.

A dissertação começou com a análise histórica da construção do santuário, a fim de compreender se o processo construtivo introduziu dano. Posteriormente, todas as inspeções, diagnósticos e monitorizações estruturais realizadas foram apresentadas para melhor se compreender como se determinaram as causas dos problemas estruturais. A intervenção de reforço estrutural foi discutida sobre todos os seus aspetos e também foi realizada uma análise para a substituição das cruzes no topo das duas torres, uma vez que estas se encontram muito deterioradas. Finalmente, os dados do sistema de monitorização estático, instalado desde 2009, foram analisados e confrontados com a situação atual (no decorrer de trabalhos de reforço), com o objetivo de avaliar o impacto da intervenção na construção e se, eventualmente,

Através da análise dos anteriores estudos foi possível determinar as características mecânicas/estruturais do santuário e as causas que levaram ao aparecimento das anomalias existentes. Foi também possível compreender o nível de atividade das anomalias e a assertividade da intervenção estrutural proposta para a estabilização das mesmas. A verificação da conformidade do projeto reafirmou a sua necessidade e permitiu melhorar a eficiência de algumas das medidas de intervenção. A análise da substituição das cruzes foi satisfatória, com a exceção de um dos modelos que deverá ser aprofundada para melhor avaliar a sua estabilidade.

Como tarefas futuras propõem-se a continuidade do acompanhamento dos trabalhos de intervenção e da análise dos dados dos sistemas de monitorização estático e dinâmico, quer durante, quer depois da intervenção. Também será necessária a realização de análises numéricas mais específicas sobre o comportamento mecânico do edifício considerando o tanto dano devido aos assentamentos da fundação, como o efeito da variação térmica na construção. Além disso, vários ensaios deverão ser realizados sobre os materiais sobrantes da intervenção (tais como os tarolos de carotagem), a fim de validar a confiabilidade dos ensaios não destrutivos realizados na estrutura.

ABSTRACT

La chiesa di San Torcato rappresenta un capolavoro nel paesaggio architettonico di Guimarães, emblema delle altissime capacità delle maestranze locali. Infelicemente, l'insorgere d'innumerevoli anomalie di moderata ed elevata intensità ha richiesto esami dettagliati dell'edificio, avviati alla fine degli anni settanta e protratti continuativamente fino ad oggi.

L'obiettivo di questa tesi e la riproposizione delle varie investigazioni che hanno permesso di identificare i fattori scatenanti dei danni dell'edificio, la discussione dei lavori di rinforzo pianificati per sopperire a tali problematiche e la verifica dell'eventuale alterazione della struttura indotta dall'esecuzione dell'intervento.

La trattazione del tema è iniziata dalla ricostruzione del processo evolutivo della chiesa, così da relazionare l'edificio al suo complesso quadro storico. Successivamente, tutti i sistemi di monitoraggio utilizzati e le indagini eseguite sono stati organizzati e descritti, in modo da ripercorrere il lungo processo logico che ha portato alla scoperta delle cause dei problemi attuali. L'intervento è stato discusso e vagliato da un attento calcolo, così da individuare e migliorare eventuali punti carenti del programma. Un progetto minore è stato eseguito personalmente come richiesto dall'istituzione coinvolta nella conservazione dell'edificio: la sostituzione delle croci sulla sommità dei campanili. Infine, i dati ricavati dai sistemi di monitoraggio statici, installati dal 2009 sono stati analizzati e confrontati con la situazione attuale, in modo da poter riscontrare la presenza di un eventuale danno indotto dai lavori.

Dalle analisi delle precedenti investigazioni è stato possibile ricostruire il quadro completo delle caratteristiche meccaniche dell'edificio e delle cause che hanno scatenato gli attuali fenomeni di decadimento. Inoltre, è stato possibile conoscere il livello di attività del danno e l'efficienza del sistema d'interventi pianificato. Una verifica incrociata di tale progetto ne ha confermato l'affidabilità, ed ha permesso di migliorare il più possibile le sue prestazioni. L'analisi della croce è stata soddisfacente ad esclusione di uno dei modelli matematici utilizzati: tale schema dovrebbe essere migliorato a seguito di esami specifici sugli elementi decorativi.

I compiti futuri dovranno prevedere l'analisi dell'effettivo sviluppo dei lavori esecutivi e lo studio incrociato con i dati dei sistemi di monitoraggio sia dinamici sia statici. Sarà inoltre necessario eseguire analisi computazionali più specifiche che tengano conto della reale mappa dei danni, oltre che modelli a elementi finiti dell'edificio che contemplino l'azione congiunta dei cedimenti differenziali del suolo e delle variazioni termiche. Inoltre, test distruttivi dovrebbero essere sviluppati sui preziosi scarti delle esecuzioni (come ad esempio i carotaggi delle torri) così da valutare l'affidabilità dei ND-test eseguiti sulla struttura e aggiornare le sue caratteristiche meccaniche.

TABLE OF CONTENTS

1. INTRODUCTION

1.1 General

The church of São Torcato probably represents the masterpiece of the granite carving skills of Minho craftsmen (Figure 1.1). The construction of this church started in 1825 and took almost two centuries for its completion. Its construction is inserted in a complex historical framework, which passed through various project managers and suffered lots of changes, nowadays reflected in its wide range of materials and constructive techniques. Several problems during its constructive phases trigged the arouse of several structural anomalies of medium and high intensity, identified since 1976, prompted the beginning of a careful examination of the building that is still ongoing.

Figure 1.1: The church of São Torcato

1.2 Objective and methodology

Aim of the following chapters is the retracing of the subsequent investigation steps that were able to identify the causes of the problems, the discussion on the strengthening works planned on the building and the relative assessment of the eventual harm induced by the intervention.

In order to perform such logical steps the data of the monitoring system will be analyzed and the subsequent conclusion will be discussed. The effectiveness of the intervention will be evaluated analyzing the objective of the design and comparing them with a rigorous verification. In this way it should be even

possible to update the project if weak points would be discovered. The assessment of the relative interference will be analyzed considering the monitoring data that is still recorded on the building since 2009.

A brief introduction and conclusion inferred by the topics discussed on the chapter will be considered in each pass.

1.3 Outline of the thesis

Next chapter will consider the historic development of the church since the beginning of its construction (and even before). Passing through the situation and the construction phases of the building, it will be possible to analyze and understand in more detail the current construction.

In the third chapter, all the monitoring systems and survey performed on the building since 1976 will be categorized in four main groups and organized in a chronological way. In this way it will be possible to understand the logical passages that were used to identify and understand the roots of the problems that are affecting the building in a severe way since, at least, 1976.

In the fourth chapter the intervention will be analyzed and discussed. In this way it will be possible to easily understand the main idea and hypothesis behind the design decisions. Such work will be personally cross-checked and verified, in order to evaluate possible weak points and update the intervention accordingly.

The fifth chapter is dedicated to the design and the verification of the replacement of the cross on top of each spire, resulted from the decay of the actual elements. Two limit analysis model and a kinematic model will be verified for this purpose.

The sixth chapter will deal with the analysis of the data and the research of possible interference of the strengthening intervention. The data will be evaluated until the beginning of the works and then compared with the data collected afterwards. The relative works will be reported and described.

Finally, conclusions and recommendation for future works will be presented in chapter 7.

2. S. TORCATO CHURCH

2.1 Introduction

The case study of this thesis is the church of São Torcato, a huge temple with a cross-Latin shape that took almost two centuries to be completed in 2008. The classical basilica three-nave scheme was planned as a combination of several architectonic styles: Classic, Gothic, Renaissance and Neo-Romanic). This trend is called in Portuguese Neo-Manuelino, as developed under the crown of King D. Manuel I. The structure, passing through various project managers, suffered lots of changes that are nowadays reflected in the range of materials used: granite, wood and reinforced concrete define the actual temple and mark the different steps of the yard.

In this chapter, the church will be analyzed considering its historical framework. Passing through the situation and the construction phases of the building, it will be possible to analyze and understand in more detail the current temple.

2.2 Situation

São Torcato is a small village in the northern part of Portugal that took its name from the homonym martyr. It is sited on the left side of the Selho river, seven kilometers north-east of Guimarães, in northern

Figure 2.1: Two panoramic views of São Torcato (Ogrizovic et al., 2013)

part of Portugal. It has historical and economical relevance due to its strategic position, which guaranteed a good settlement for the inhabitants and an agricultural wealth during the centuries. Moreover, a strong industrial sector, mainly focused in the footwear sector, provides a good income to the area. For all these reasons, São Torcato was always considered one of the most important village in the Minho Region. Nowadays, the natural and historical patrimony represents the most important values of the village: The Sanctuary of São Torcato, the Church, the Chapel of Fonte do Santo and the main park, attract thousands of pilgrims every year (Figure 2.1).

2.3 The martyr and the birth of the sanctuary

Figure 2.2: The preserved body of São Torcato

São Torcato was the first martyr of the Iberian Christianity, and his body, perfectly preserved to the present day, is a relic that makes the village a place of pilgrimage. According to the Dicionário de Santos (Tavares), he was born in Toledo during the end of the Visigoths dynasty in Spain. He became arch-priest of Toledo, bishop of Iria Flávia and Porto, and successively archbishop of Braga. In the meanwhile, the Spanish Crown was under the threat of the Islamic army, which had started to occupy the territories of the Iberian Peninsula. When the Arabs arrived in Guimarães, on the 26 of February 719, São Torcato tried, with other twenty seven men, faced the general accusing him for his cruelty and for the committed murders. They were all martyred and their bodies were thrown in a pit, in which they remained for many centuries.

The sepulcher of São Torcato was initially placed inside a small chapel and then transferred to a Benedictine monastery in the 16th century. The opening of the tomb left everyone astonished: the body of the Saint was perfectly conserved (Figure 2.2). A primitive chapel was built to house the remains of the saint, which were shown once a year. But soon, the miraculous event attracted so many pilgrims, that in 1805 the archbishop of Braga and the Irmandade de S. Torcato were forced to order the construction of a new temple more suited to the needs. The place chosen to erect the monument was the “Penedos de Maria do Monte Maio”.

2.4 Main building phases in historical perspective

The works started in 1825, according to the baroque conception of the Portuguese architect Luis Ignacio Barros Lima. The construction began as usual starting from the apse, which was concluded in 1855. From June 1852 the relic was exposed permanently in the apse for devotes. The engineer Cesário

(a)

(b)

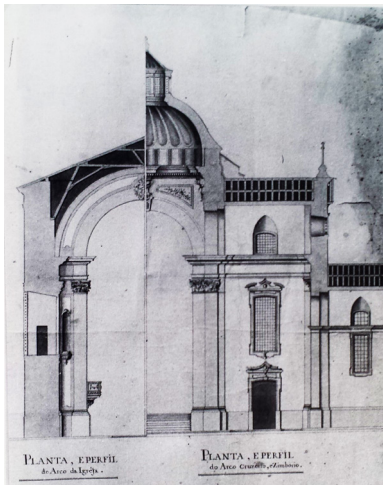

(c)

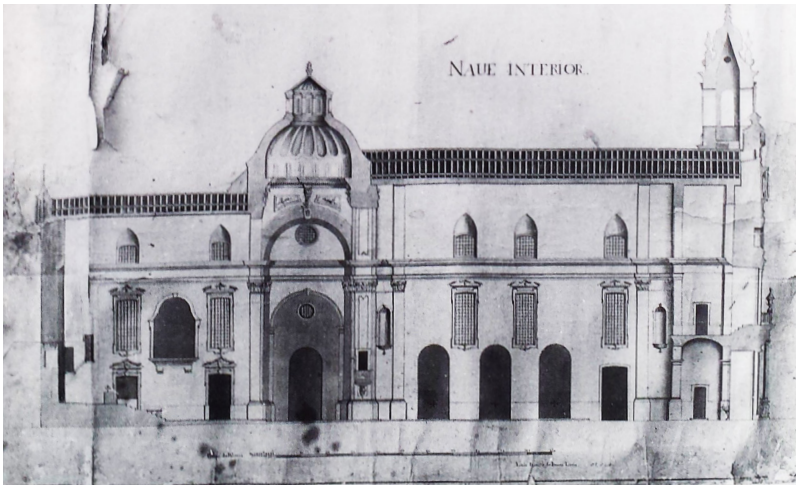

(d)

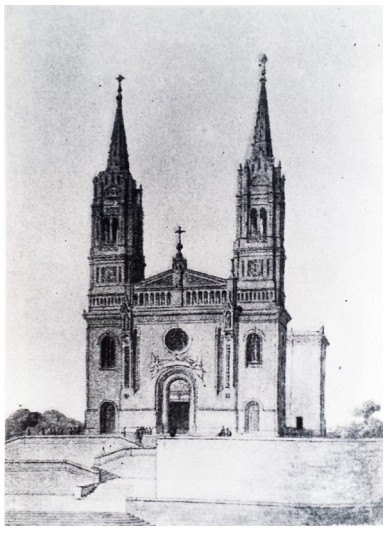

(e)

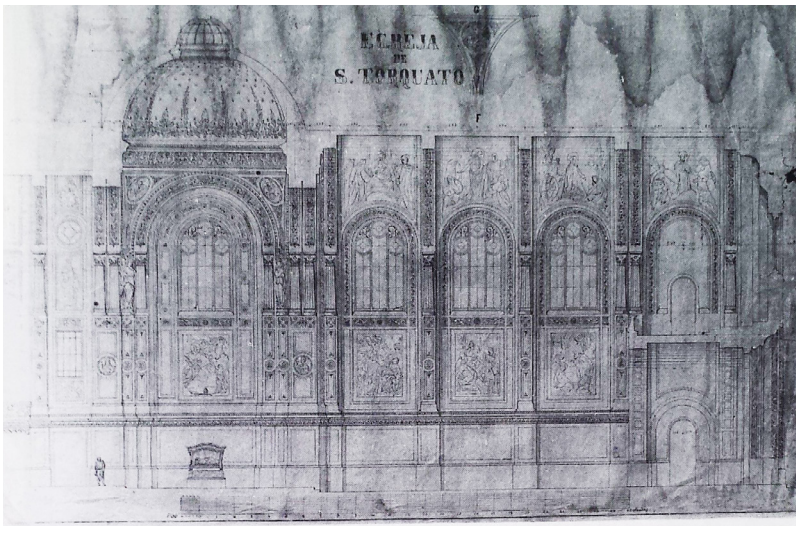

(f)

Figure 2.3: Development of the sanctuaries: (a) the first chapel built where the Saint was buried (b) chapel adjoins to the parish church (c) section of an arch and the transept from L. I. Barros de Lima, 1824 (d) transversal section of the project of L. I. Barros de Lima, 1824 (e) the façade in the project of L. F. K. Bohnstedt, 1866 (f) transversal section of the project of L. F. K. Bohnstedt, 1866 (S. Torcato museum, Reimaginar Guimarães and Baptista, 1997)

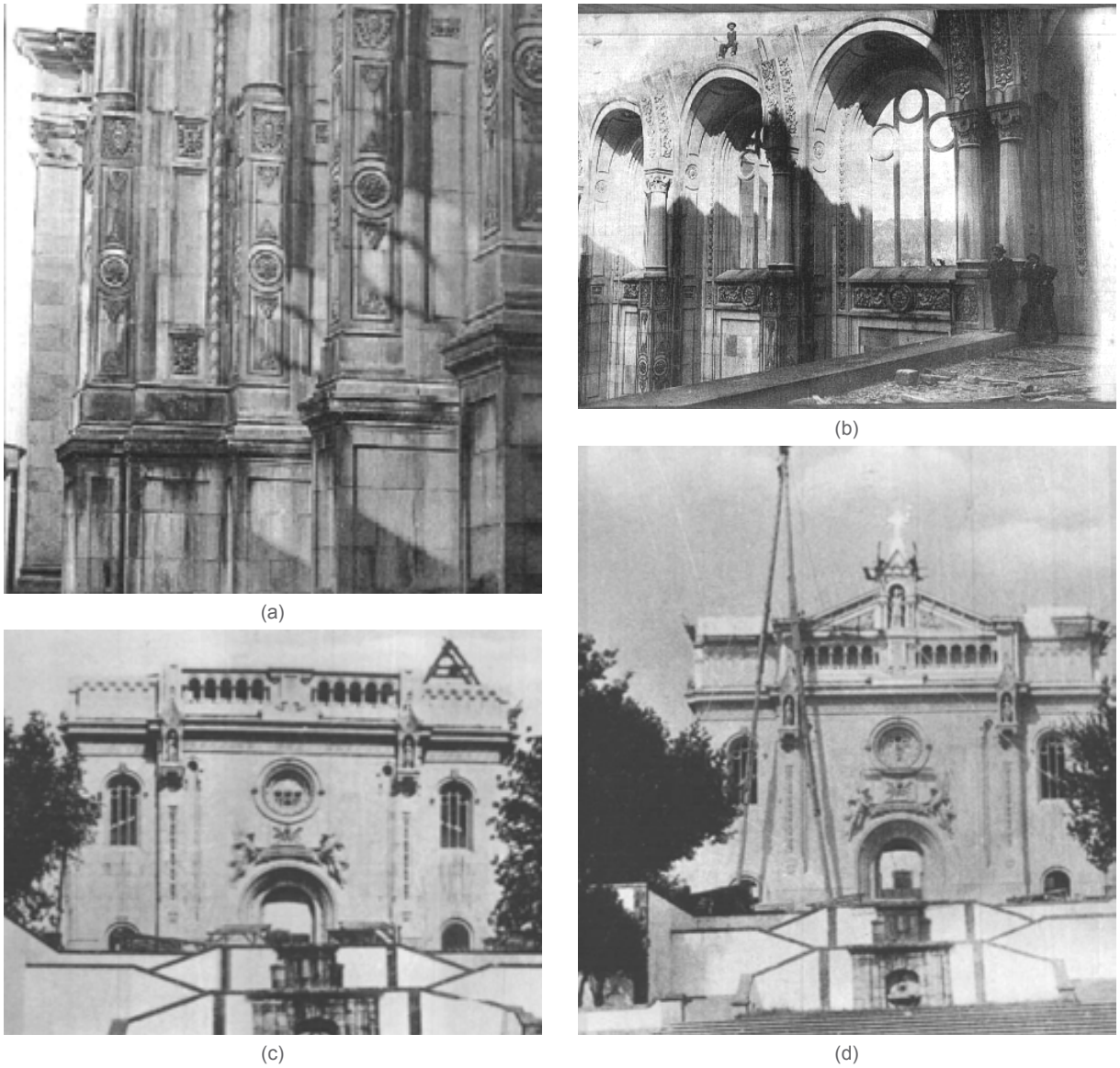

(a) (b) (c) (d)

Figure 2.4: Construction phases: (a) detail of the pillars of the arches of the nave (b) completion of the side walls (c) construction of the balustrade in front (d) Termination of the lintel of the facade and starting to build the first tower (S. Torcato museum)

Augusto Pinto, responsible for the construction since 1866, criticized the project due to the excessive simplicity of it; for him the building was not able to reflect the importance of the represented institution and was not worthy for pilgrims. For this reason, in the same year, the Association of Civil Architects and Portuguese Archaeologists proclaimed a competition for the transformation of the church, which was won by the German architect Ludwig Franz Karl Bohnstedt. The aesthetic and stylistic changes were allowed, but with the obligation to utilize the ancient foundations. In 1871 the foundation where finished and the new construction was set up, starting from the left transept and proceeding up to enclose the interior space, until the high of the main doors. This process will over in 1877. In the same date, fourteen bells were provided to the temporary tower built in 1857. In 1896 architect Marques de Silva was chosen to continue the work of his deceased predecessor. His change in the project concerned the decorations of the two towers and the central dome, which was enlarged. In 1910 the main nave was virtually over, with the exception of the transept and towers: the left one was lacking of the spire, the right one had just been started. In 1915 the church suffered a collapse, extent of which is not clear, and the

(a)

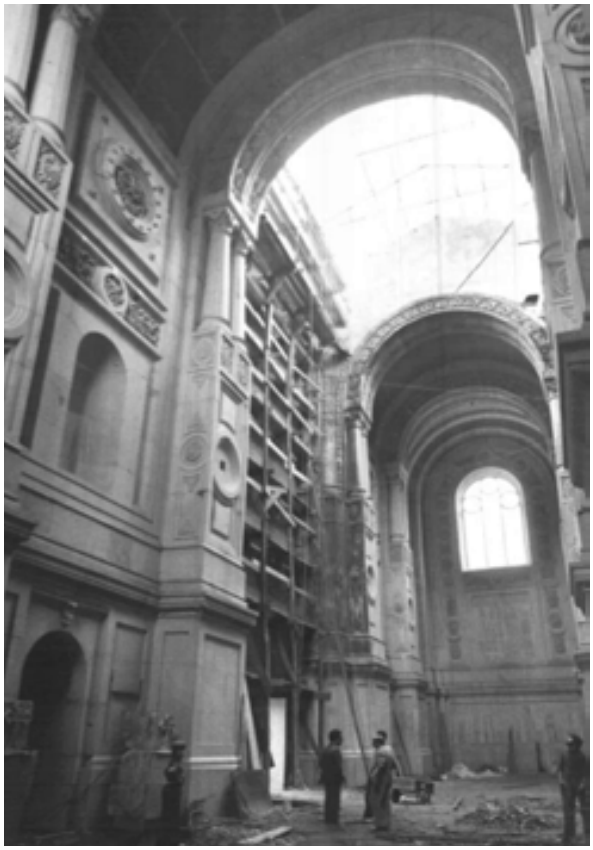

(b)

(c)

(d)

(e)

Figure 2.5: Construction phases: (a) completion of the first tower (b) interior of the altar during the beginning of the covering (c) termination of second tower (d) detail of the chapel, still uncovered (e) Construction of the dome (S. Torcato museum)

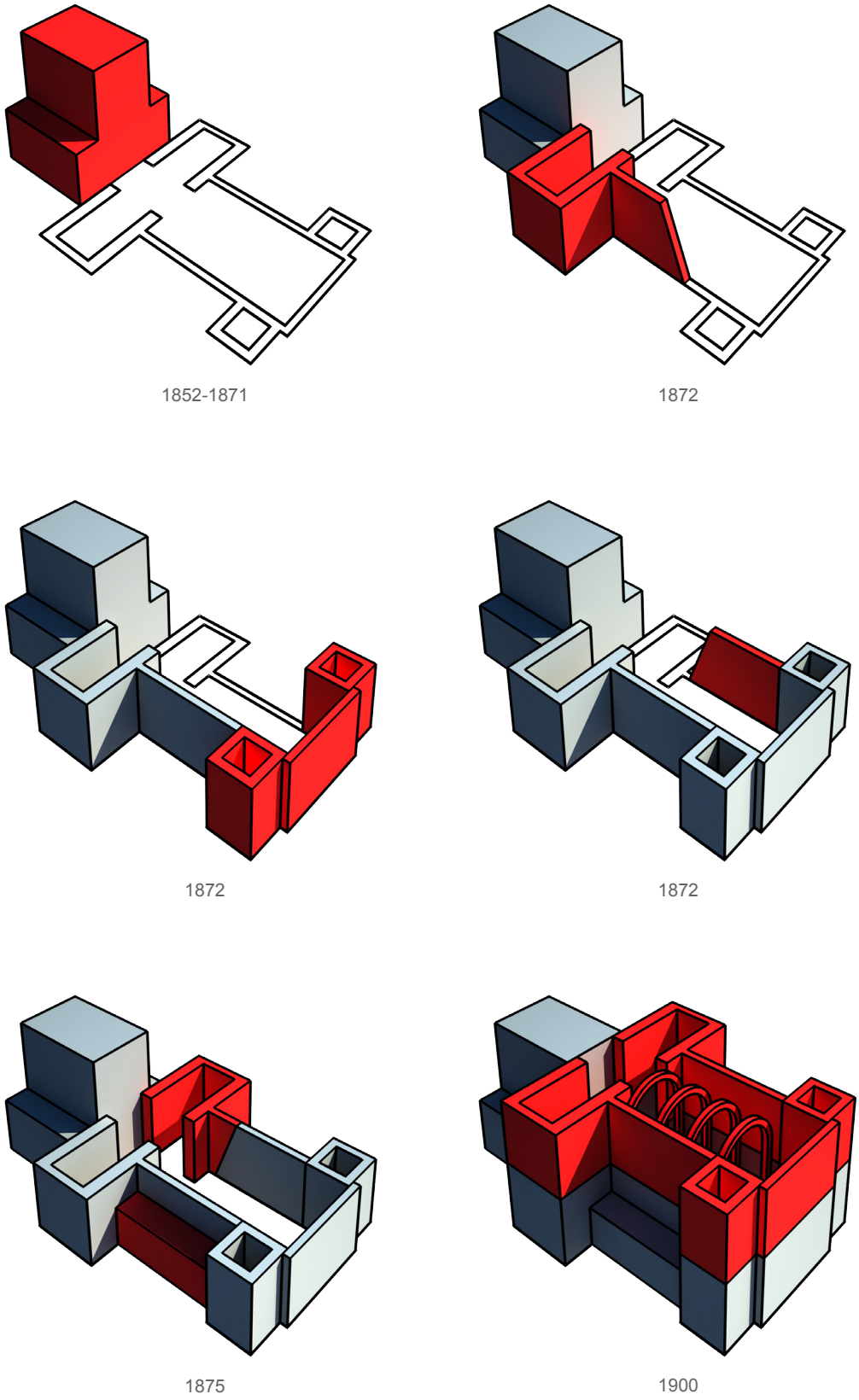

Figure 2.6: Development of the church until 1900

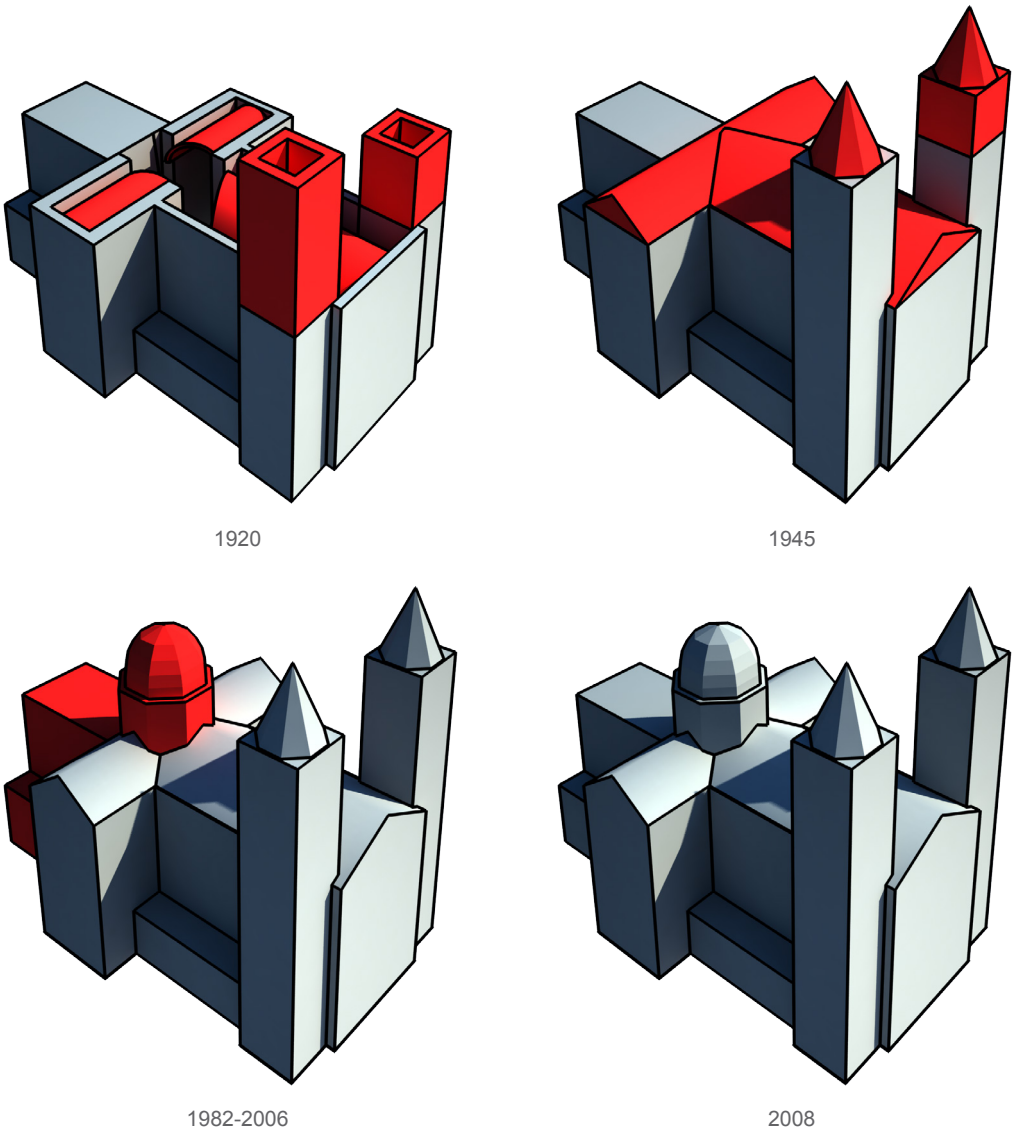

Figure 2.7: Development of the church after1900

project was significantly changed. In 1946 the church was inaugurated and few years later the construction of the transept was accomplished (Baptista, 1997).

The yard was stuck for almost half a century due to lack of money, until the Irmandade de S. Torcato was able to receive financial support from the State. The main aim of such grant was the rehabilitation of stonework art, accomplished by the institution of a professional school for stone carving, in 1982. From that moment, the construction could proceed: the cover of the apse, 18 meters higher than the roof of the church, was accomplished as the dome in reinforced concrete above the main altar. Between 1982 and 2006 the old apse was demolished and replaced by a new one, the dome was finished and few lateral chapels were added in the main nave (Figure 2.5).Comparing the original drawings of the apse made by Luis Ignacio de Barros Lima with the newest one, it is possible to notice the similarity of the two projects: perimeter, thickness of the walls and position of the stairs have not changed (Figure 2.8). Summing up the previous point, the construction process can be resumed in:

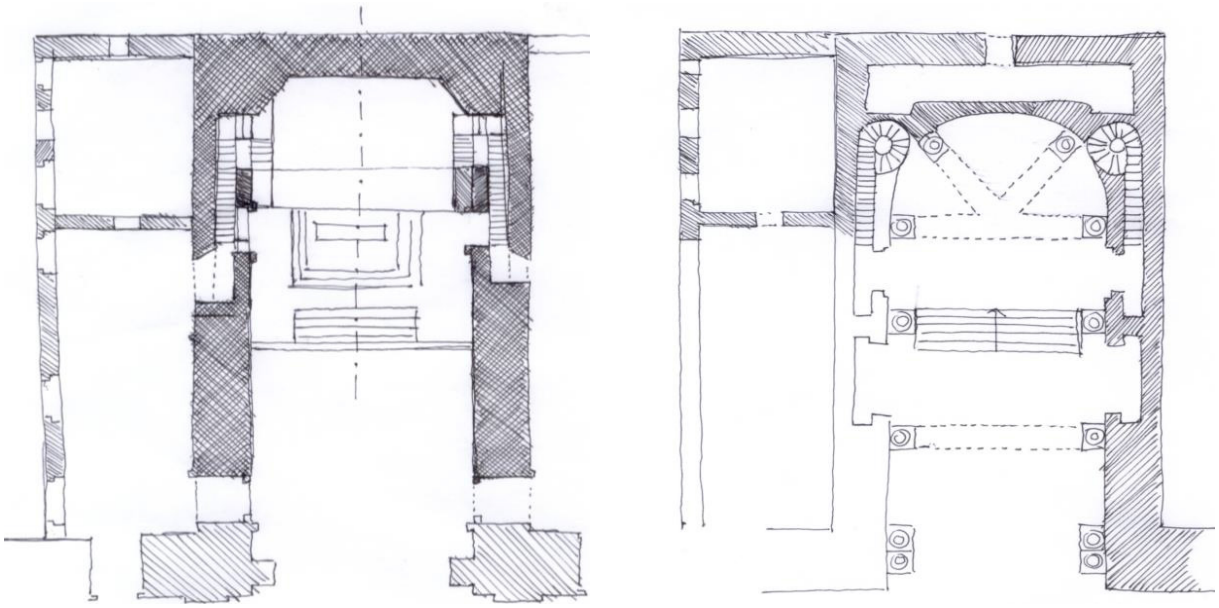

Figure 2.8: Comparison between old and new apse (Betzer et al., 2014)

- The apse is finished around 1852, and the foundations are completely settled in 1871
- The left transept and the left lateral wall was built until the half of its height since 1872
- The main façade is built until the half of the height, so as for the towers
- The right lateral wall had been started soon after
- The construction of the lateral transept reach the half of its height in 1875; lateral volumes started to be added since the same period (the addiction is still visible because of the joints and the difference of granite color)
- The main façade, the lateral walls and the transversal arches were completed around 1900; the building is basically completed with the exception of the towers, the dome and the roof
- The barrel vault were constructed both the main nave and in the transept since 1910. The left tower was completed in 1912, with the exception of the spire, and the right tower reached half of its total height in 1920
- In 1945 the barrel vault and the roof structure was finished. In the same period both the towers and their relative spires were accomplished.
- The octagonal dome was carried out between 1982 and 2006. In the same period, at an unspecified date, the apse was replaced with a reinforced concrete one. The difference is visible due to the color change of the granite veneer with respect to masonry walls inside the nave.
- The church is complete in 2008

A diagram of the construction process can be seen in Figure 2.6 and 2.7, For other historical pictures see the Annex A.

2.5 The actual state

As mentioned in the introduction, the building presents the classical Latin-cross setting for the basilicas in Neo-Manuelino architectural style. The choice of such hybrid style and the dimensions of the church reflect the assertion of authority and the symbol of grandeur. In fact, the sizes of the building are considerable. The image of the church is homogeneous and sober. From the most recent surveys carried out by means of laser measurements (Sánchez Aparicio et al., 2014), it is possible to establish (Figure 2.9):

- The dimensions of the central nave are 58,19 m of length, taken from the façade to the apse, and 8,24 m of width, without take into account the lateral chapels. The average height of the interior is 17,72 m at the keystone of the transversal arches and 13,45 m at the set of those. The height of the roof that covers the main arch reaches 26,29 m.

- The transept has a lenght of 34,76 m and a variable width from 6,40 m and 8,40 m, considering the interior space.

- The towers façade are of 7,46 m length by 6,15 m width from the exterior space. The height of the tower is 42,70 m until the set of the spire and reach a total of 61,12 m until the upper part of the crosses.

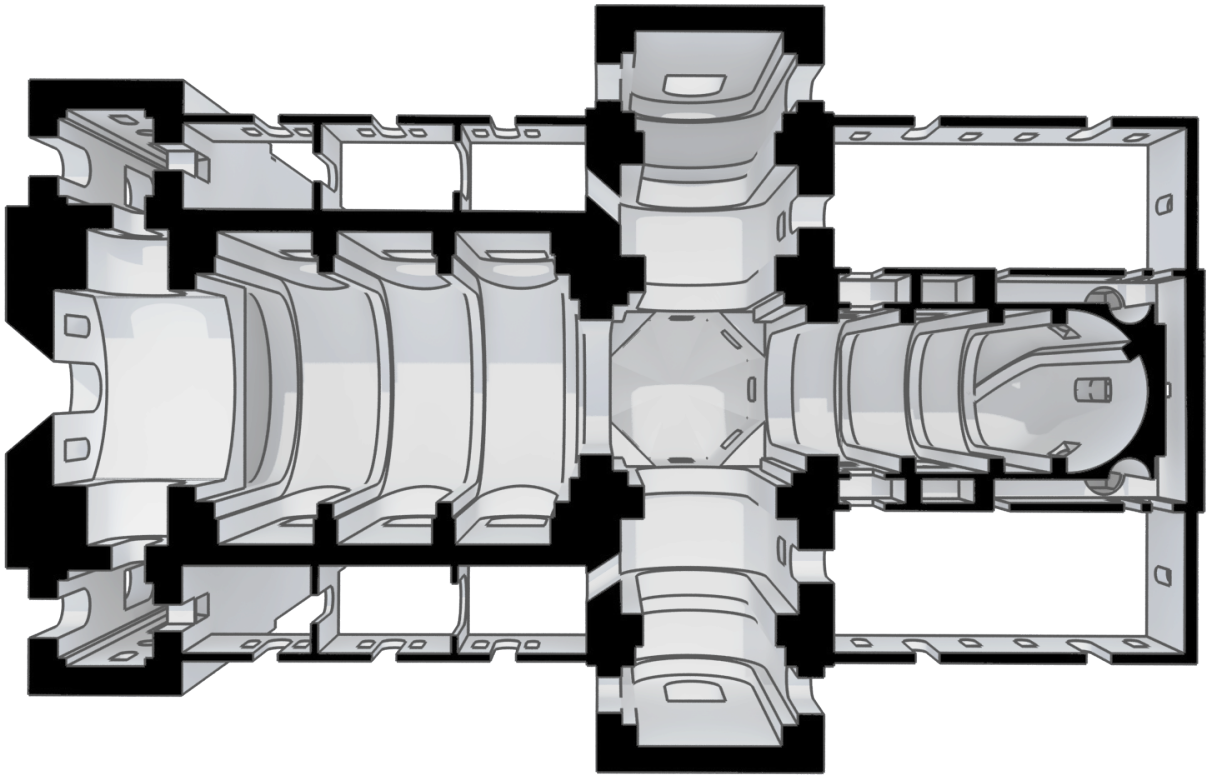

Figure 2.9: Plant and interior of the building inferred by the laser model made by Sánchez Aparicio

(a)

(b)

(c)

(d)

Figure 2.10: Details of the towers: (a) the internal staircase (b) a detail of the tower from a old picture (c) one of the spires (d) the rosette and the upper gallery (personal works and Baptista, 1997)

(a)

(b)

(c)

Figure 2.11: Interiors of the church: (a) the octagonal dome (b) with the roof structure and the of vault extrados are visible in the attic (c) one of the spires (d) the main nave (Betzer et al., 2014)

• The thickness of lateral walls vary from 1,05 m (in the windows) to 1,30 m (where the pillars are sited). The average thickness of the towers is 1,42 m, and is constant through the height of it. The thickness of the façade is 2,28 m in the bottom part and changes at the choir level, where is reduced to 1,39 m.

The façade is symmetrical and presents two quadrangular towers, in both of which there is a stone spiral staircase that allow the access to the bells. The towers present impressive windows and culminate in a pyramidal spire, whose decorations represent the fine art of the craft-men. In the façade is present, above other things, a rosette of 2,2 m of diameter and a balustrade accessible from the choir and the towers (Figure 2.10).

The main nave is covered by barrel vault leaning on the side walls and on a series of arcs supported by pillars. An octagonal dome made of reinforced concrete overhangs the transept. The main altar represents the focal point of the building: it is possible to recognize that was transformed from the original conception because the stone has evident differences with respect to the rest of the building. The Gothic choir occupies two of the entrance arcades and has a height of approximately 8,7 m, with a balustrade that allows the global vision of the main nave. Above the vault of the main nave, a wooden truss structure supports the roof (Figure 2.11).

The church is mainly built in granite masonry walls with thin joints: the details that are carved on the

(a) (b)

Figure 2.12: Examples of the carving skill of the local artisans: (a) the statue of S. Torcato that adorns the main façade (b) the rich decoration of arches and columns (Baptista, 1997)

blocks, on the arches and in the spire of the towers shows the enormous skills of the local artisans. The phases of construction and the development of the tools can be seen by naked eye in a careful observation. The façade and the entrance of the church were worked by hand with the help of simple tools, because are carved in coursed way with respect to the stone of the newer part of the apse (recalling that the former one was replaced) that were definitely carved through saws. It is significant in the presence of reinforced concrete covered in granite veneer in many parts of the building, like the apse and the main dome. The barrel vault is also constructed by a 30 cm layer of poor concrete with a reinforced mesh of 8-10 mm in diameter.

3. BUILDING ANOMALIES AND PREVIOUS INVESTIGATIONS

3.1 Introduction

As previously mentioned, São Torcato church suffers of several damages of medium and high intensity, mainly concentrated in the façade and the side parts that are closest to the entrance. Such anomalies are basically structural cracks of considerable dimensions, some of which 50 mm of width.

The date of first manifestation of these phenomena is uncertain, but for sure it happened more than forty years ago. In fact, since 1976, a detailed investigation campaign has been carried out on the church to evaluate the level of activity of the cracks and, more important, the causes that trigged the damages arouse.

Aim of this chapter is the study of all the inspections, monitoring and diagnosis works performed during the years and report their conclusion, in order to build a complete picture of the method that were used to discover the causes of the problems and the characteristics of the building. For each investigation it will be described the systems and tool sets used, the methodology and the main conclusion that were inferred by them.

The different techniques will be grouped according to four categories (Visual inspections, Monitoring, Non-Destructive testing and Diagnosis), inside of which each investigation will be organized in a chronological way, in order to understand the logical process that pushed the analysis on a specific path. A n outline of all the methods that were performed on the building since 1976 can be seen in the scheme shown in Figure 3.1.

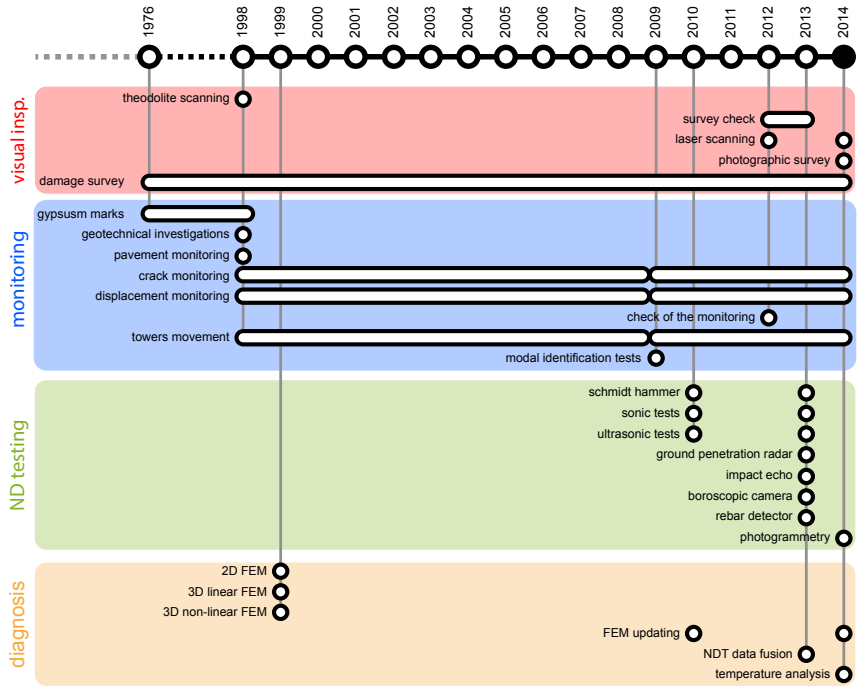

Figure 3.1: Resuming scheme of the different studies performed on the building

3.2 Visual inspections

The visual inspection is the first step that has to be performed in order to evaluate the state of equipment and structures. Is the easiest method of quality control and data acquisition that can be performed with the help of raw human senses or others non-specialized equipment, such as cameras.

Three type of visual inspection will be briefly described in the following paragraphs. Such campaign represents a fundamental point for the comprehension of the building problems; without it, in fact, it would not have been possible to notice the damages.

3.2.1 Geometrical survey

The first goal of the inspections is the check of the reliability of the existing data. The geometrical survey can establish, with more or less approximation, the effective dimensions of structural parts, building elements and details, more generally defined as the building envelope. It is possible to build in this way a reference system that can be translated into blueprints and real or digital models. It is necessary to remark the need of accuracy of this step; a coarse description could lead, in fact, to wrong results of further analysis carried out based on such investigation. The geometrical survey is usually compared with historical data, such plans, drawing or pictures, and was carried out in S. Torcato initially by means of a theodolite, and more recently with a laser scanner.

3.2.1.1 Theodolite scanning (’90)

The first survey was carried out with the help of an optical theodolite (Lourenço and Ramos, 1999). This precision instrument is able to measure angles in horizontal and vertical planes. The instrument is mounted on a tripod leveled by a laser or analogical plummet, and consists on a telescope that is movable within two perpendicular axes, the vertical and the horizontal ones, also called trunnion axis. The precision of the modern theodolites is high, approximate to seconds of arc. However, its accuracy and its manageability are lower compared to total stations (already present in the market during the considered scanning) and laser scanning. The main dimensions and the blueprints inferred by that survey (Lourenço and Ramos, 1999) are reported in the following list (Figure 3.2):

- The dimensions of the central nave are 57,5 m of length, 17,5 m of width and an average height of 26,5 m.

- The transept is of 37 m length and 11,5 m width.

- The façade towers are of 7,5 m length, 6,5 m width and 50 m height.

- The thickness found for the structural elements are 1,3 m in the lateral walls, 1,45 m in the tower, and varying from 2,5 m to 1,5 m in the façade.

A mistake is visible both in the plants that in the elevation of the developed blueprints. There is in fact a lack of information regarding the lateral chapels of the main nave. Those volumes were built around

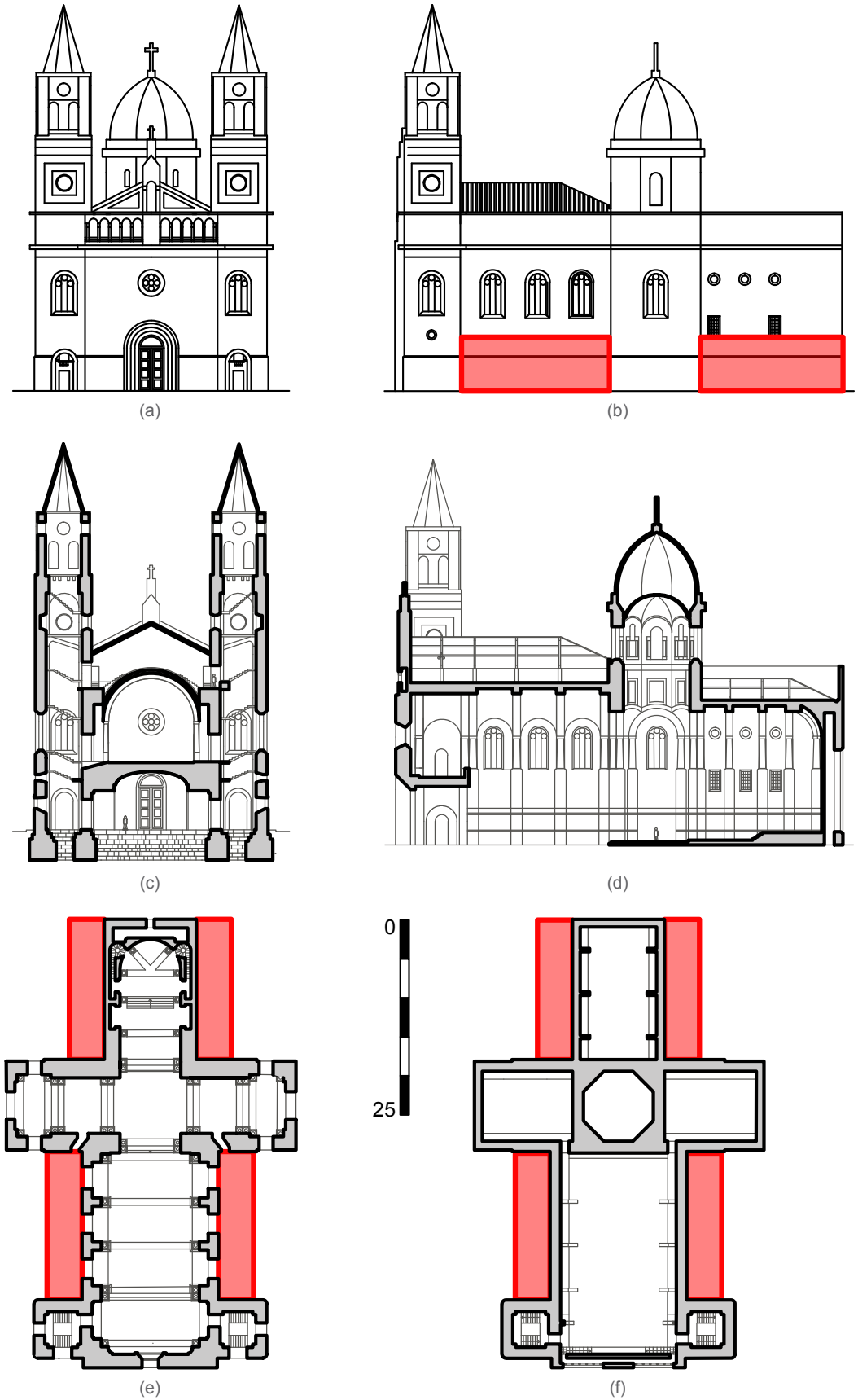

Figure 3.2: The blueprints resulting from the theodolite scanning, in red are marked the parts omitted during the analysis: (a) façade (b) eastern elevation (c) transversal section (d) longitudinal section (e) ground floor plant (f) roof plant

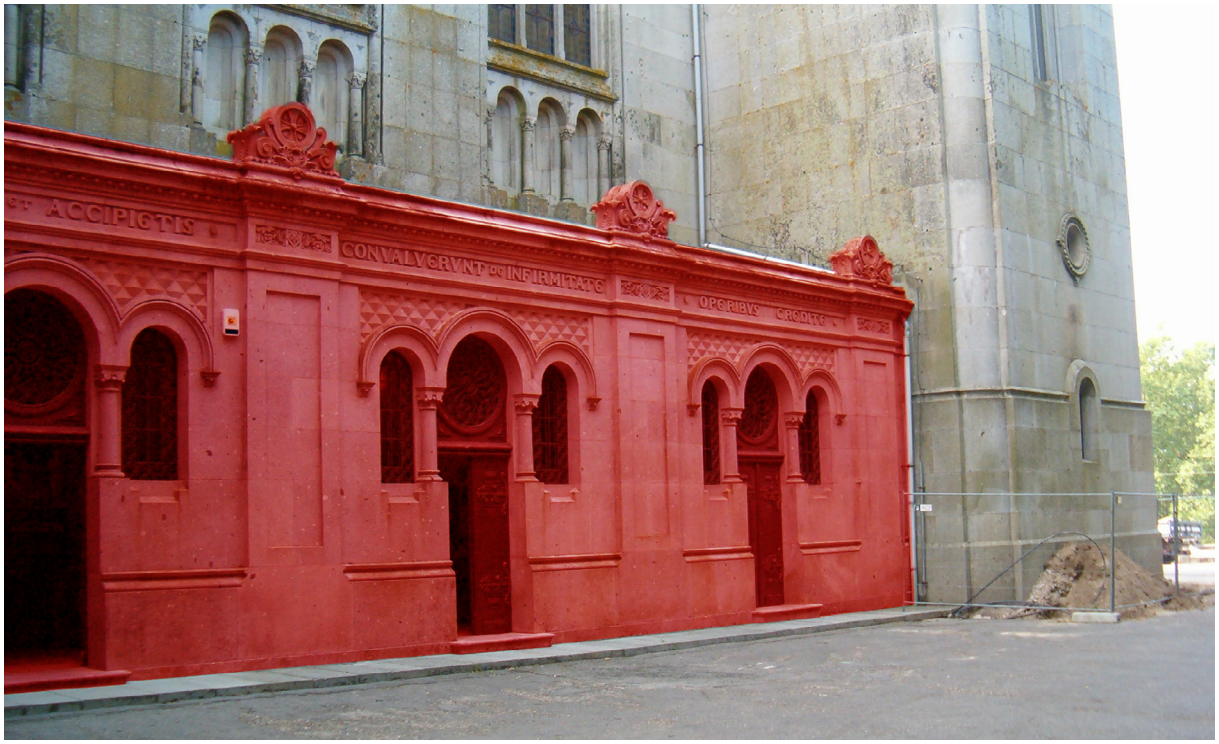

Figure 3.3: The parts omitted during theodolite scanning

1875 (see Chapter 2) thus they were present during the scanning and should be identified by it (Figure 3.3). Even the apse part is not reliable with the real building for lack of information, but this point is more delicate because this part of the building was replaced in between the last thirty years, operation that could have been performed after the survey (see chapter 2.4). This omission could be attributed to a mistake during the scanning, a mistake during the transferring of the image from the CAD file to the report or even an arbitrary choice of separate those later additions with respect to the structural parts. However, recalling that the aim of the geometrical survey is the recovery of objective data, even the last hypothesis would be incorrect. This mistake, together with others, has been pointed and discussed by former SAHC students. Their consideration will be presented in the following paragraph.

3.2.1.2 Survey check (2013)

In the first semester of the present academic year the church was a case study during the “Inspection and Diagnosis” course of SAHC. During the survey performed by the students different measures were taken to check the existing blueprints. Various errors were discovered and reported to update the previous information. As previously mentioned, they noticed that some parts of the building were omitted and the dimensions in the drawings were not enough reliable. The main nave has a difference of two meters in height, resulting in a stretched drawing well exposed in the following figures. Several minor mistakes are described in the student reports. The difference of more than 6 meter in length with respect to real measurements can be considered as a “test“ made by the professor during the SAHC course of visual inspection: the difference of the blueprints with respect to the real measurements cannot have, in fact, such a wrong level of approximation.

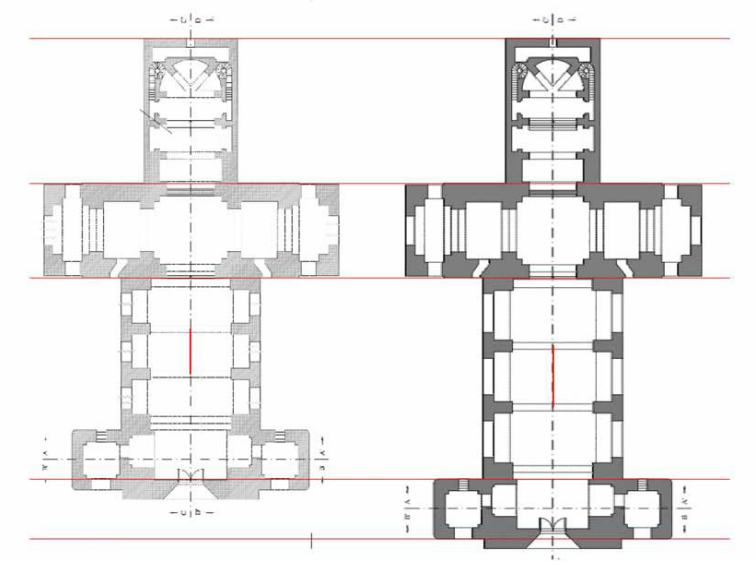

Figure 3.4: The irrealistic difference discovered by the students during their the geometrical survey: the blueprint developed after the theodolite scanning (left) the updated drawing (right) (Ogrizovic et al., 2013)

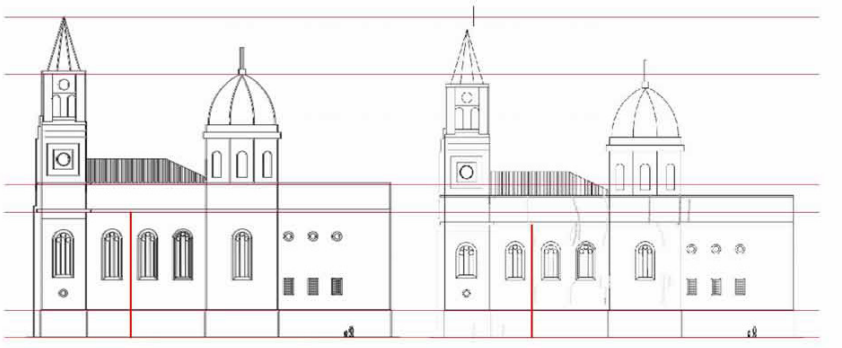

Figure 3.5: Difference in height discovered by the students during their the geometrical survey: (a) the blueprint developed after the theodolite scanning (b) the updated drawing (Ogrizovic et al., 2013)

3.2.1.3 Laser scanning (2012)

On the 12th of December 2012 a laser scan on the façade of S. Torcato was carried out by Belén Riveiro, a researcher at the University of Vigo. The main aim of this analysis was the update of the plans of the building and the check of the real inclination of the towers (this last part will be discussed in Paragraph 4.3.1.6). Because of the lack of time just two scans were carried out, one in the front and one in the sides of the façade (Figure 3.6). The laser scanning was useful to reveal the mistakes of the drawings and the plans were updated as shown in Figure 3.7.

3.2.1.4 3D laser scanning (2014)

The 3D laser scanning represent the most advanced methodology of geometrical survey nowadays. Such inspection was carried out in the church by means of a FARO Focus 3d and a Rielg Z390I portable laser scanning during four days (Sánchez Aparicio et al., 2014). Those systems are mounted on a tripod and consist on a fixed laser beam that projects a ray on a rotating screen, a receiver and an internal pro-

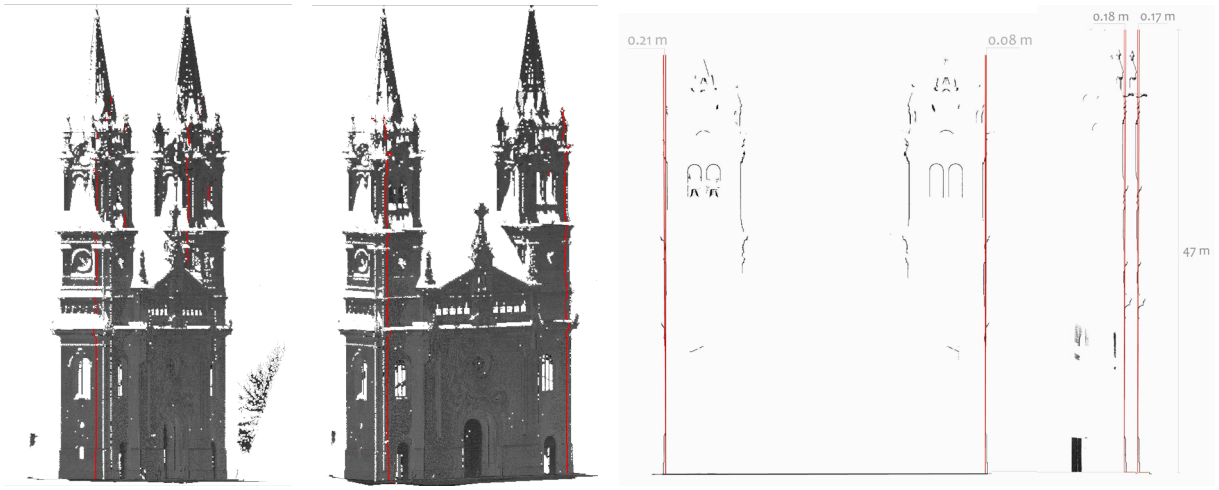

Figure 3.6: The first laser scanning: (a) laser scan of the sides of the church (b) laser scan of the front of the church (c) lateral displacements inferred by the students (d) displacements of the façade inferred by the students (Facelli et al., 2013)

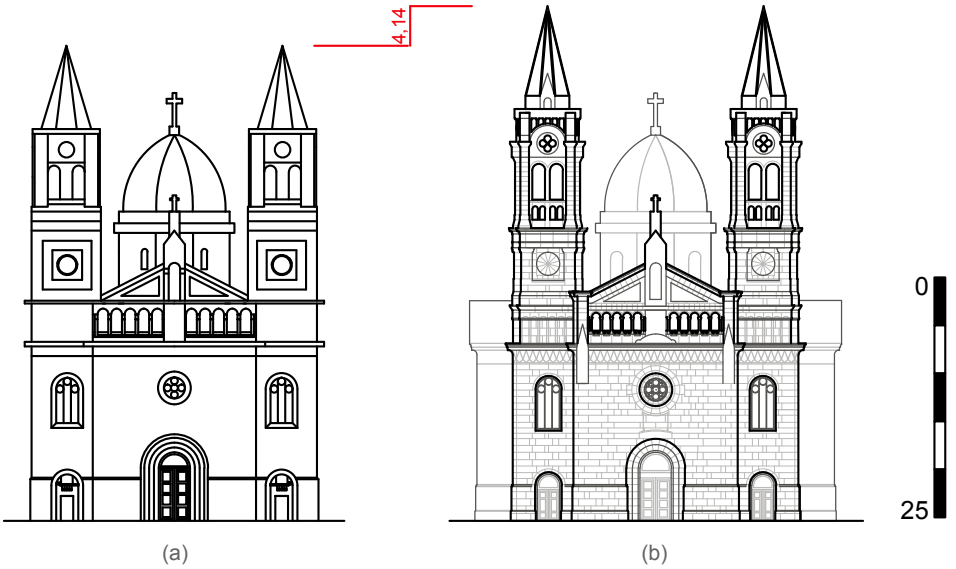

Figure 3.7: Updating of the building plans (a) the blueprint derived from the theodolite scanning (b) the drawings developed from laser scanning

cessor, the whole system can rotate with respect to the base. The difference of the instruments regards the physical principles that govern the data acquisition. The FARO scanner works for phase shift: the laser is shot on a surface and reflected to the receiver, the difference of phase determine the distance of the body with respect to the scanner. The Rielg system considers, instead, the time of fly of the laser: calculating the time necessary for the ray to rebound on a surface and return to the receiver it is possible to define the distance between the scanner and the body. Both instruments works register the measurement in polar coordinates and then transformed in Cartesian coordinates. The whole system of points is outputted as point cloud. The laser is able to measure distances directly on the line of sight of the tool, thus it is always necessary to collect data from several different point. In the case study, the exterior was completely covered, with the exception of the roof, by a ring path around its perimeter. In the interior the laser systems were moved through the nave and the transept, more difficult was the survey of the attic.

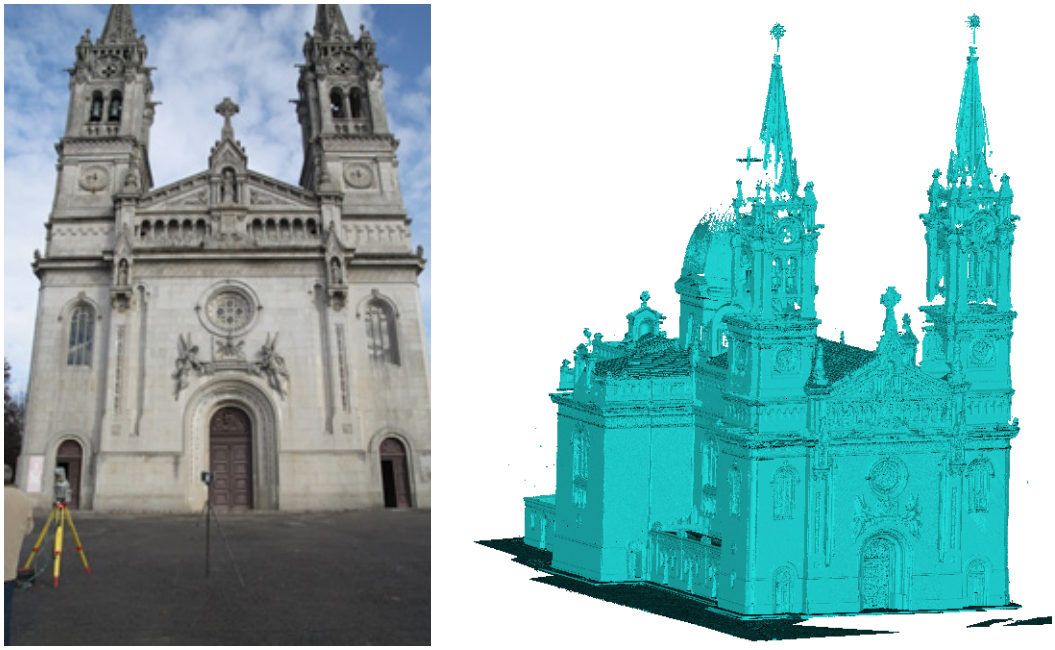

(a) (b)

Figure 3.8: The last 3d laser scanning (a) the two different systems used during the survey (b) the final output of the systems presented as point cloud, with an extremely high detail (Sánchez Aparicio et al., 2014)

The various point cloud were registered and unified in a single file by means of proper reference points (Figure 3.8).

The main aim of this inspection was the acquisition of data that, interpolated with photogrammetry data (see paragraph 1.4.8), were able to create a reliable digital model, suitable for a Finite Element analysis (see paragraph 1.5.7). The power of those tools is in the extremely high precision and the speed of data acquisition, but is an expensive instrument and requires long time of post-processing for the analyst. Even with this level of accuracy, laser scanners are not reliable for crack monitoring because it is hard to establish the crack pattern from the point cloud. Other more suitable methods for this purpose will be described in the following paragraphs (see paragraph 1.4.8).

From the laser data it was possible to establish the precise dimensions of the building. The discussion of the difference with respect to the theodolite scanning measurement will be exposed in the next paragraph. The main dimensions of the sanctuary are:

- The dimensions of the central nave are 58,19 m of length, taken from the façade to the apse, and 8,24 m of width, without take into account the lateral chapels. The average height of the interior is 17,72 m at the keystone of the transversal arches and 13,45 at the set of those. The height of the roof that covers the main arch reaches 26,29 m.

- The transept has a lenght of 34,76 m and a variable width from 6,40 m and 8,40 m, considering the interior space.

- The façade towers are of 7,46 m length, 6,15 m width from the exterior space. The height of the

tower is 42,70 m until the set of the spire and reach a total of 61,12 m until the upper part of the crosses supported by the.

• The thickness of lateral walls varies from 1,05 m (in the windows) to 1,30 m (where the pillars are sited). The average thickness of the towers is 1,42 m, and is constant through the height of it. The depth of the façade is 2,28 m in the bottom part and changes at the choir level, where is reduced to 1,39 m.

3.2.1.5 Conclusions on Geometrical Survey

The development of tools and techniques of analysis have considerably increased the accuracy and the rapidity of measurement. This paragraph wants to remark the importance of a geometrical survey as the first task of a building analysis. In fact, if detailed analysis were carried on using a wrong base, they would certainly leads to errors or wrong approximation of the relative results. The differences observed between the drawings developed after the theodolite scanning and the newest model result of the laser scanning will be summarized in Table 3.1, considering the relative percentage of error. It is possible to see that the most relevant mistake is in the tower, were the measuring differs for almost 15%.

	Theodolite (m)	Laser (m)	Difference
Length of the church (walls exterior side)	57,52	58,20	1,17%
Length of the nave (walls interior side)	52,46	53,12	1,24%
Span of the nave (at pillars level)	10,20	11,07	7,86%
Span of the nave (at niches level)	14,85	15,20	2,30%
Façade width	17,18	17,55	2,11%
Building width	29,90	29,79	0,37%
Façade height until the tympanum	22,95	23,15	0,86%
Total height of the towers	49,50	57,57	14,02%
Height of the dome before the cross	40,20	39,50	1,77%

Table 3.1: Differences in measurement between theodolite and laser scannings

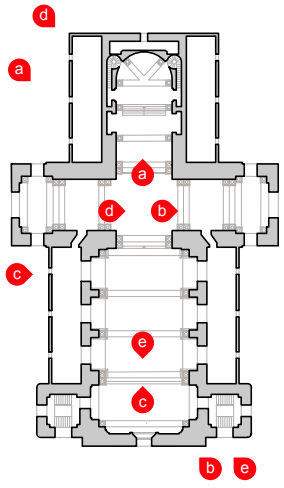

Figure 3.9: photographic survey scheme

3.2.2 Photographic Survey

The main aim of the acquisition of photographic material is the creation of a detailed archive that could be used to check the progress of crack patterns, observe the developments of building conditions or just provide historical bases for further investigations that could be supported and facilitated from such dossier, as described in previous paragraphs. The Irmandade of S. Torcato has already a big archive that former SAHC students helped to enlarge providing their own files. In this chapter will be shown just few personal shots taken on site (Figure 3.10 and 3.11), accompanied by an explanatory scheme (Figure 3.9). Additional personal pictures will be placed in the Annex A, together with historical photographs.

(a)

(b)

(c)

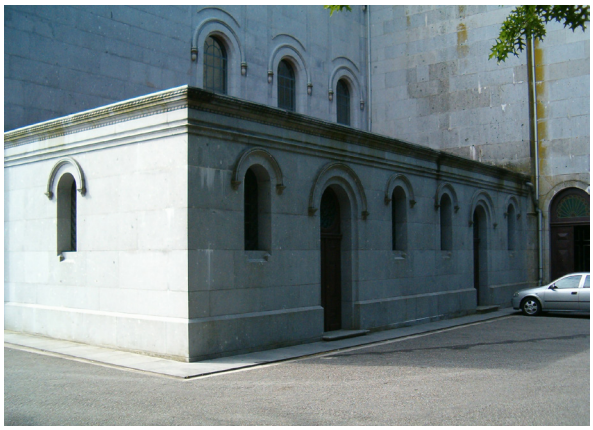

(d)

(e)

Figure 3.10: Photos of the exterior

(a)

(b)

(c)

(d)

(e)

Figure 3.11: Photos of the interior

3.2.3 Damage survey

The church is affected by several structural and non-structural decays. The external walls present discolorations, delamination, encrustation, patinas, soiling, corrosion of the metallic parts and biological attacks. Causes and intervention methods of those pathologies were suggested by SAHC students during 2013. The actual damage pattern has been well represented by the students (Figure 3.12).

However, the most critical damage phenomenon is represented by the cracks that are developing on bearing walls and balconies. In fact, the main façade of the Temple is affected by a several cracks that reach 50 mm of width in some parts. The crack starts on the top of the main door and develops until the rosette, where it forks and proceeds up to the balustrade and the tympanum. It can be inferred that the area bounded by the cracks, that in some points are passing-through, represents a macro element detached from the rest of the façade. The crack pattern can be seen in Figure 3.13 and 3.14.

The balustrade presents five vertical cracks with maximal width of 5 mm, spaced approximately one meter between them. The major cracks of the façade are extended to the interior wall of the choir and on the upper part of the barrel vault. In in the choir the prolongation of three of the main cracks are visible on the floor. Moreover, in the main nave of the church is visible a horizontal crack that passes through the central part of the barrel vault.

Both sides of the buildings are affected by cracks, with maximal width of 20 mm, in the keystone of the first two rows of arches. Such damages are protracted until the roof (Figure 3.14).

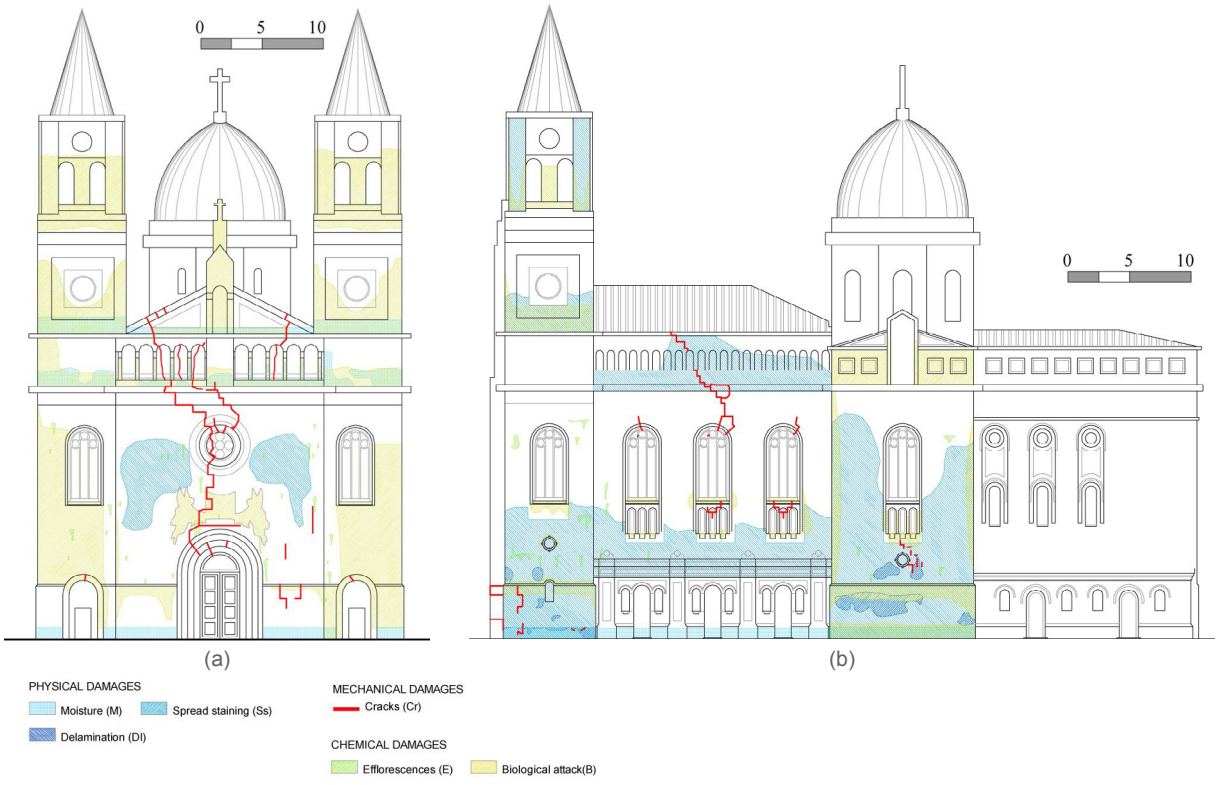

Figure 3.12: Damage map: (a) façade (b) eastern elevation (Ogrizovic et al., 2013)

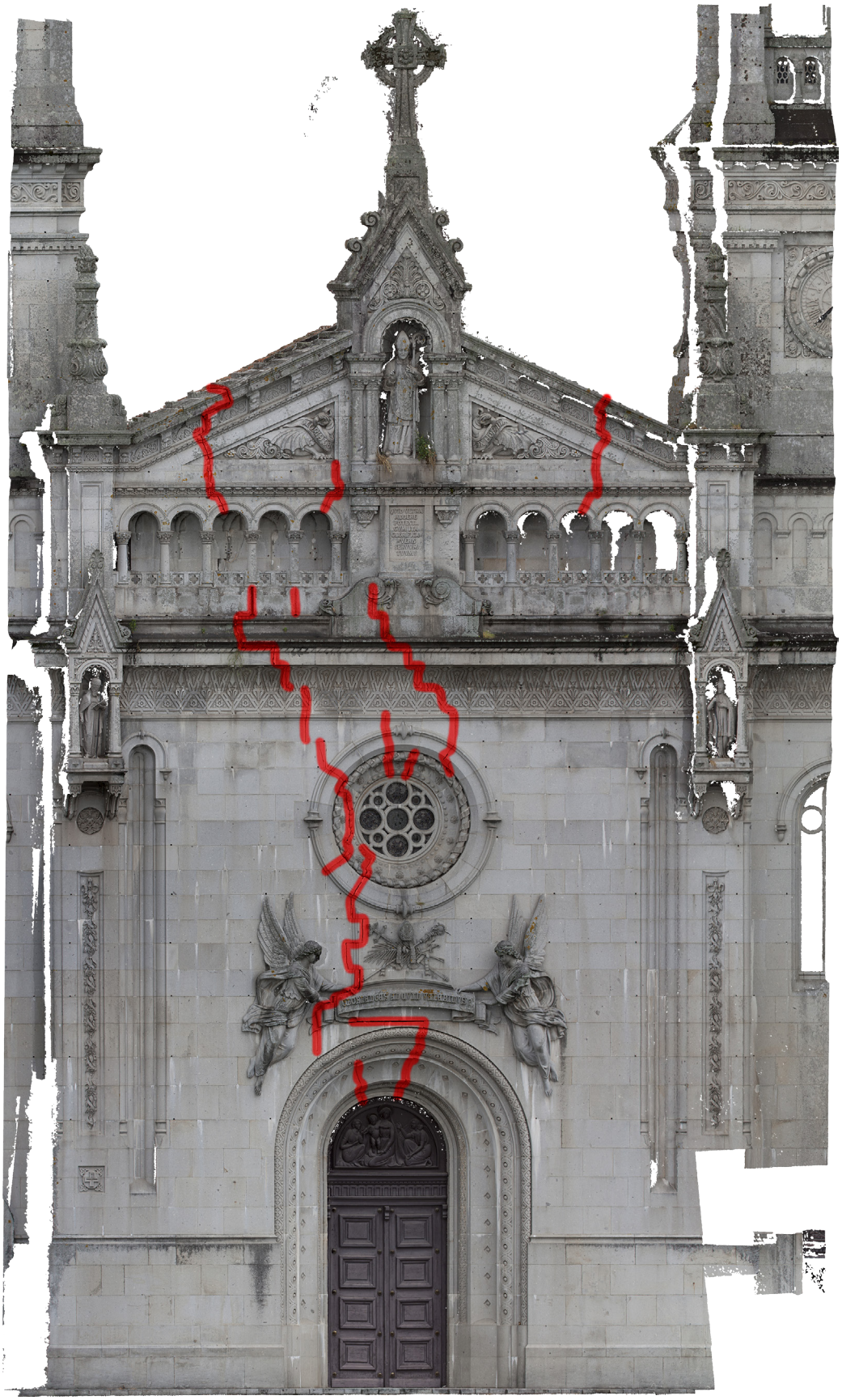

Figure 3.13: Identification of the crack in the façade, based on photogrammetric survey of Sánchez Aparicio

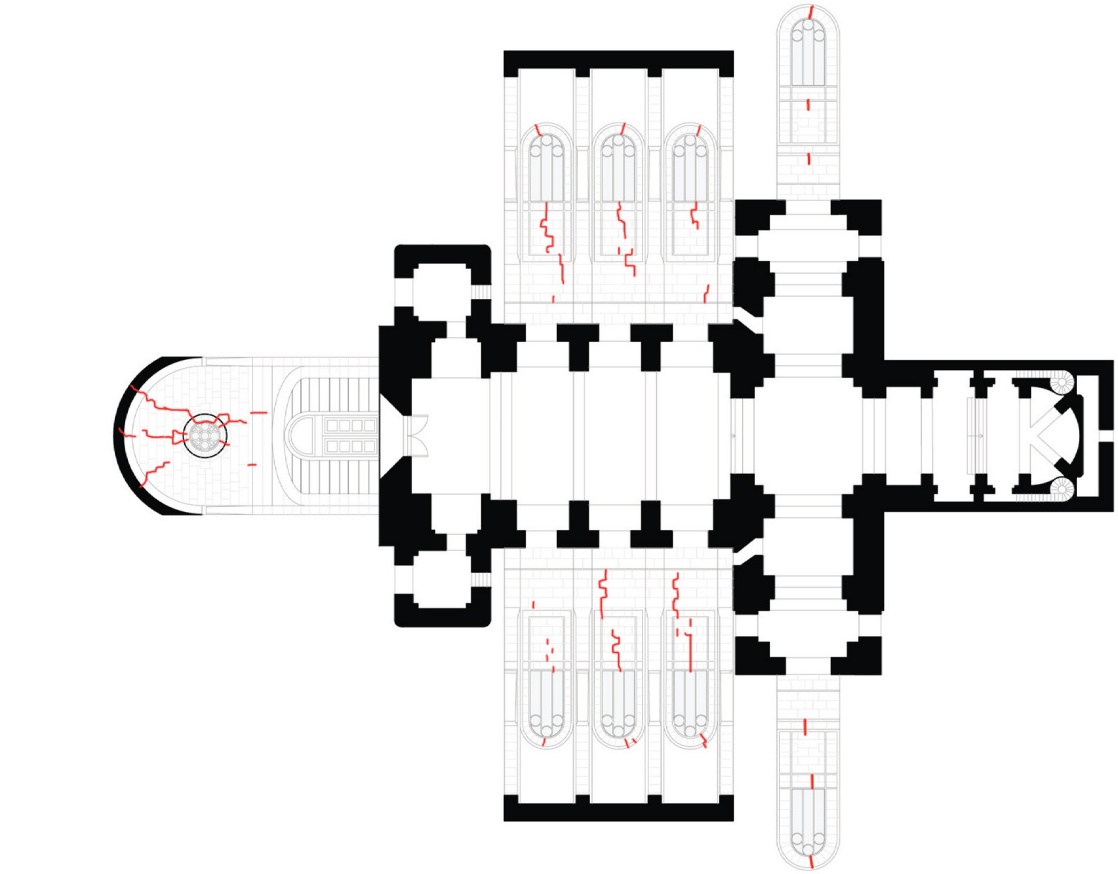

(a)

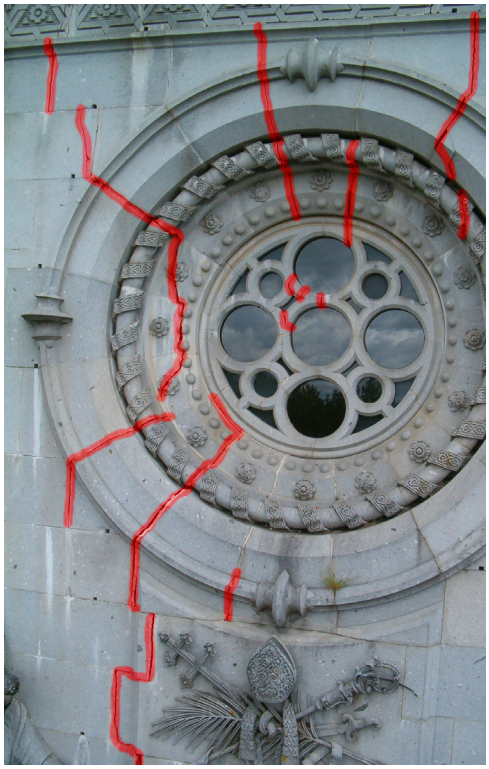

(b)

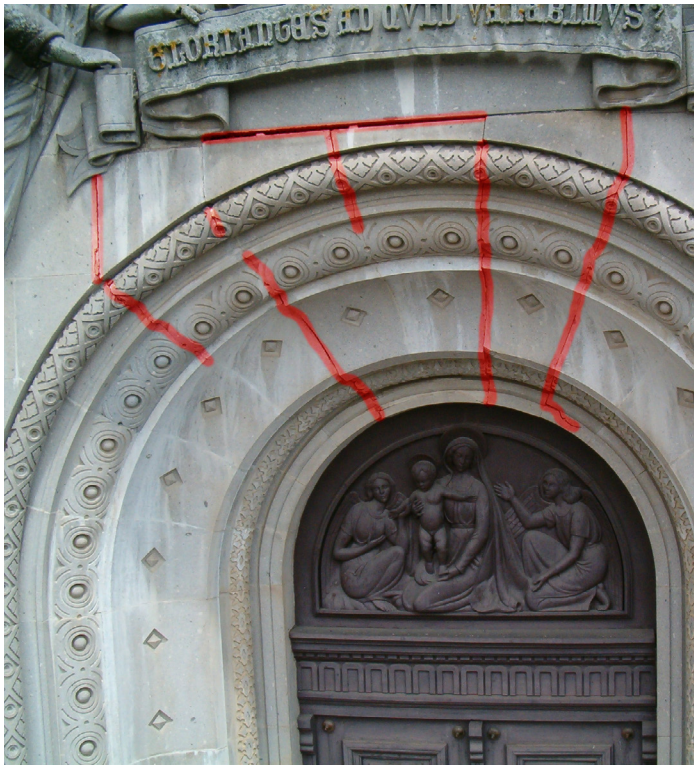

(c)

Figure 3.14: Cracks of S. Torcato: (a) scheme of the the damage patter in the interior of the church defined by Gutscoven (b) detail of the cracks visible on the rosette (c) the damage revealed on the main entrance

3.3 Monitoring

3.3.1 Static

The aim of static monitoring systems is the check of the buildings movements in terms of displacements or rotations. With several devices, it is possible to discover the activity level of a crack and its trend, or the development of mechanisms or settlement of the whole building. Because the main problem of the building is given by the crack pattern, the static monitoring systems are mainly focused on the study of slits activity.

3.3.1.1 Gypsum marks monitoring (1976)

Figure 3.15: Gypsum marks

The gypsum marks present in the interior side of the external balustrade represent the first attempt of crack monitoring. The data of such system, if collected, have been lost and it is unknown who performed and monitored them. However, just by means of superficial analysis, it is possible to deduct that the cracks had to been appeared more than forty years ago. Furthermore, the cracks widths have increased several millimeters since the application of the marks.

3.3.1.2 Geotechnical investigations (1998)

The investigation developed for the Irmandade de São Torcato (Lourenço and Ramos, 1999) reports that thirty dynamic cone penetrations and four extractions of soil samples for laboratory tests, of variable depth between four and eight meters, were performed around the church in order to understand the soil composition of the area. The results of the test indicate the presence of a wide range of layers. Moreover, it was discovered that the tower and the façade are leaning on landfill earth mixed with topsoil whit very poor mechanical characteristics. The distribution of the soil layers through the church section can

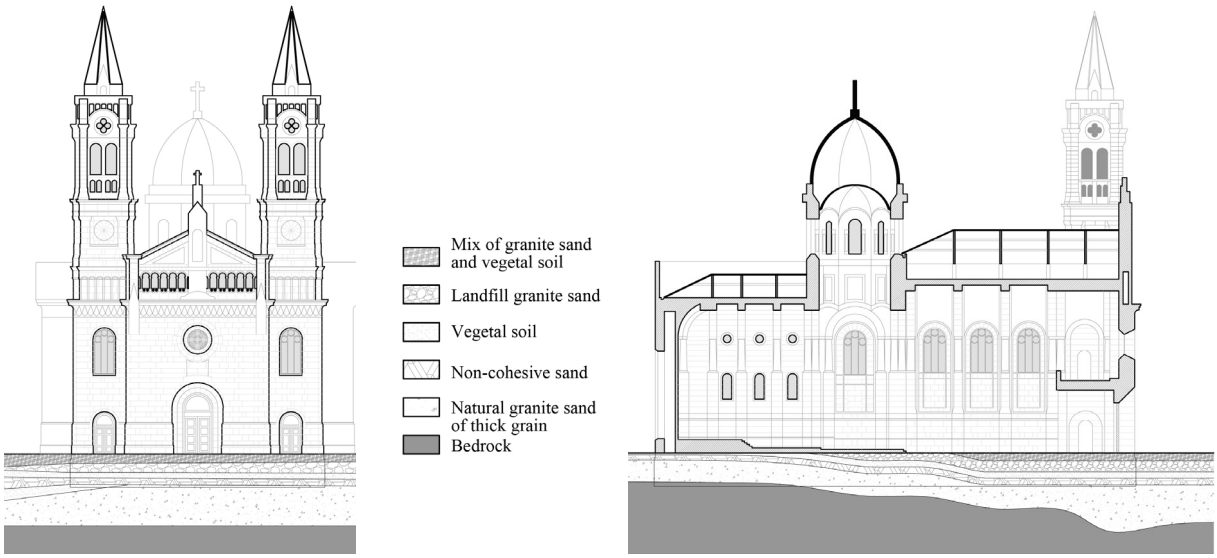

Figure 3.16: Distribution of soil layers according to the geotechnical investigation (Lourenço and Ramos, 1999)

be seen in Figure 3.16.

The results of this test are really important, because can imply the presence of a soil settlement as an underlying cause of the cracks. In fact, the building could be affected by differential soil settlement because is standing on various layers with different mechanical behavior. Furthermore, the presence of the cracks in the area that directly supported on the soil with poorest quality could validate such hypothesis.

3.3.1.3 Pavement level survey (1998)

It was considered necessary to perform a survey of the pavements due to the results of the geotechnical survey and the imperfections observed from the analysis of the arches, which showed a vertical difference in level of about 20 cm. By means of a total station, such difference was confirmed for the pavement and the plan reported in Figure 3.17 was drawn.

The results of the displacement monitoring confirmed the hypothesis of the differential settlement of the subsoil. It was possible to observe that the entire building, with the exception of the apse, is basically sinking following the distribution of the mechanical resistance of soil layers.

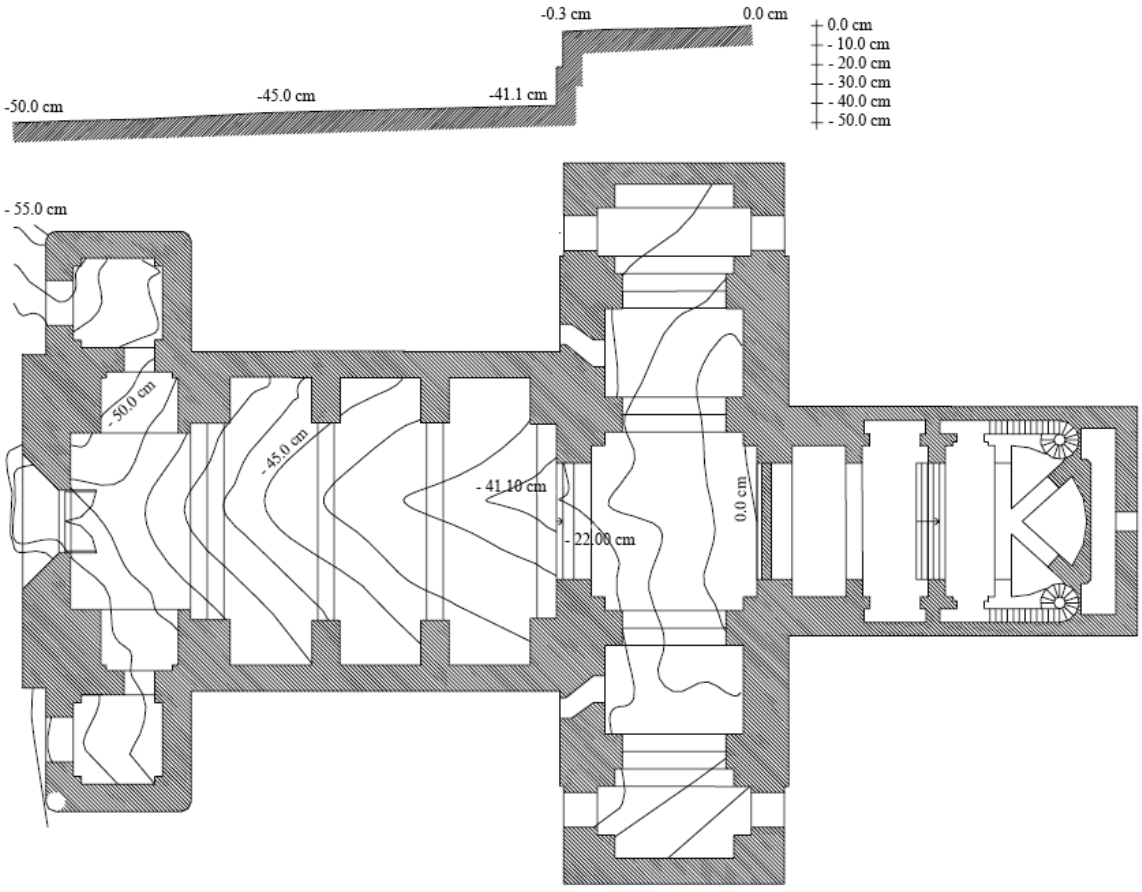

Figure 3.17: Plan that shows the distribution of the difference in level of the pavement (Lourenço and Ramos, 1999)

3.3.1.4 Crack monitoring (since 1998)

Once clarified which cracks were active by means of plaster marks, fourteen of them were chosen and daily monitored. This monitoring system consisted on the application of six analytical crack meters fixed on the walls combined with fourteen demountable Demec strain-gauges. The fixed crack meters have two overlapping transparent slips which are fixed to both sides of a crack. In case of crack expansion or contraction such slips could slide and the relative movement would be marked by an analytical meter (Figure 3.18). The strain gauge consist of three steel plates glued to the structure, used to measure the relative displacement in transversal and longitudinal directions by means of a Vernier caliper (Figure 3.18). Those sets were also coupled with a thermometer, so as to demonstrate the influence of temperature in the behavior of the slits. The weakness of such monitoring is the duration of data acquisition cycle, lasted only a year, and the number of measurements of little significance.

The crack monitoring demonstrated that the temperature affects the movement of the slits, and that the fourteen specimens are all active and present a differentiated movement that varies from 0,02 mm/year to 0,11 mm/year. The last check of the systems validated the projections of the crack development. In October 2012 an increase of the slit width of 1,0-2,9 mm was revealed by those crack meters. The Demec measurements demonstrated, a development of the cracks width around 2,5 mm.

In 2009 the previous set was discarded to give way to an automated monitoring setup. Two linear variable differential transducers (LVDT) were installed for the remote monitoring of the cracks width, together with three temperature sensors and one relative humidity sensor (Figure 3.19).

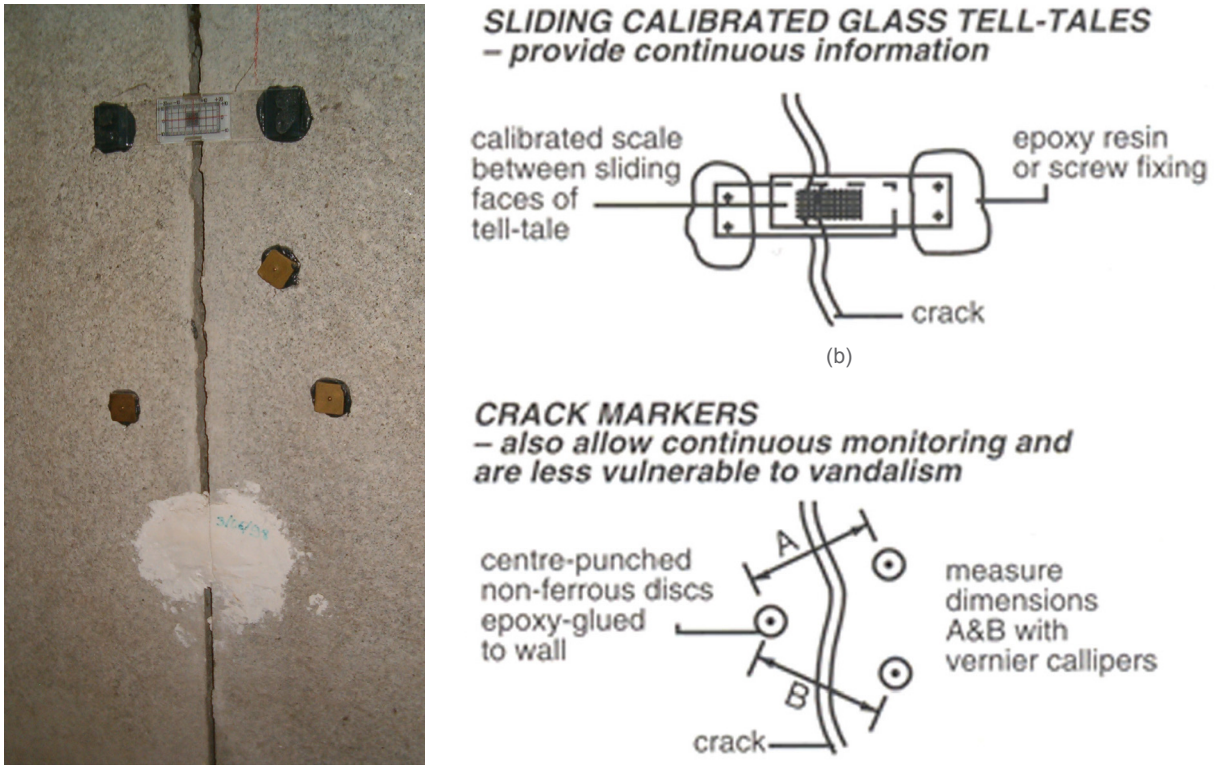

Figure 3.18: Monitoring tool set used in '98: (a) fixed crack meters (b) working scheme of the analytic crack meter (c) working scheme of the strain-gauge analytic system (Gutscoven, 2014)

(a)

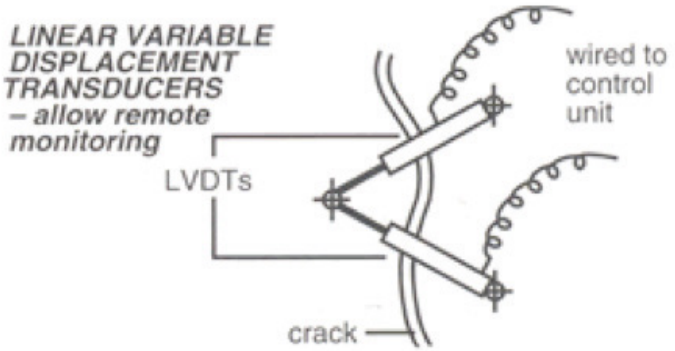

(b)

Figure 3.19: Crack monitoring tool set on-going since '99: (a) one LVDT (b) working scheme of a LVDT (Gutscoven, 2014)

A detailed analysis of the data until today will be described in Chapter 6. However, a brief conclusion that was inferred of the analysis of the data until 2012 will be reported here (Manning et al., 2013). It was found an average crack width increase varying from 0,1 to 0,15 mm/year. The tendency of the cracks follows inversely the temperature trend, that is to say the cracks width increase when the temperatures decrease (Figure 3.20).

3.3.1.5 Tower displacement monitoring (1998)

During the same period of installation of crack measurement tools, an analysis of the two towers displacement was carried out by means of an optical theodolite, which was used even for

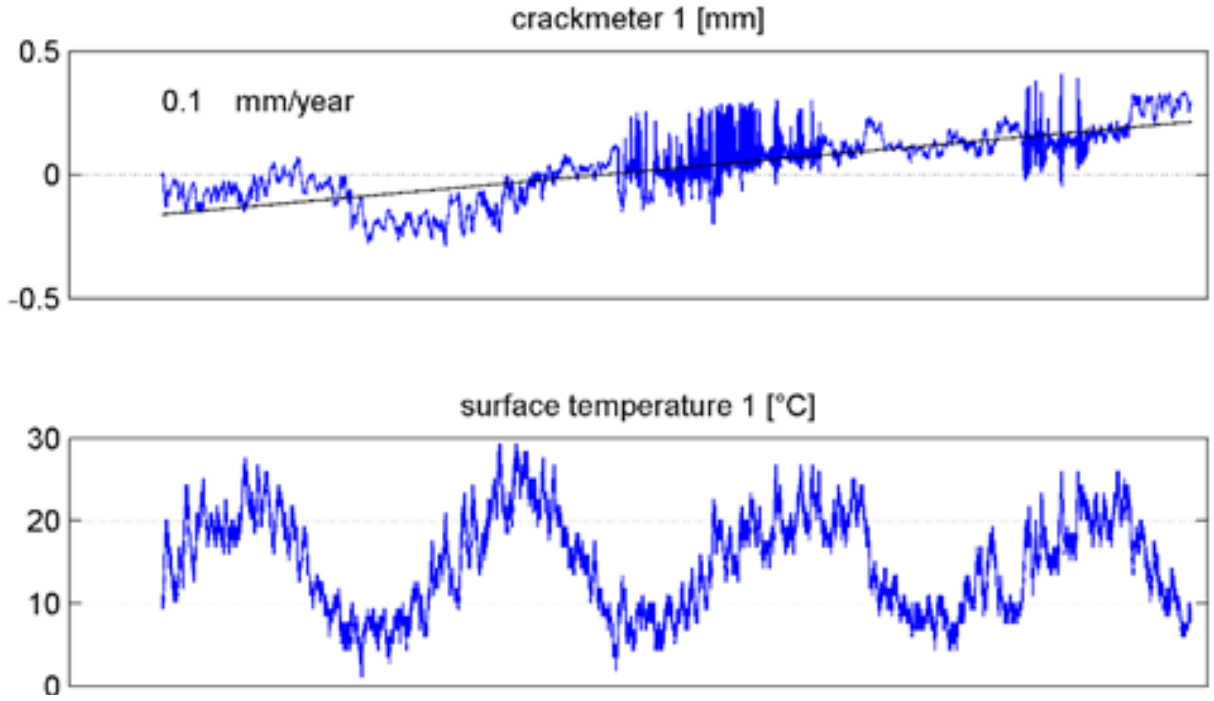

Figure 3.20: First results of the LVDT data regarding one of the cracks (Manning et al., 2013)

the survey for the arches of the barrel vault. The investigation on the towers shows that both of them are leaning on the same side with differential inclinations of about 0,0016 mm/m (left tower) and 0,0020 mm/m (right tower) (Figure 3.21).

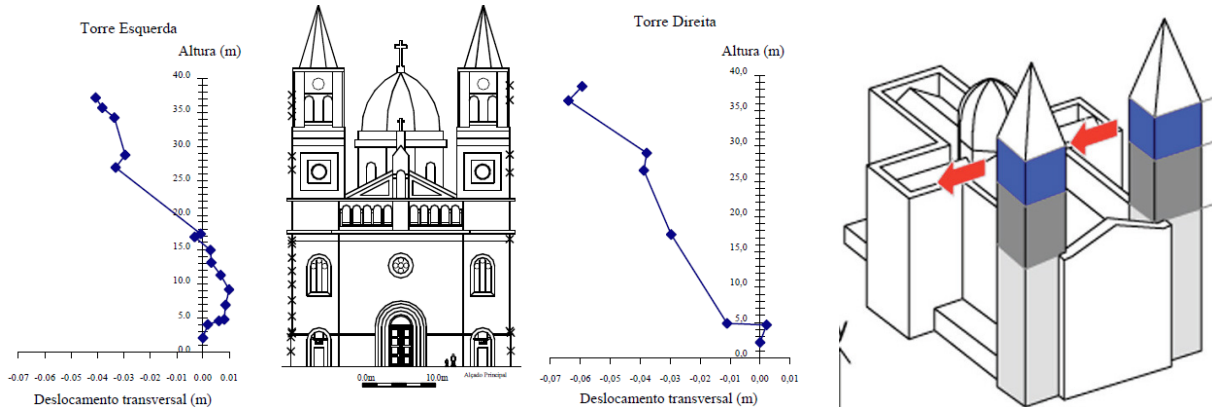

Figure 3.21: Tower displacement monitoring made by means of a optical theodolite: (a) results of the analysis (b) resuming scheme developed by Gutscoven (Lourenço and Ramos, 1999)

3.3.1.6 Check of the displacement monitoring (2012)

The laser scanning carried out during 2012 permitted to state the real tilting of the towers. Of course this analysis cannot represent the real movements of the structure, because it denotes just the situation at the moment of the snapshot. However, it is possible to confront the data collected during the theodolite survey and the displacements detected by the laser scanning. This comparison shows that to data collected analytically were probably wrong, but it is necessary to remark that the precision of a theodolite is much less than a laser station (Figure 3.22). Further analysis of the tilting, using the monitoring system data, will be carried out and described in Chapter 6.

3.3.1.7 Tower movements monitoring (since 1998)

Two simple clinometers were fixed in the upper parts of the two towers in conjunction with the installation of the crack monitoring systems. The devices were formed by two heavy pendulum submerged in a high density liquid with a maximal accuracy of $4{,}1 \times 10^{-5}$ mm/m (Figure 3.23). In this way it was possible to monitor the movements of the structures during two consecutive years.

The monitoring demonstrated that the towers were moving and that the order of magnitude is about $8{,}2 \times 10^{-5}$ mm/m/year. Moreover, the right tower presents oscillations more marked than the other one.

The devices were replaced by an improved monitoring system in 2009. Two automatic tilt meters (both for the measurement of horizontal displacements in perpendicular directions) per tower were installed at the bells level. The output data of the system will be deeply analyzed in Chapter 6.

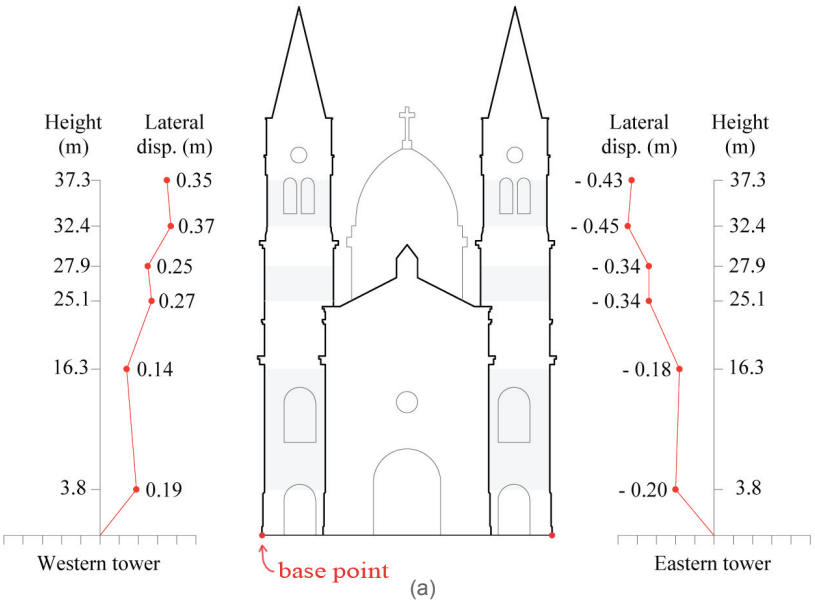

(a)

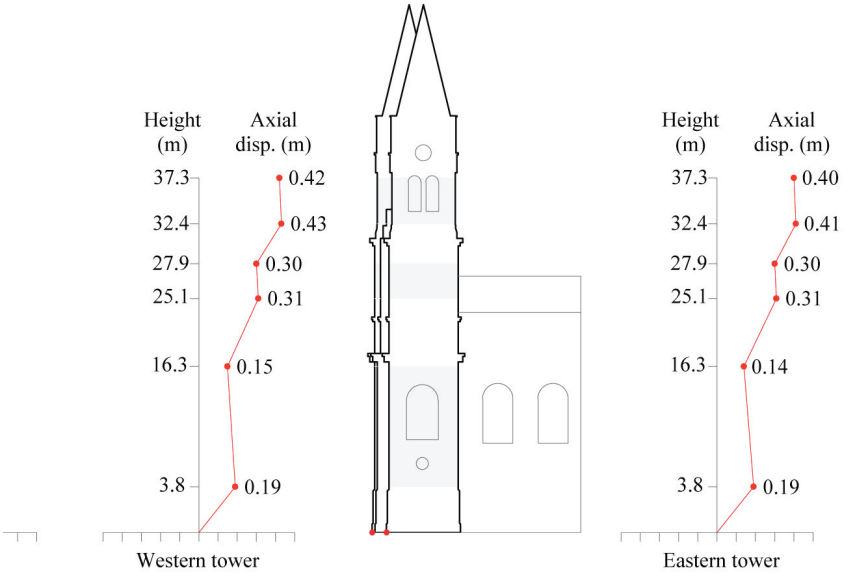

(b)

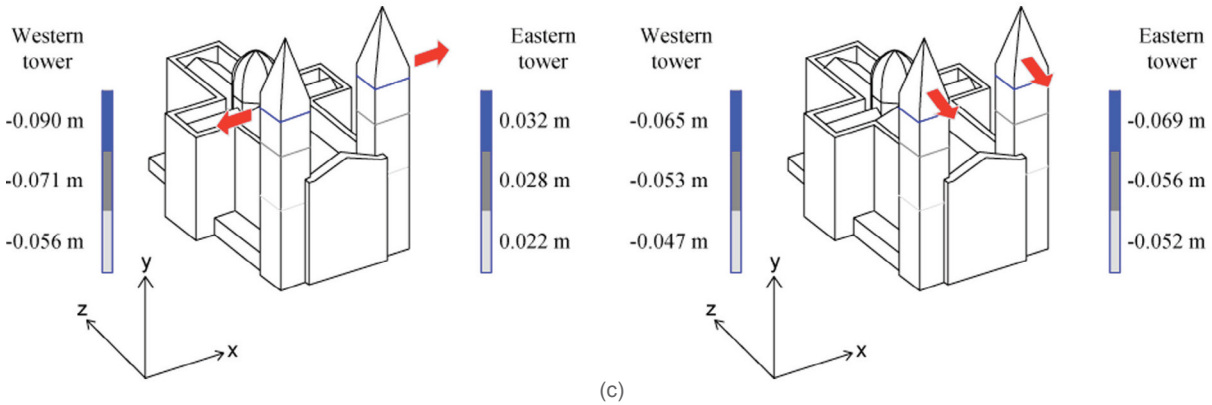

(c)

Figure 3.22: Check of the displacement monitoring by means of a laser scanninh: (a) differences in the transversal direction (b) differences in the longitudinal direction (c) reming scheme of the analyzed displacements (Gutscoven, 2014)

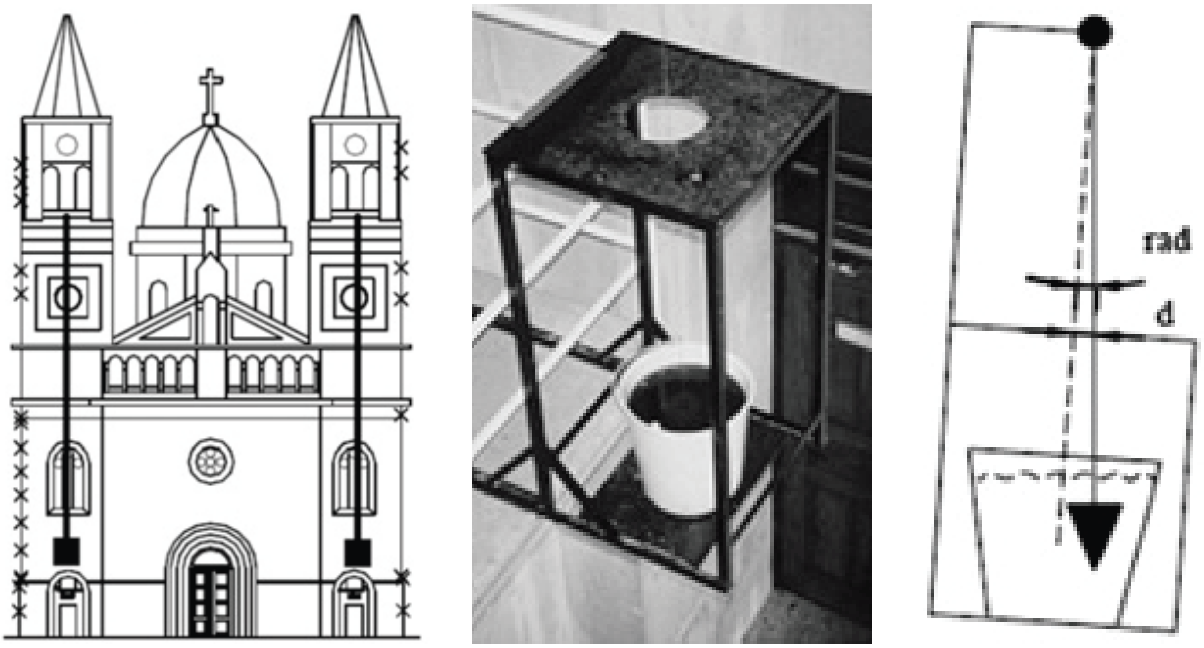

(a) (b) (c)

Figure 3.23: Pendulums: (a) location of pendulums (b) bucket in which is dipped the weight of the pendulum (c) reading scheme (Lourenço and Ramos, 1999)

3.3.2 Dynamic tests

The information inferred by non-destructive or destructive tests (see Section 3.4) can be local or insufficient. Nowadays, perform campaigns of dynamic tests is the best way to discover the global properties of a structure without damage it. For this reason, experimental dynamic techniques are reliable to obtain natural frequencies, mode shapes and damping coefficients that can be related with global values of the building, such as Young's modulus, density, etc.

3.3.2.1 Modal identification tests (since 2009)

The building was involved in an extensive campaign of Operational Modal Analysis (OMA) since 2009. The power of this analysis is the capacity of assess global properties of the structure without affect it directly. Ten uniaxial piezoelectric accelerometers with 10 V/g sensitivity, 0,5 g measuring range, 8 μg rms broadband resolutions were installed with a 16-bit resolution data acquisition. Thirty-five sensors were placed in order to record the acceleration of the building every ten minutes in a sampling rate of 200 Hz (Figure 3.24).

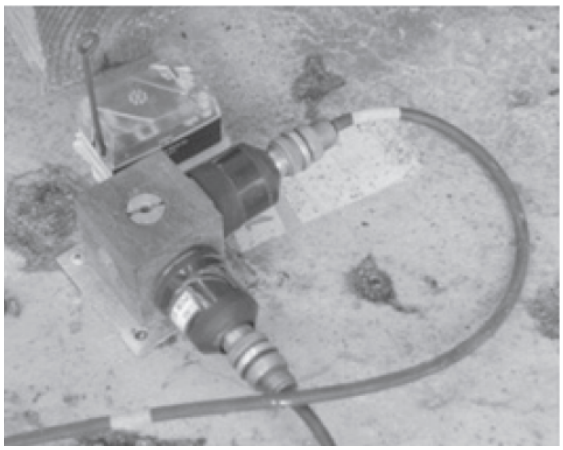

Figure 3.24: A two node accelerometer used for the modal identification test (Lourenço and Ramos, 1999)

Three OMA routines were used to determine the modal properties of the church (Alaboz, 2009): Frequency Domain Decomposition method (FDD), En-

hanced Frequency Domain Decomposition method (EFDD) and the Stochastic Sub-Space Identification method (SSI). Thanks to those tests, four modal frequency, two reflecting transitional movements and two representing torsional displacements, were identified with their relative damping ratio (Table 3.1). Subsequently, the FEM models were updated until reach an appropriate convergence with the experimental results. The product of the analysis can be seen in Section 3.5.

	SSI		**FDD**	**EFDD**	
	f (Hz)	ε (%)	*f* (Hz)	*f* (Hz)	ε (%)
Mode 1	2.14	1.5	2.15 (0.5%)	2.14 (0.01%)	1.8 (20%)
Mode 2	2.63	1.1	2.64 (0.4%)	2.62 (0.4%)	1.5 (36%)
Mode 3	2.85	1.4	2.89 (1.4%)	2.89 (1.4%)	0.8 (43%)
Mode 4	2.93	1.5	2.97 (1.4%)	2.94 (0.3%)	0.8 (47%)

Table 3.1: Results of the experimental modal analysis tests (Alaboz, 2009)

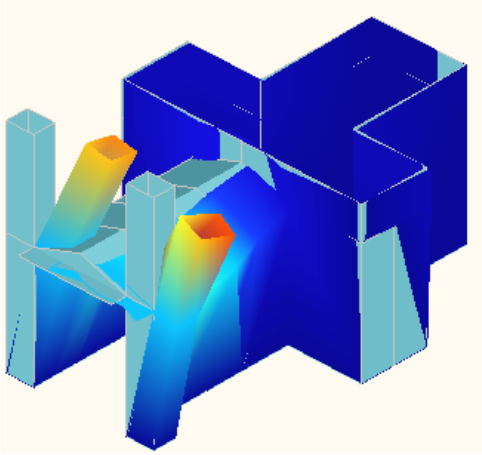

Mode 1 (2,14 Hz)

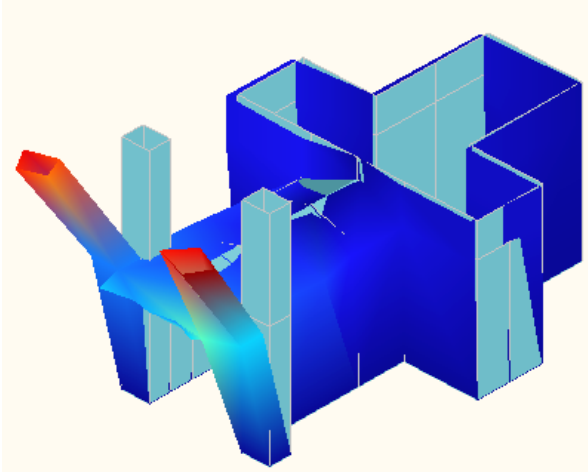

Mode 2 (2,63 Hz)

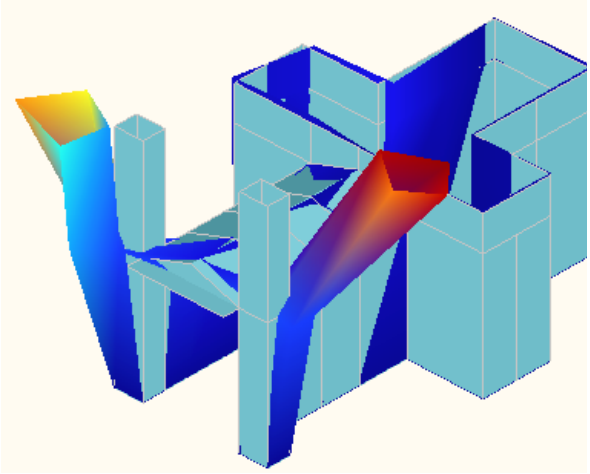

Mode 3 (2,85 Hz)

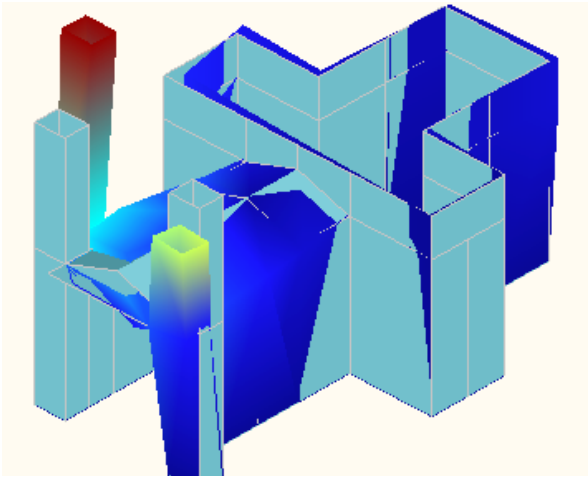

Mode 4 (2,93 Hz)

Figure 3.25: Results of the modal identification, in terms of natural modes and relative frequency (Alaboz, 2009)

3.4 ND testing

Non-destructive tests (NDT) campaigns were performed on São Torcato since 2009. The aim of those inspections is the characterization or the updating of the building's properties without harm the structure it-self. It is possible to carry out a wide range of tests that are able to define mechanical properties, material quality, decay level and construction techniques of the church.

3.4.1 Schmidt hammer (since 2010)

The rebound hammer is able to determine in a quick way the compressive resistance of a material according to its surface hardness. The tool is formed by a cylinder in which a metallic pin that is shot to the surface of the specimen with a given impact energy of 2,2 Nm applied by a spring. An analogical display on the cylindrical cover displays the relative rebound value of the material (Figure 3.26). It is possible to correlate such value with the compressive resistance of the material by means of proper graphs.

Figure 3.26: The Schmidt hammer tool (www.schmidthammerhire.co.uk)

The first tests were carried out in 2010 with the purpose of comparing the granite of one the building towers with the stone taken from the same quarry that supplied the S. Torcato construction. In this way it should be possible to estimate if there is a correspondence between their material strength and compressive strength. Taking into account that it is not possible to carry out destructive test on the granite, this correlation would be a powerful statement that could permit to perform compressive tests on suitable specimens without damage the real structure. Two samples were taken from the quarry (Figure 3.27) and three tests were performed on each face of the specimen; the same tests were performed in the interior walls of one of the towers. The results were robust for specimens as for the real structure, and, more important, they were comparable: the average rebound value of all the tests performed on the quarry stone was 64,3 with a standard deviation of 2,1 and a coefficient of variation of 3,2% while the response of the real structure was around 63,0, with a standard deviation of 2,8 and a coefficient of variation of 4,4%. From those values the compressive strength of building granite was assumed equivalent to the one of granite taken from the quarry.

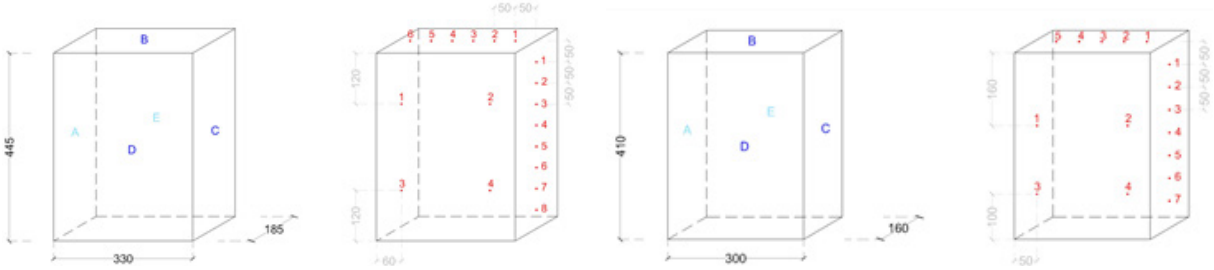

Figure 3.27: Granite block sonic and ultrasonic test locations: Stone 1 (on the left) and Stone 2 (on the right) (Manning et al., 2013)

Several Schmidt Hammer tests were also performed by SAHC students during 2013. Such investigations were focused in the building on façade walls, towers and the vault. The results carried out on the façade (Guimarães et al., 2013) and the towers (Facelli G. et al., 2013) are very close to the previous survey: the average rebound value is respectively 62,4 and 64,8. However, Tests performed on the vault and on the damaged part of the façade (Greco et al., 2013) gave different values: the average value for the vault is lower (but it is normal, because is a concrete structure), around 40, while the façade presented an average value of 54, lower with respect to the tests performed on sound masonry, and a higher coefficient of variance of 11%. An important difference was inferred by the tests performed on the exterior of the church (Guzmán Corredor et al., 2013), the newer part of the building is more resistant than the older one: in the first the average values is in fact 55 while in the second is 68. A comparison of the results on the granite can be seen in the following table.

	Rebound value	St. deviation	COF	f_c[MPa]
Manning et al.	63,0	2,8	4,4%	-
Guimarães et al.	62,4	-	0,8%	78,4
Facelli et al.	64,8	3,47	5,86%	65
Greco et al. (damaged part)	54,0	6	11%	-
Guzmán et al. (old-new part)	55 - 74	7 - 2	13% - 2%	70 - 106

Table 3.2: Comparison of the results of the various rebound hammer campaings performed

3.4.2 Sonic test (since 2010)

A sonic wave is able to propagate elastically through a body depending on its characteristics. From the recorded velocity of the signal it is possible to infer quickly the elastic modulus and the Poisson's ratio of the material, presence of cracks and its depth, detachments, voids, change in density distribution or any generic defect of the material. The investigation was performed using a transmitter (it can be an instrumented hammer, electrodynamics or pneumatic devices) that generate a wave subsequently collected by a receiver trigged by such stress signal, usually an oscilloscope or an accelerometer adhering

(a)

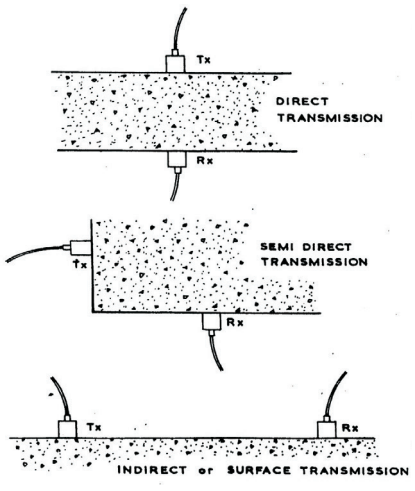

(b)

Figure 3.27: Sonic test: (a) the instrument used during student analysis (b) three different methods of test that can be performed (Facelli G. et al., 2013)

to the surface (Figure 3.27). Depending on the relative position between the transmitter and receiver it is possible to perform three different methods: direct, semi-direct and indirect analysis.

The first campaign of sonic tests was carried out in 2010 with the same aim of Schmidt hammer tests: the comparison between S. Torcato granite and the granite taken from the relative quarry (Manning et al., 2013). Direct test could not be performed in the church, because the presence of stones passing from side to side of the walls was not sure. For this reason, it was possible to compare just semi-direct and indirect test performed on the building and on the quarry specimens. However, the specimens were analyzed with the three transmission methods and compared with sonic and ultrasonic tests performed on the building (see next paragraph). Five signals were generated in the samples for each configuration of transmitter and receiver (Figure 3.7); the subsequent wave velocity was calculated considering their relative distance. Due to the small dimensions of the specimens, the direct test data were not accurate and lots of values were not realistic. Even the indirect test did not succeed: the difficulty of distinguish P-waves from R-waves and the high coefficients of variation determined a low reliability of the data, thus even the comparison of S. Torcato with this test was rejected. The semi-direct tests presented the same values of the direct tests, but with a higher variance; for this reason it was hard to understand the reliability of the data. The results on the two specimens are summarized in the following Table 3.4.

	Direct		**Semi-direct**		**Indirect**	
	velocity [m/s]	COV	velocity [m/s]	COV	velocity [m/s]	COV
Stone 1	4945	15,8%	4716	20,1%	3552	21,7%
Stone 2	4530	17,0%	4845	16,9%	3212	31,1%

Table 3.3: Results of the sonic tests performed on granite specimens

Several stones of S. Torcato were then selected, marked and analyzed with direct tests to discover the constructive method of the tower walls (Figure 3.29). The average results can be seen in Table 3.3.

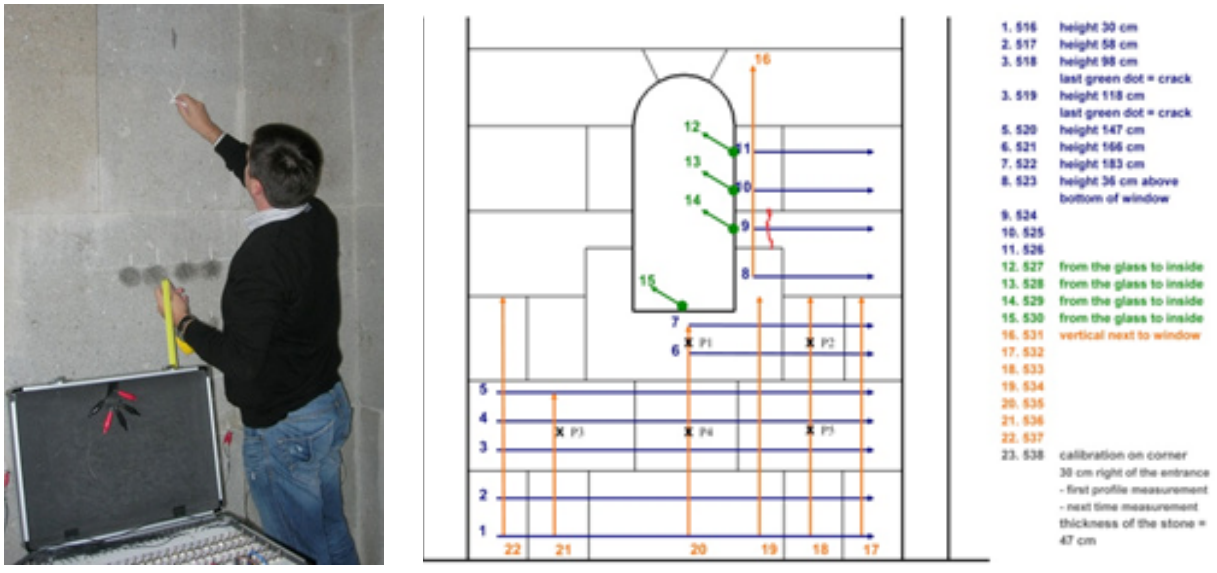

(a) (b)

Figure 3.29: Sonic Test Setup: (a) Marking the locations for the sonic tests on the interior northwest wall of the west tower (b) test locations, P1 through P5 (Manning et al., 2013)

Location	Average velocity [m/s]	COV [%]
P 1	2073	1.84
P 2	4220	4.54
P 3	3244	2.39
P 4	3821	3.38
P 5	3322	2.39
Average	3336	24.26

Table 3.3: Results of the direct sonic tests performed on S. Torcato

Comparing those data (3300 m/s) with the one taken from the sample (4500 m/s) it is possible to see a reduction of average speed in the tower's granite. However, it was inferred the presence of a passing through stone in Point 2 and Point 4, because the value is quite close to the specimen value. In Point 3 and 5 were considered the presence joint between each side of the wall while Point 1 could represent a wall with two joints or made with rubble masonry.

A second campaign was developed by SAHC students during 2013. Probably the most interesting conclusions can be inferred from the direct tests performed on the right tower of the church (Facelli G. et al., 2013). A grid of twelve points separated at least 50 cm was defined in both sides of the structure. The average velocity calculated was 4450 m/s, with a maximum coefficient of variation of 5,2% per measurement. Comparing this velocity with the measurement on the specimens it is possible to notice the strict correlation; a passing through stone with good condition was discovered in the analyzed points. Several indirect tests were also performed in different locations of the church: exterior walls, choir and on the top of the vault. The main results on the granite walls were two: it was possible to establish the difference in velocity in continuous stones (around 4500 m/s) with respect to one of the test performed at the joints level (around 3500 m/s). Even with such difference, the students considered that the joints were in good condition (Guzmán Corredor et al., 2013). The morphology of the choir, defined by a mixture of regular stone bound with filling mortar, was deduced by sonic tests (Guimarães et al., 2013).

3.4.3 Ultrasonic Test (since 2010)

The physical principles that govern those tests are the same as the previous paragraph, but consider ultrasonic waves instead of sonic ones. The instruments are similar as for the sonic tests: an ultrasonic pulser sends a signal at 54 kHz that is catch by a receiver connected to a computer. Transducers are coupled to the masonry surface silicon sheet or gels that maximize the energy transmissions.

The first experiments with ultrasonic instrument was carried out, as previously described, to evaluate the affinity between granite from the S. Torcato quarry and the granite of the building itself (Manning et al., 2013).

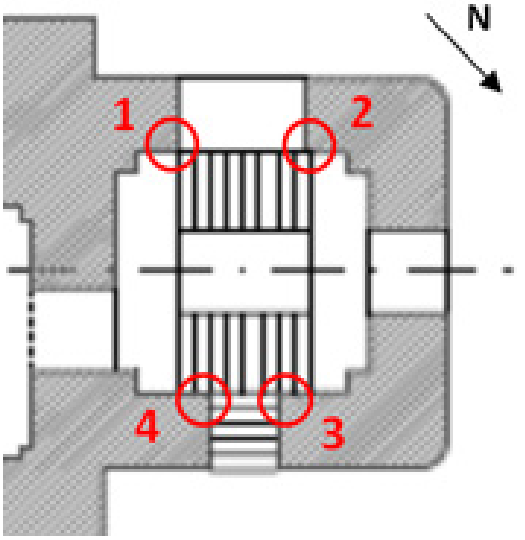

Figure 3.30: In-situ ultrasonic tests locations (Manning et al., 2013)

Direct, semi-direct and indirect ultrasonic tests were performed both in the granite specimens and in one of the towers of the church. The corners of the interior part of the towers were analyzed in several point distant 5 cm one to each other, as shown in Figure 3.30.

The results of direct ultrasonic tests on the samples were much more consistent with respect to the sonic tests (with an average wave velocity of 3800 m/s) while it was not possible to make a comparison between indirect tests due to high variability of sonic. The average value for semi-direct tests was around 3700 m/s, with the velocity of the second specimen slightly higher than the first one. The semi-direct ultrasonic tests performed in-situ showed an average speed around 4500 m/s (as for the specimen's sonic tests). The sets of points and their relative distance were similar in the specimen and in the building, thus it was possible to compare the two granites. The values taken from the building are considerably higher than the specimens, and this could suggest that the material from the quarry was different in mechanical properties or in composition. However, the different environmental conditions (such humidity and temperature) could have affected the results of the tests. A numerical comparison of the measurements can be seen below.

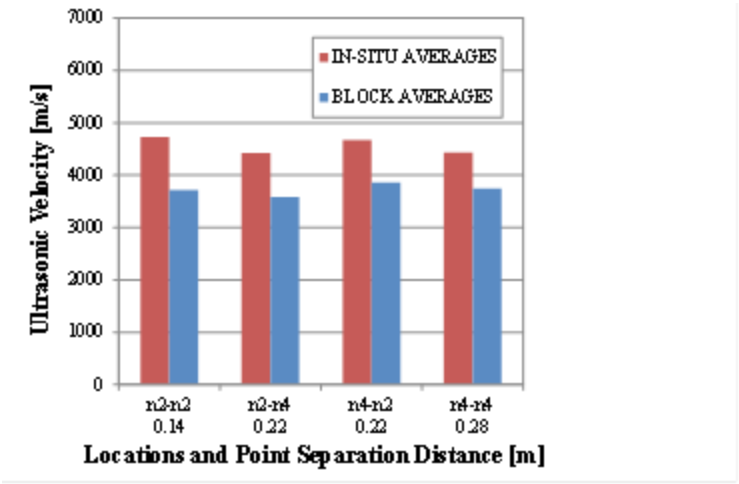

Figure 3.31: Comparison of semi-direct ultrasonic tests in-situ and in separate granite blocks (Manning et al., 2013)

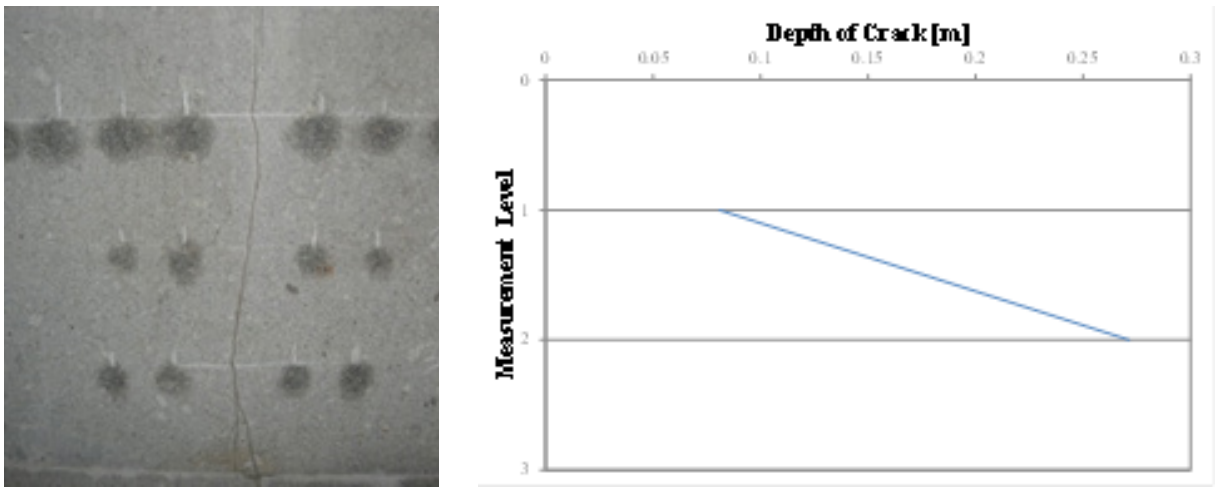

(a) (b)

Figure 3.32: Ultrasonic tests over a crack in the west tower of the S. Torcato church (a) locations and levels of the crack depth readings (b) crack depth results (Manning et al., 2013)

Another set of tests was performed also to define the depth of a crack visible in the exterior wall of the left tower. The fissure was measured at three different heights resulting on a maximal depth of 25 cm (Figure 3.32).

Another thirty centimeter-width crack of the same tower was checked in 2013 (Facelli et al., 2013). This time the crack depth was investigated with a set of six coupled point distant 10 cm from each other, disposed at six different levels spaced 5 cm. A maximal depth around 6 cm was discovered thanks to his analysis (Figure 3.33).

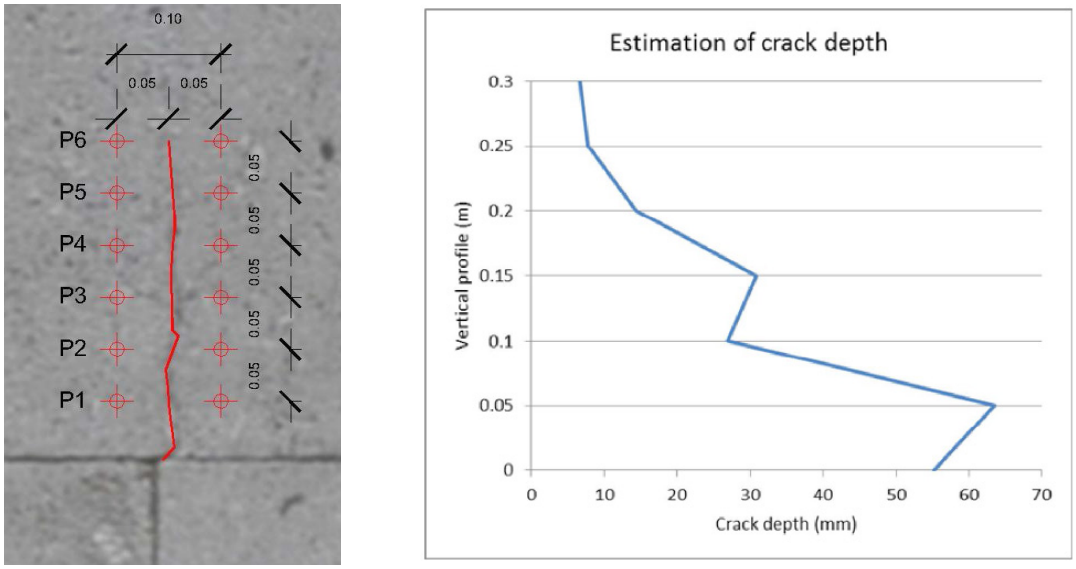

(b)

Figure 3.33: Ultrasonic tests performed by students on a crack (a) locations and levels of the crack depth readings (b) crack depth results (Facelli G. et al., 2013)

3.4.4 Ground Penetrating Radar (2013)

The ground-penetrating radar is a geophysical non-destructive method able to reproduce a continuous cross-sectional analysis that can identify internal anomalies. During the process a microwave band signal is sent inside a body and is reflected depending on the structure. It is possible, in this way, to evaluate the thickness of internal layers, the presence of cracks, inhomogeneity of materials or reinforcing bars. The microwaves are generated by a transmitter, recorded by an internal antenna and then sent to a processor. The antenna have band range that varies between 200 MHz and 1,5 GHz depending on the depth of the body that has to be analyzed: higher frequency give more resolution of the results but are easily dissipated inside the body while lower frequency can reach deeper levels with less accuracy.

Among the studies that were done by SAHC students during 2013, probably the most interesting is the analysis performed on the exterior walls of the transept (Guzmán Corredor et al., 2013). Four horizontal sections and two vertical sections were traced in the southeastern wall in order to determine its thickness, the constructive techniques and the presence of any defect on it. An 800 MHz antenna was chosen because it was able to reach two meters of depth, a dimension close to the thickness of the structure. In the output the joints can be easily detected as well as the presence of three different areas

distributed through the thickness of the wall: the surface, an irregular layer and the last area defined by the interior leaf of the wall (Figure 3.34). Due to the high level of noise in the internal layer, the student inferred that the wall could not be massive and instead a multi-leaf constructive method was used for the transept. The thickness of those layers is: 65 cm for the exterior side, 35 cm for the interior and 40 cm for the infill, with a total of 140 cm. Because of the interference of the signal, they also considered the possibility that the stone was well worked just in the surface while the other sides were worked in a coarse way. Passing-through stones were also discovered by means of this analysis. The interesting conclusion proposed by the student was the drawing of the most likely section of the transept wall, shown in Figure 3.35.

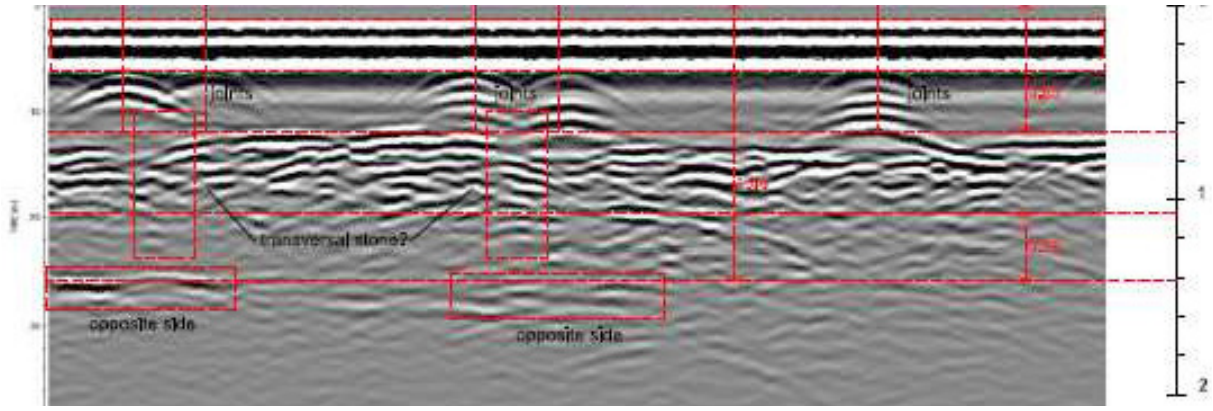

Figure 3.34: The output of one of the GPR horizontal tests (Guzmán Corredor et al., 2013)

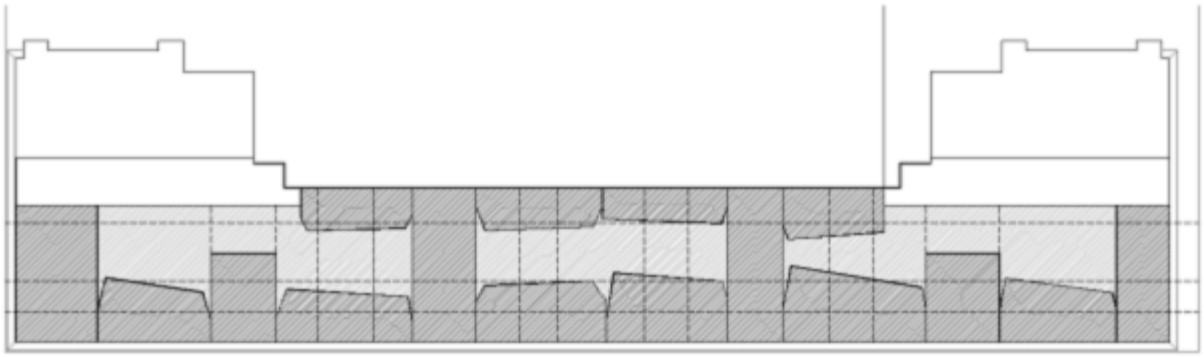

Figure 3.35: The horizontal section based on the analysis of GPR output (Guzmán Corredor et al., 2013)

3.4.5 Impact echo (2013)

The data regarding the acceleration response of the structure, collected with sonic test tools set, can be processed and transformed in a Fourier spectrum. Impact echo tests permit to estimate the thickness of an analyzed body. In fact a wave sent through a structure is reflected and rebounded several times until the signal fades out. The echo on the wave will generate a peak on Fourier function, and it is possible to correlate its frequency with the depth of the surface.

The values found on the transept were not reliable, because the thickness was about the double or the real one (Guzmán Corredor et al., 2013). Instead, the test performed on the vault was completely successful (Greco et al., 2013). The peak value recorded from of the receiver (Figure 36) corresponded to

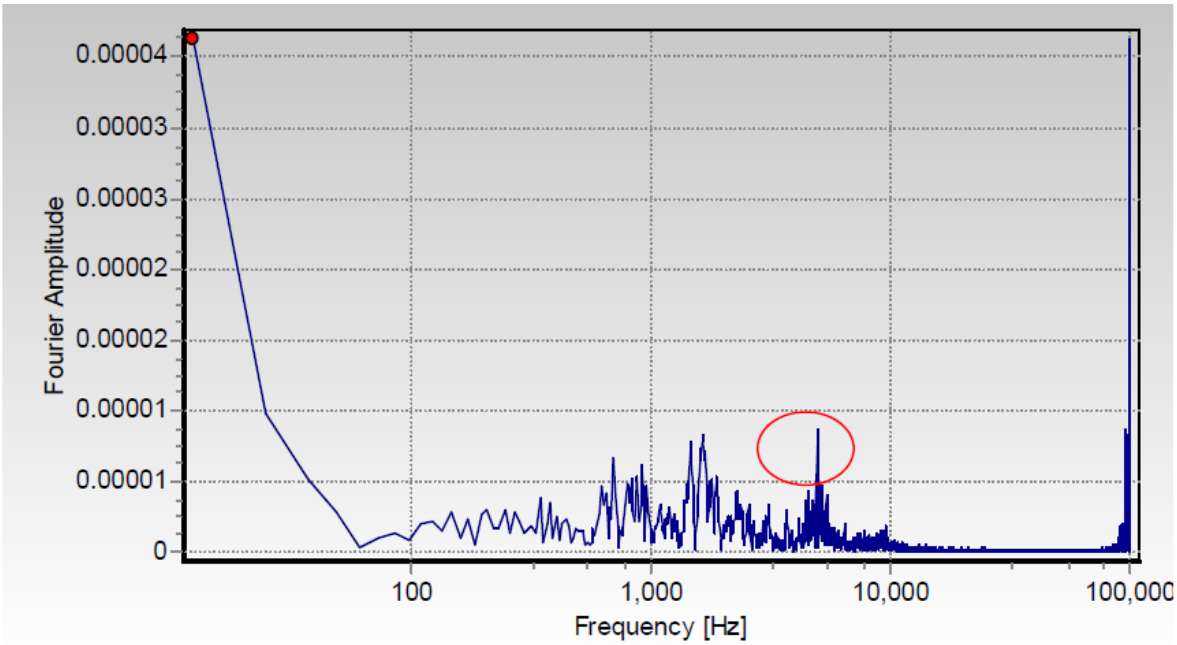

Figure 3.36: The Fourier spectrum from the test on the vault (Greco et al., 2013)

a thickness of the vault of 28 cm; this measurement was then checked and confirmed lately by means of a Boroscopic camera, with the relative error of 10 %.

3.4.6 Boroscopic camera (2013)

This minor destructive test permits to check in a direct way both the thickness that the composition of a structure. The camera, which can be rigid of flexible, permits to the operator to check the interior of a borehole drilled in the structure directly or by means of a digital display.

Figure 3.37: Rigid boroscopic test device (www.directindustry.com)

Several tests were performed on the vault (Greco et al., 2013), on the choir and on the façade of the building (Guimarães et al., 2013). It was possible to estimate that the thickness of the vault

Figure 3.35: Borehole, from left to right, the regular section of the whole changes to irregular and then a big void appears at the depth of 60 cm (Guimarães et al., 2013)

Figure 3.39: Boroscopic test image from the façade (Guimarães et al., 2013)

was around 25 cm and was probably made by hollow-brick quarterdecks. For the test performed on the choir, a crack was chosen as place to analyze so that the drilling was minimized. It was possible to check until 60 cm, and during the survey was discovered the presence of non-adherent layers of concrete (Figure 3.38). Another crack was used as base for the analysis of the façade. In this case, the light at the end of the hole demonstrated that the fracture passes through the entire wall (Figure 3.39).

3.4.7 Rebar detector (2013)

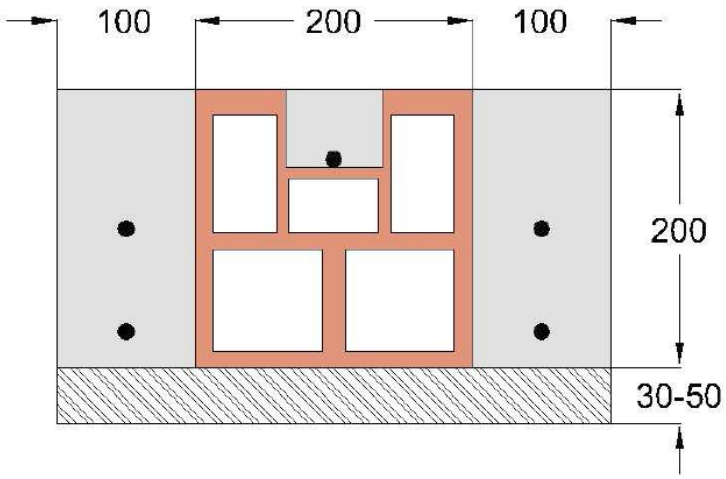

Figure 3.40: Barrel vault sections approximated geometry (Greco et al., 2013)

Specific devices can quickly and accurately determine the location of the reinforcing bars in the concrete. In this way it is possible to avoid unwanted drilling on the metallic mesh (it should be more difficult to perform with respect to pure concrete drill) or just know the exact position of each rebar.

The vault was analyzed with a rebar detector to evaluate the position of the bars and their diameter (Greco et al., 2013). The Figure 3.40 was drawn according to the results.

3.4.8 Photogrammetry (2014)

Photogrammetry is an estimative method that can be used to recover exact positions and motion pathways of designed reference point located on any moving object. The data collected during the analysis is subsequently elaborated with computational models that are able to transform the 2D images in a 3D model.

Several pictures of the façade and the interior were taken by means of a Canon EOS 450D camera mounted on a UAV moved by remote control. Several tie points were automatically defined by an A-SIFT algorithm; such references are used to set the camera in the space. Once oriented, a Mic-Mac algorithm is used for the 3D reconstruction of the dense point clouds.

Figure 3.41: The UAV system used for the survey of S. Torcato (Sánchez Aparicio et al., 2014)

This method is suitable for the analysis of parts that are difficult or impossible to reach by the operator of the laser scanner, like the backside of the spires or the roof. The main improvement with respect to a laser scanning is the possibility of apply photo-realistic textures on the model. In this way it is easy to establish the crack pattern and have a global idea of the damage. The crack pattern revealed on the building can be added on the final FE model so that is possible to check the real behavior of the structure. If the method is repeated during a long range of time, it should be possible to check the crack development too.

(a) (c)

(b) (d)

Figure 3.42: Resluts of the photogrammetry: (a) the image obtained from the laser is too precise and the flat to notice the crack (b) with photogrammetric textured model the crack is more visible (c) a detail (d) exterior balcony (Sánchez Aparicio et al., 2014)

3.5 Diagnosis

The previous test and monitoring were able to recreate the “medical history” of the building. Several numerical models were run in order to check the reliability of the hypothetical cause of the damage phenomena. The use of finite element analysis was a forced choice induced by the complexity of the problem, given by the geometry of the building and the soil interaction with it, which could not be analyzed in an analytical way.

3.5.1 2D Finite element analysis (1999)

With the data collected in the previous analysis, two plane stress Finite Element Models (FEM) of the façade were run in 1999: (a) one linear model; and (b) a non-linear model were analyzed considering the interaction with the soil. The inputs of the program were the following:

	Symbol	Value
Young’s modulus	E	15 GPa
Poisson coefficient	ν	0,2
Specific weight	γ	25 kN/m^3
Fracture energy	G_f	0,05 Pa
Tensile strength	f_t	0,2 MPa

Table 3.4: Imput data of the first FEM in 1999

The construction sequences were considered in a second stage of the analysis. Taking into account the long period of construction, it was considered just the self-weight, the load of the roof and the weight of the atmospherics condition and accidental actions were neglected. The foundations were considered and five different type of soil with their relative Winkler coefficients were added, in order to simulate the real soil composition (Figure 3.43).

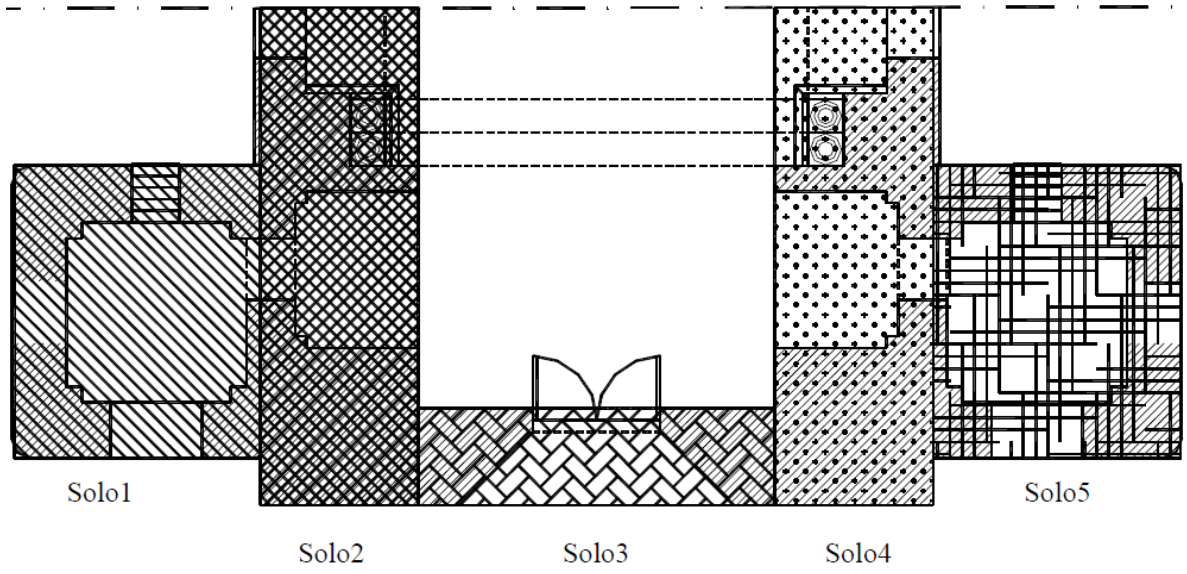

Figure 3.43: The different soil characteristics modeled in the FEM (Lourenço and Ramos, 1999)

The linear analysis of the model showed a range of stresses varying from -2,5 MPa to 2,5 MPa and a rotation of the building that follows the distribution of soil properties, as expected (Figure 3.44). From this value of tension it can be inferred that the material will crack. The position of the potential crack fits the damage pattern of the structure: a tensile stress concentration is present on top of the rosette and follows a triangular pattern until the top of the tympanum. It was also discovered that applying the construction phases the results were not affected.

The results of the non-linear model were slightly different. The range of the stress is going from -4,5 MPa to 0,2 MPa. The distribution of stresses is not symmetrical due to the settlement of the structure. The crack pattern in the FE model is in agreement with the real damage distribution of the real building. It can be inferred that the structural defects on the structured can be attributed to differential settlement on the foundations. The tilting measured with the optical theodolite was compared with the displacements found in the FE model. Even is the distribution of the displacements along the FE tower were difficult to understand, it was found a rotation of 0,0016 mm/m, value that approximate the rotation detected on the real structure (around 15 - 25 x 10^{-3} mm/m).

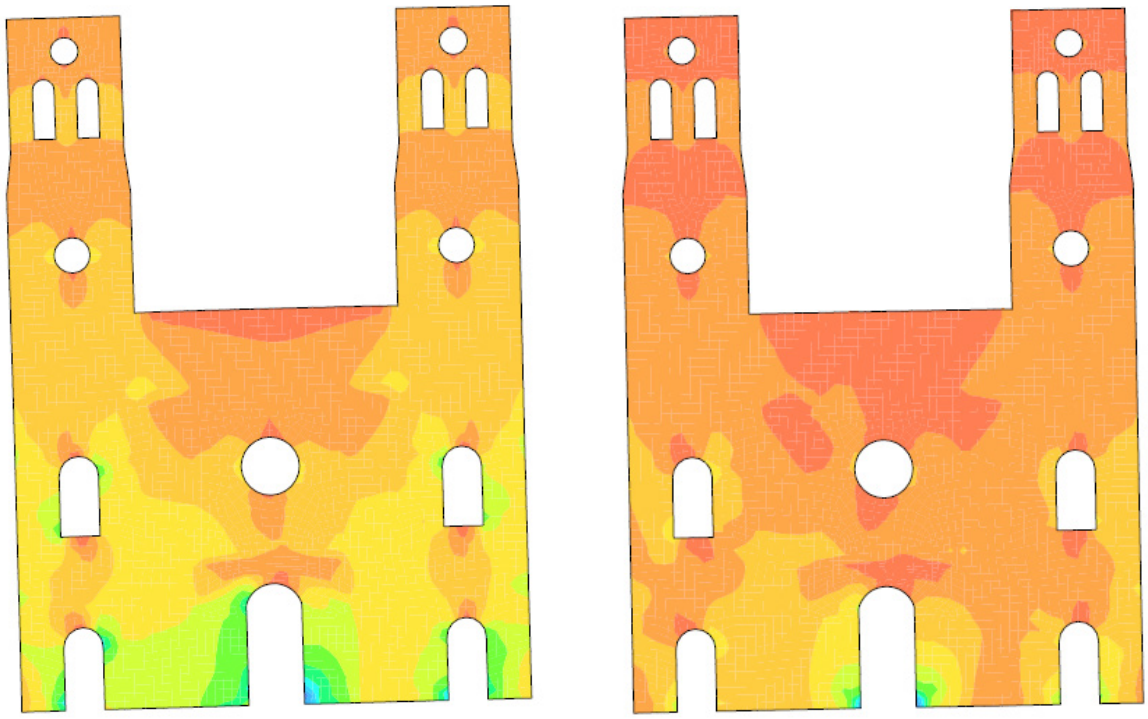

(a) (b)

Table 3.44The result of the linear 2D analysis, the gradient shows the minimal principal stresses distribution (a) linear model with range from -2,5 MPa, in blue, to 2,5 MPa, in red (b) non-linear model with range from -4,3 MPa, in blue, to 0,2 MPa, in red (Lourenço and Ramos, 1999)

3.5.2 3D Linear FEM (1999)

A plane model was not sufficient to understand the global behavior of the structure. For this reason a simplified 3D model was designed in AutoCAD and two linear analyses were carried out in Diana: one considered the interaction between the soil and the structure while the other did not. The apse was

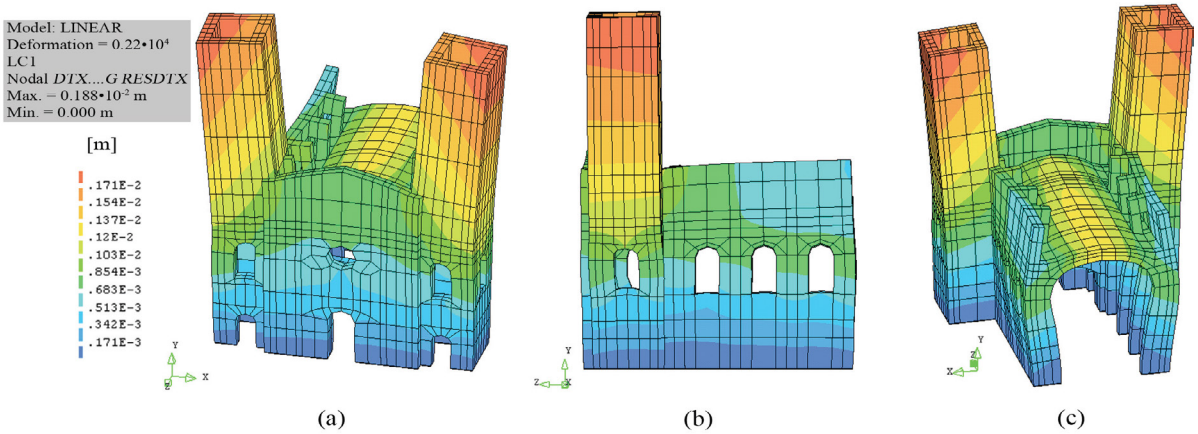

Figure 3.45: Displacements [m] and deformations of the linear model without soil interaction (Lourenço and Ramos, 1999)

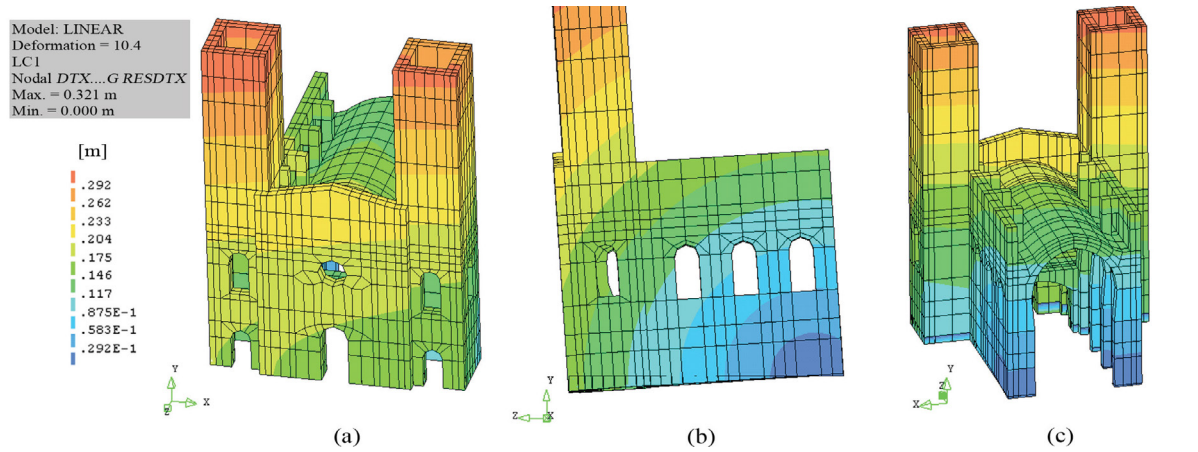

Figure 3.46: Displacements [m] and deformations of the linear model with soil interaction (Lourenço and Ramos, 1999)

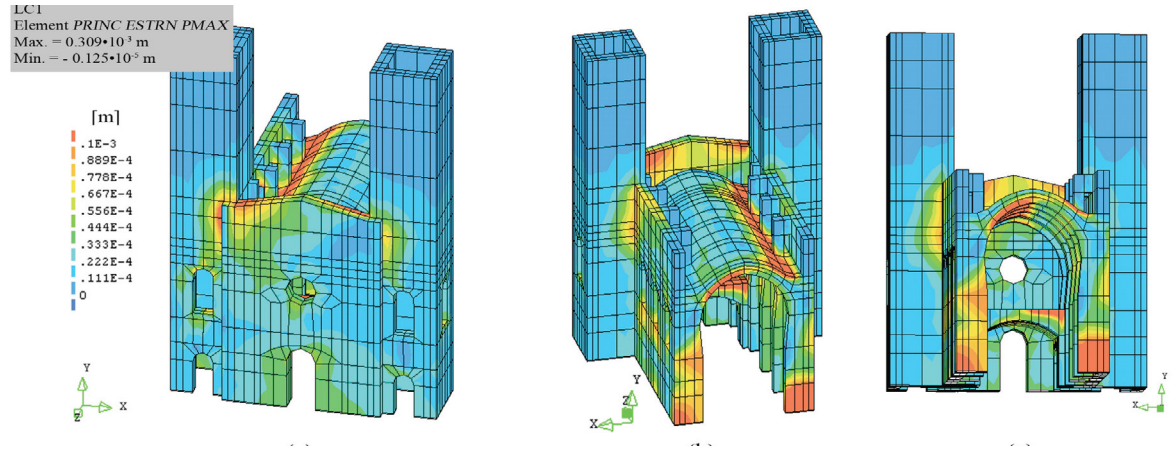

Figure 3.47: Strains of the linear model with soil interaction (Lourenço and Ramos, 1999)

not modeled and the main nave was considered fixed in the backside because in this part, made of reinforced concrete, because the presence of any damage or settlement was not revealed during the previous monitoring. The same inputs of the previous model were used to define the 3D FEM.

The linear analysis without the soil interaction was carried out to evaluate the behavior of the structure itself and check for the presence of anomalous stress concentrations. The main results of this analysis are visible in the Figure 3.45, 3.46 and 3.47. The main nave works as a rigid frame: the arches transmit the deformation to the bearing walls that are bended because are perfectly fixed to the soil. For this reason the towers and the façade, that prevent the movement of the walls, are stretched and twisted. The separation induced on the towers develops in this way tensile stresses on the façade. This, with the concurrence of load in the entrance, could explain the up-lifting arouse of the back side.

With the introduction of the soil properties the analysis changes completely. The displacement patterns marked on the previous analysis are changed, because the thrust line generated by the arches is transferred to the ground. The settlement of the left tower is slightly higher than the other one and for this reason the stress distribution is not symmetric. The compressive stresses reach peak values of 3 MPa, which is quite reduced. The maximal tensions reach values of 2,5 MPa in the arches, and 2,0 MPa in the choir: they will lead surely to the development of a crack. The order of magnitude of tensions and compression stresses determined a non-reliability of a linear model for the actual problem. It is necessary to verify the non-linear behavior of the structure to enhance the approximation (Figure 3.47).

3.5.3 3D Non-Linear FEM (1999)

The previous 3D model was analyzed with a non-linear analysis. The building was studied once again without and with the soil-structure interaction. The results of the FEM without the soil model are similar to the one discovered for the linear model (Figure 3.48, 3.49 and 3.49).

More interesting are the results of the analysis that takes into account the interaction with the soil. The displacements found in this analysis are similar to the previous 2D case, but the strain pattern is has a really good approximation of the real damage of the building. The strain distribution range is much more realistic, reaching maximal tension stresses of 0,9 MPa (compatible with the material) and maximal compression values of 7,0 MPa, that could represent the risk of incipient collapse of some part of the building (namely the arches). The left tower settlement reaches 0,19 m and the differential settlement of the tower with respect to the first arch is 8,1 cm, a value that represent closely the situation detected during the theodolite scanning. However, The difference between the first and the fourth arch is too elevated with the differential settlement identified during the pavement survey.

This FEM analysis definitely confirmed that the damage of the building is due to soil settlement. However, some cracks that are not present in the real structure were found (see Figure 3.49, number 6). The cracks on the main vault are more central than the one resulting from the FEM (see Figure 3.49, number 6). Furthermore, in the interior of the façade just one crack is developing while in the reality there are two slits (see Figure 3.49, number 8). For all this reason, even if the results are really good and give a significant explanation on the damage causes, it was considered necessary to update the model by means of dynamic system data.

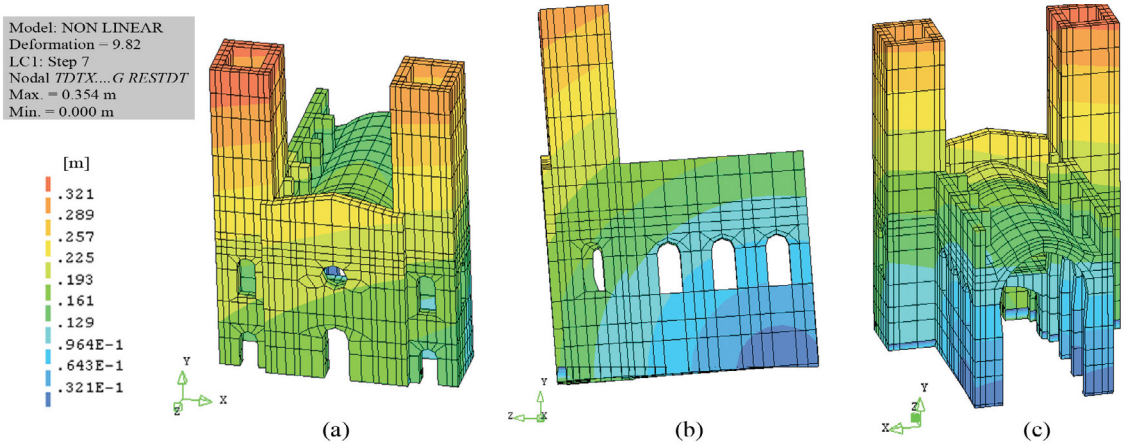

Figure 3.48: Displacements [m] and deformations of the non-linear model with soil interaction (Lourenço and Ramos, 1999)

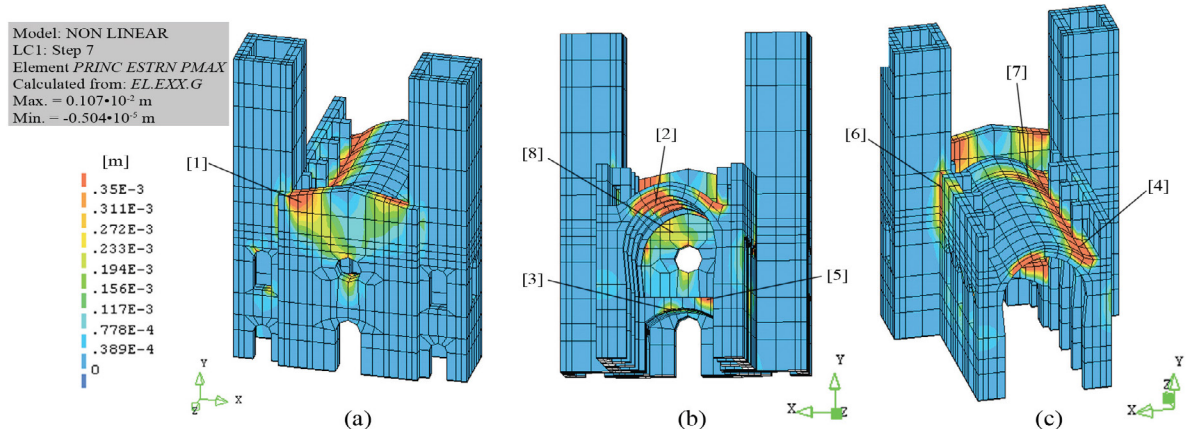

Figure 3.49: Strains [m] of the non-linear model with soil interaction (Lourenço and Ramos, 1999)

3.5.4 Finite element updating (2010)

The dynamic analysis data collected until 2010 were used to tune the FE model that was considered not enough reliable for the motivation previously described. Considering correct the geometry of the model (this is not true because based on wrong plans) it was chosen to change the model parameters.

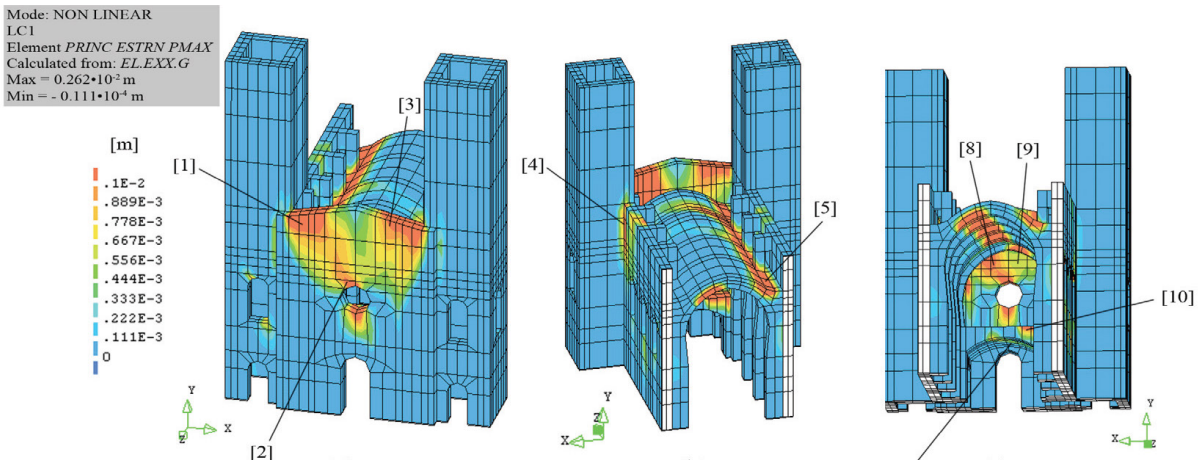

Figure 3.50: Strains of the optimized model with soil interaction (Ramos et al., 2012)

Some properties of the model were calibrated by means of the Douglas-Reid method, implemented considering lower and upper bounds for the updating variables (Table 3.5). A difference in value of 80% was found in the first model with respect to the updated. The Model Assurance Criterion (MAC) was used to compare the numerical model with the experimental results. The reliability of the updated model with respect to the experimental data can be seen in the Figure 3.51. The analysis carried out on the updated model was able to recreate the real crack pattern in a better way (Figure 3.50). All the mistakes described in the previous paragraph concerning the non-linear 3D FEM are now reduced. The adjustment induced to the Young's modulus has led to an increase of tensile stresses in the façade, which now presents a crack more similar to the real one.

	Initial value	Optimizing interval of values		Updated value
		Lower bound	Upper bound	
E_m (GPa)	10	4,0	15,0	5,64
E_s (GPa)	3,9	0,039	3,9	0,63
Et_n (GPa)	0,1	0,001	0,1	0,05
Et_s (GPa)	100	1	100	21,59

Table 3.5: Update of the imput data of the first FEM in 1999 (Ramos et al., 2012)

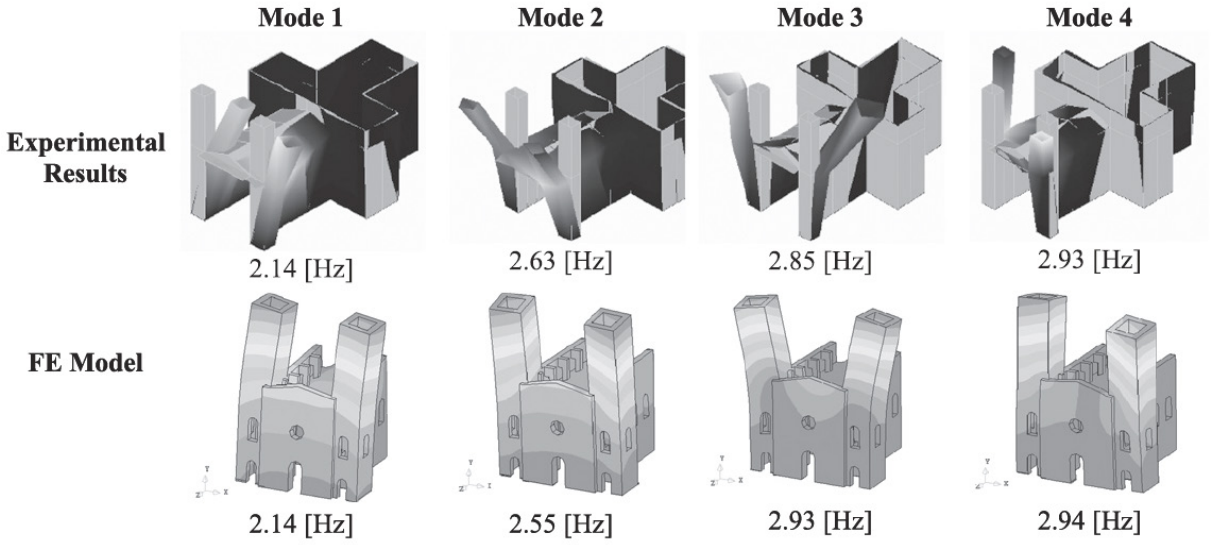

Figure 3.51: Comparing the real frequencies with the ones of the updated model it is possible to infer that the new FEM presents a good accuracy (Ramos et al., 2012)

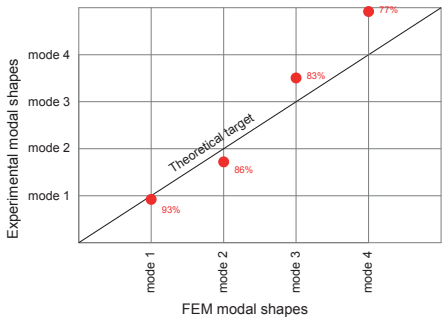

Figure 3.52: Result of the FE model updating progress, the circles reppresent the MAC values

3.5.5 NDT Data Fusion with a Bayesian approach (2013)

The main aim of this analysis was to combine information gathered NDTs and fuse it by using Bayesian approach, as a single technique might be not sufficient to gain enough information of a structure. NDTs data were transformed in a single and uniform format in order to define the probability distribution function for Elastic modulus (E) and compressive strength (*fc*) of granite blocks (Figure 3.53). The updated value for the Young's modulus was 32,3 GPa while the *fc* was 89,2 MPa.

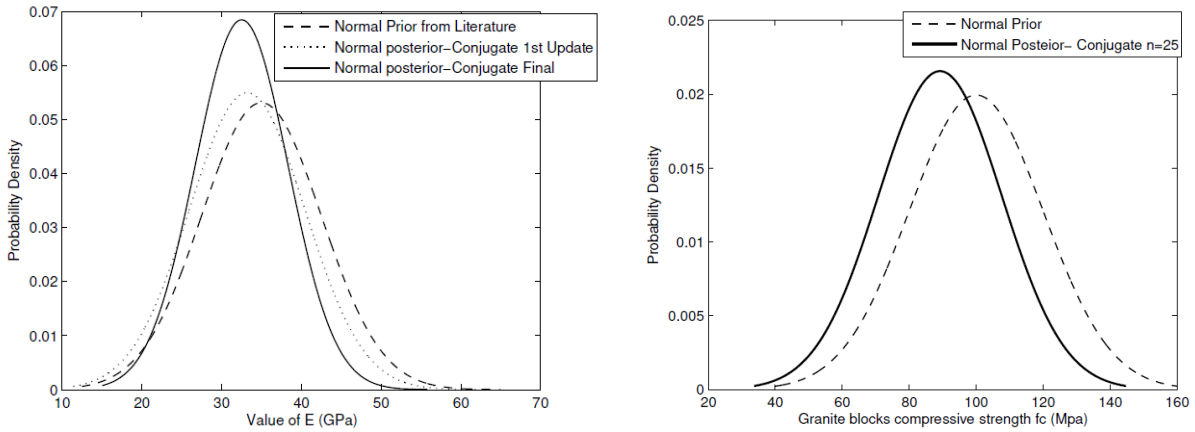

Figure 3.53: Results of the NDT Data Fusion: (a) stochastic distibution of the Young's moduls values (b) stochastic distibution of the compressive strenght of the material (Mayank., 2013)

3.5.6 Temperature analysis (2014)

Once discovered the correlation with crack openings and temperature, it was considered to perform a linear analysis of the temperature effect on the structure. Three point of the same updated model previously described were used to analyze the displacement of the structure (Figure 3.54). A coefficient of thermal expansion of 8 x 10^{-6} °C^{-1} was defined for this purpose. Two different analyses were carried out:

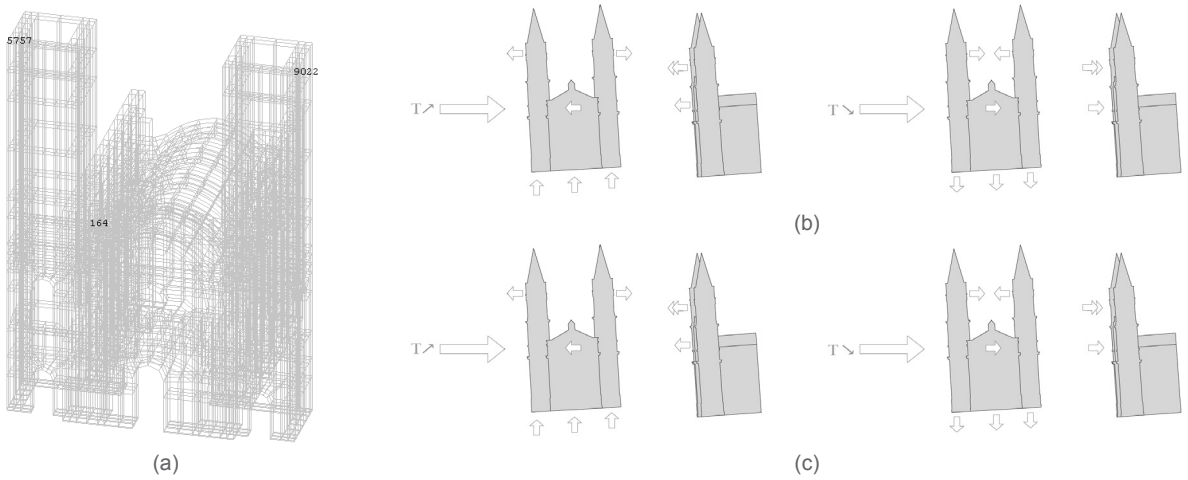

Figure 3.54: Temperature FEM analysis: (a) the reference points used for the evaluation of the responce (b) conclusion of the linear analysis under global thermal loads (c) Conclusion of the linear analysis when a thermal load is applied on the front and the east face of the eastern tower (Gutscoven, 2014)

the first considered a global variation of the temperature while the other considered a local variation that would represent the solar radiation on the façade. The first case represented a symmetrical distribution of the displacement while the second an anti-symmetrical one. However, it was observed that the influence of the thermal variation on the structure displacement is less important compared to the effect of soil settlements.

3.5.7 FEM updating with cracked model (2014)

The 3D geometry resulted from the last laser scanning (Figure 3.55) will be used to develop a detailed non-linear FE analysis that takes into account the interaction between soil and structure (Sánchez Aparicio et al., 2014). Until today, the model have been tuned and updated by means of comparison with dynamic data. Initially, it was chosen to input the same material and soil properties used during the 1999 analysis. The analysis was restricted on the main nave and the towers-façade system. The interaction of the transept with the rest of the structure was introduced by means of “contact and target” methods that considered the relative displacement of the system depending on the rigidity of the transept. The real crack pattern was introduced directly on the model (Figure 3.56). The model was run a first time and then updated by means of FEM-Tools program using again the Model Assurance Criterion (MAC) and the natural frequency, that are slightly different because were introduced in the model with a different algorithm. The results of the dynamic update can be seen in Table.

This analysis represents a better approximation of the real structure with respect to the previous investigations. It was discovered that the dynamic answer of the building is in fact highly influenced by the

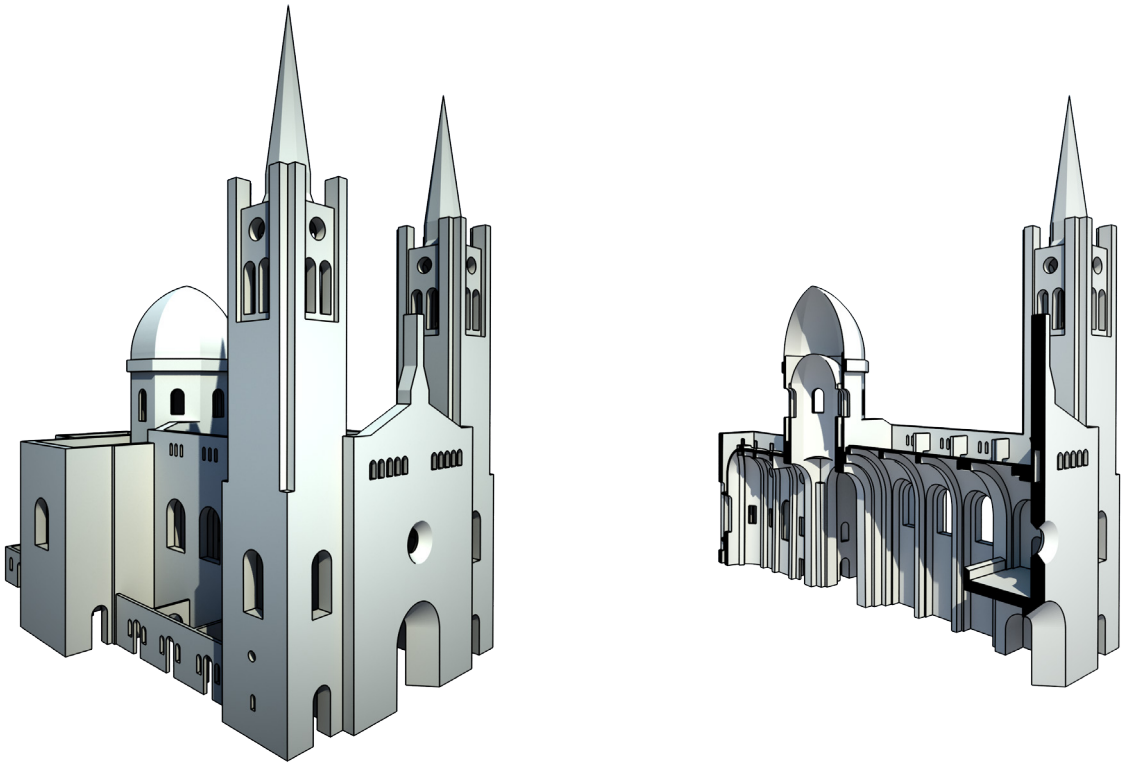

(a) (b)

Figure 3.55: The model developed by Sánchez for the FEM updating in 2014: (a) view of the whole building (b) longitudinal section in the middle of the main nave

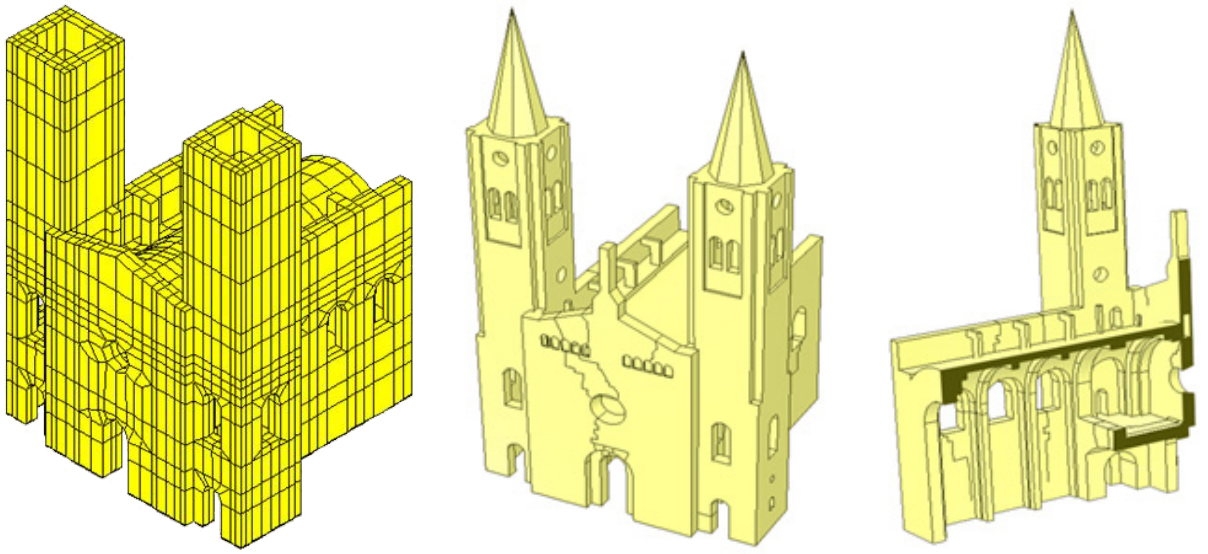

(a) (b) (c)

Figure 3.56: The model used by for the FEM updating: (a) view of the whole meshed model (b) cracks added on the façade (c) crack pattern considered in the interior of the church (Sánchez Aparicio, 2014)

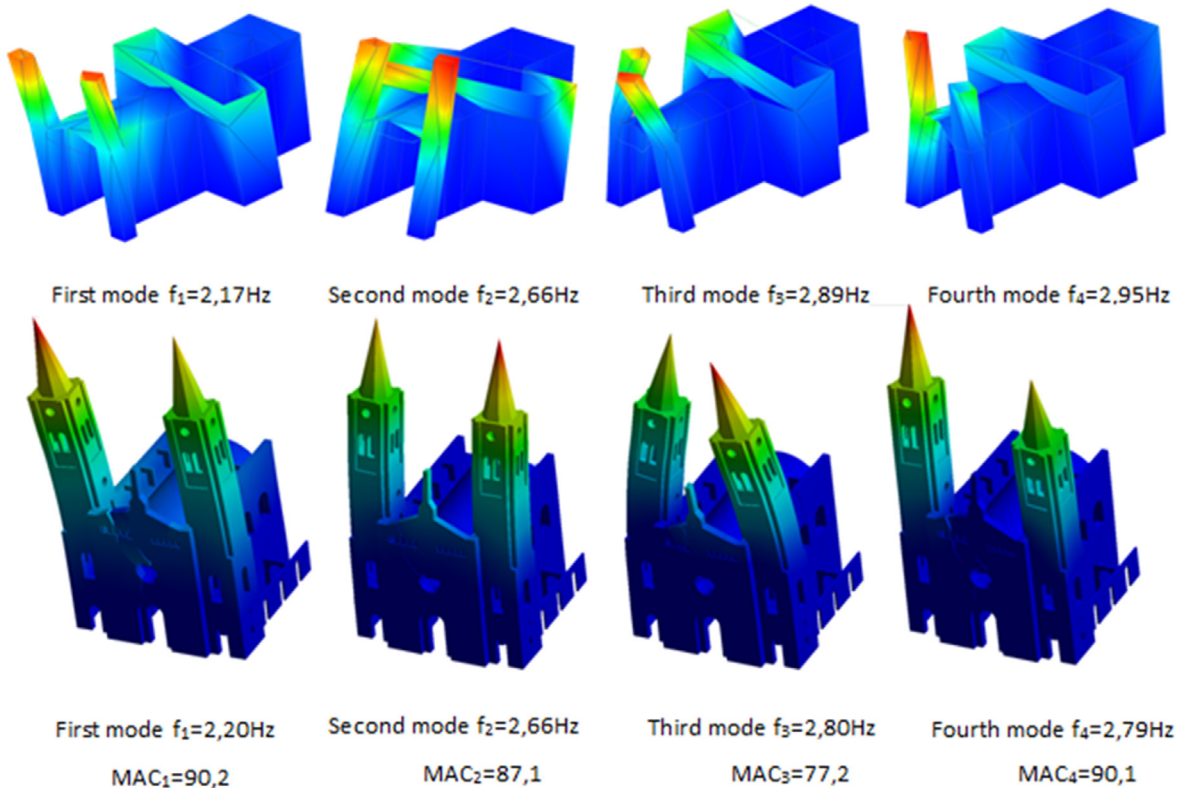

Figure 3.57: Corrispondence of the FEM modes and the results of the experimental campaign (Sánchez Aparicio, 2014)

presence of the crack on the façade. Consider the crack pattern on the model changes substantially the global properties that define the building behavior: the elastic modulus is higher than the previous update and the specific weight is more precise (Table 3.6). A complete FEM analysis with the last updated properties will be carried out soon, and surely it will define the building behavior in a more precise way.

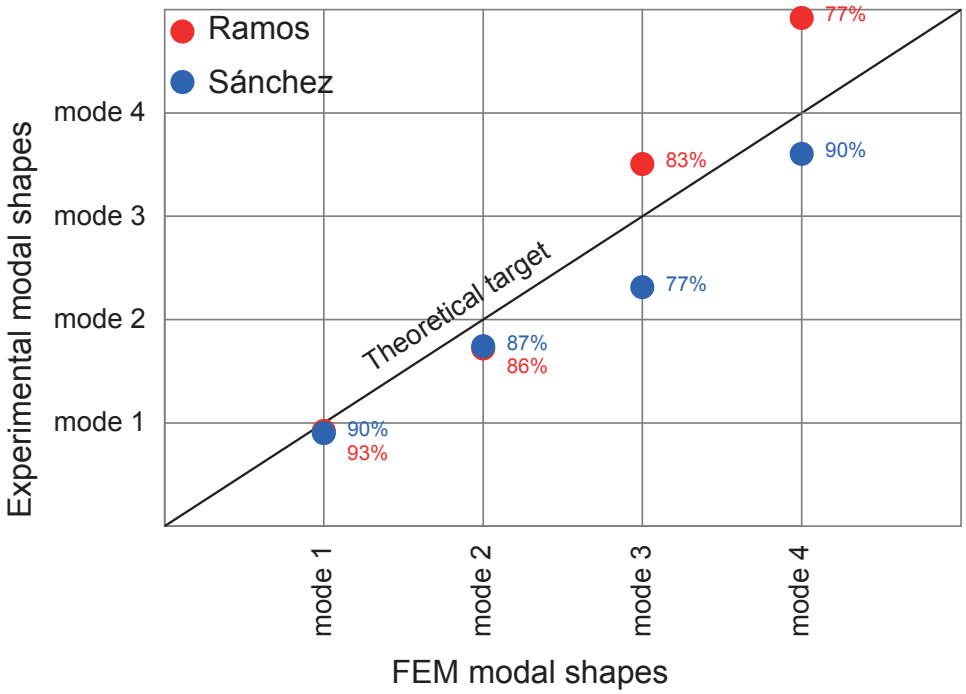

Figure 3.58: Comparison of the FE model updating progress, the circles reppresent the MAC values

	Initial value	Optimizing interval of values		Updated value
		Lower bound	Upper bound	
$E_{masonry}$ (GPa)	10	5	15	9,19
$\gamma_{masonry}$ (kg/m^3)	2500	2400	2700	2600
$K_{N\text{-}façade}$ (GPa/m)	0.0001	0.00005	0.01	0.0004
$K_{T\text{-}façade}$ (GPa/m)	0.1	0.05	1	0.53
$K_{N\text{-}firstcap}$ (GPa/m)	1	0.05	5	0.40
$K_{N\text{-}soil}$ (GPa/m)	0.585	0.0585	5.85	0.627
$K_{N\text{-}transept}$ (GPa/m)	0.1	0.005	1	0.29
$K_{T\text{-}transept}$ (GPa/m)	0.0001	0.00001	0.01	0.00002

Table 3.5: Update of the imput data of the first FEM in 1999 (Sánchez Aparicio, 2014)

3.6 Conclusions

The tests conducted on São Torcato church were able to explain the damage phenomena with a precise approximation. It was discovered that the crack pattern, developed since forty years at least, is mainly caused by a differential soil settlement. The apse part can be considered practically fixed. On the contrary, the entrance part and the towers, heavier and directly supported by a weak soil, are basically sinking according to the mechanical resistance of the different layers. Besides defining the causes of the damages, it was possible to investigate and precisely determine the mechanical properties of the structure, as well as its dynamical characteristic. Thanks to these valuable results it was possible to set the intervention project that will be discussed in the next chapter.

4. THE STRENGTHENING DESIGN

4.1 Introduction

In the previous chapters, a general view of the building problems and the crack patterns were discussed. From the former information it was possible to identify the causes of the damage phenomena. It could be established that the problem of the building was trigged by the soil underneath the façade, that is affected a differential settlement due to its poor mechanical characteristics.

The aim of this chapter is the discussion of the retrofitting and strengthening works that were planned to face and solve the problems on the church. After that, the intervention will be personally checked. Such control will be initially developed without knowing the in-deep assumptions and hypothesis were taken during the conception of the project. Once the personal design is carried out, hypothesis and results of both projects will be confronted and discussed.

4.2 General overview of the intervention

The damage is concentrated in the façade and in the entrance side of São Torcato, thus the design will be focused on that area (Figure 4.1). The main idea of the project can be split in three parts. Firstly, it is necessary to solve or at least reduce the effect of the soil settlement. In order to reach this goal, it was thought to transfer directly part of the towers weight to a better soil, by means of micro-piles. Secondly, it is important to consider the differential leaning of the towers and the subsequent splitting of the façade in different macro-blocks. The solution of this problem will be given by a systems of steel ties anchored to the towers, that will be able to reunify and ensure the monolithic behavior of the façade. Finally, the cracks on the façade wall will be filled by a suitable grouting system.

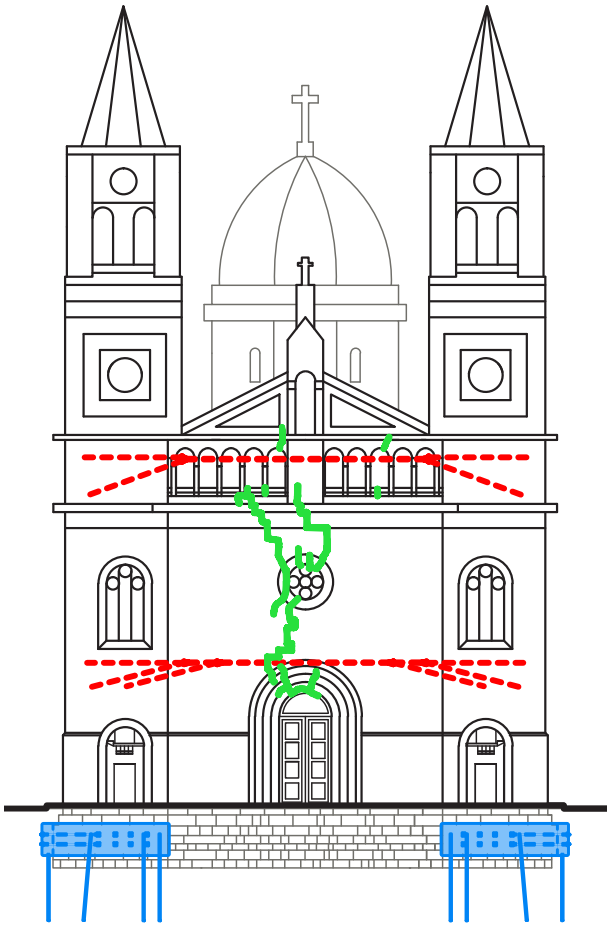

Figure 4.1: The scheme of the intervention designed by professor Ramos: the foundation strengthening, in blue, the anchoring of the towers by means of tie rods, in red, and the filling of the cracks, in green

It is important to remark that this intervention was design considering a step-by-step solution of the building problems. This means that the main assumption of the strengthening is that the soil settlement is practically stabilized. In this case, the design could prevent further damage of the building with a low economic impact. If the church, however, were still affected by damage

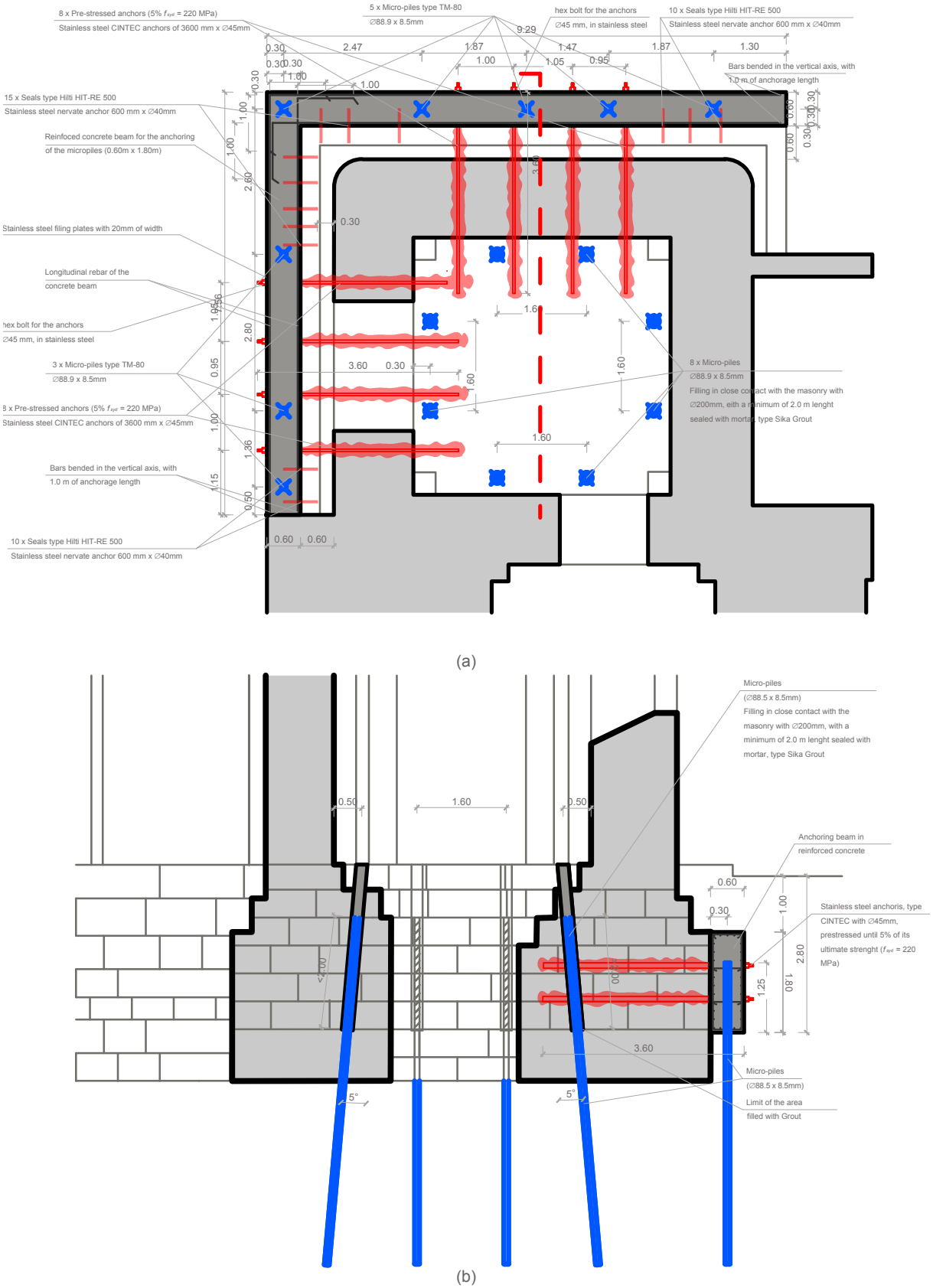

Figure 4.2: The system of foundation strengthening designed: (a) plant (b) section

developments, a new more invasive and expensive intervention would be necessary.

4.2.1 Micro-piles design

A system of micro-piles, type M-80, will be used to transfer part of the towers weight directly to the resistant bedrock. A set of eight vertical piles will be placed in the lateral and in the façade sides of both towers. In addition, other six piles will be positioned along the perimeter of the interior area of each tower to collaborate with the external ones (Figure 4.2).

The length of the micro-piles will be as sufficient as to reach the bedrock layer, sited around eight meters below the street level. The weight transferred by such ancillary structures will be around 20% of the towers dead load, estimated considering a simplified geometry of the towers and a mean specific weight of the granite. Each pile is a hollow structure of steel of 8,5 cm of diameter and 8,5 mm of thickness, with a bear capacity of 590 kN in compression. The piles will be filled with high resistance concrete CEM I 45,2 R after their positioning. On the exterior side, a concrete beam with L shape will be added and anchored to the foundations in order to create a bridge through which the loads would be transferred from the towers to the micro-piles. The insertion of micro-piles into a concrete beam is known as “underpinning” method. The attaching of the concrete beam will be provided by eight pairs of active stainless-steel bars (four on the façade and four on the tower side) of 3,6 m length and 45 mm of diameter, placed in proper holes previously drilled and fixed by grouting. Several steel reinforcing bars of 40 mm diameter will be sealed to the structure to improve the anchoring level of the beam (figure 4.2).

It was not possible to develop the same system in the interior of the towers because of the shape of its foundations. For this reasons, the micro-piles sited in the interior will be installed directly on the masonry basement and will work for friction with it. This ancillary structure will be drilled pointing to the exterior of the building, so that different stone elements will be crossed; a minimum of four bond layers will be involved in the anchoring system. It is important to remark that, to avoid rotational instability of the forces, the starting of the micro-piles adherence with the masonry structure will begin in the same level both for internal that for external sides (figure 4.2).

The constructive phase will be the following:

- The exterior and interior pavement along the tower perimeter will be removed so as to expose the foundations
- The micro-piles will be drilled and inserted in sequence by means of low pressure technology
- The holes that will host the anchoring bars will be drilled from the exterior of the towers
- The rods will be inserted in the holes and fixed to the towers with a grout
- The micro-piles will be filled with high resistance concrete
- The concrete beam will be casted into formworks, sinking both anchorages and micro-piles in

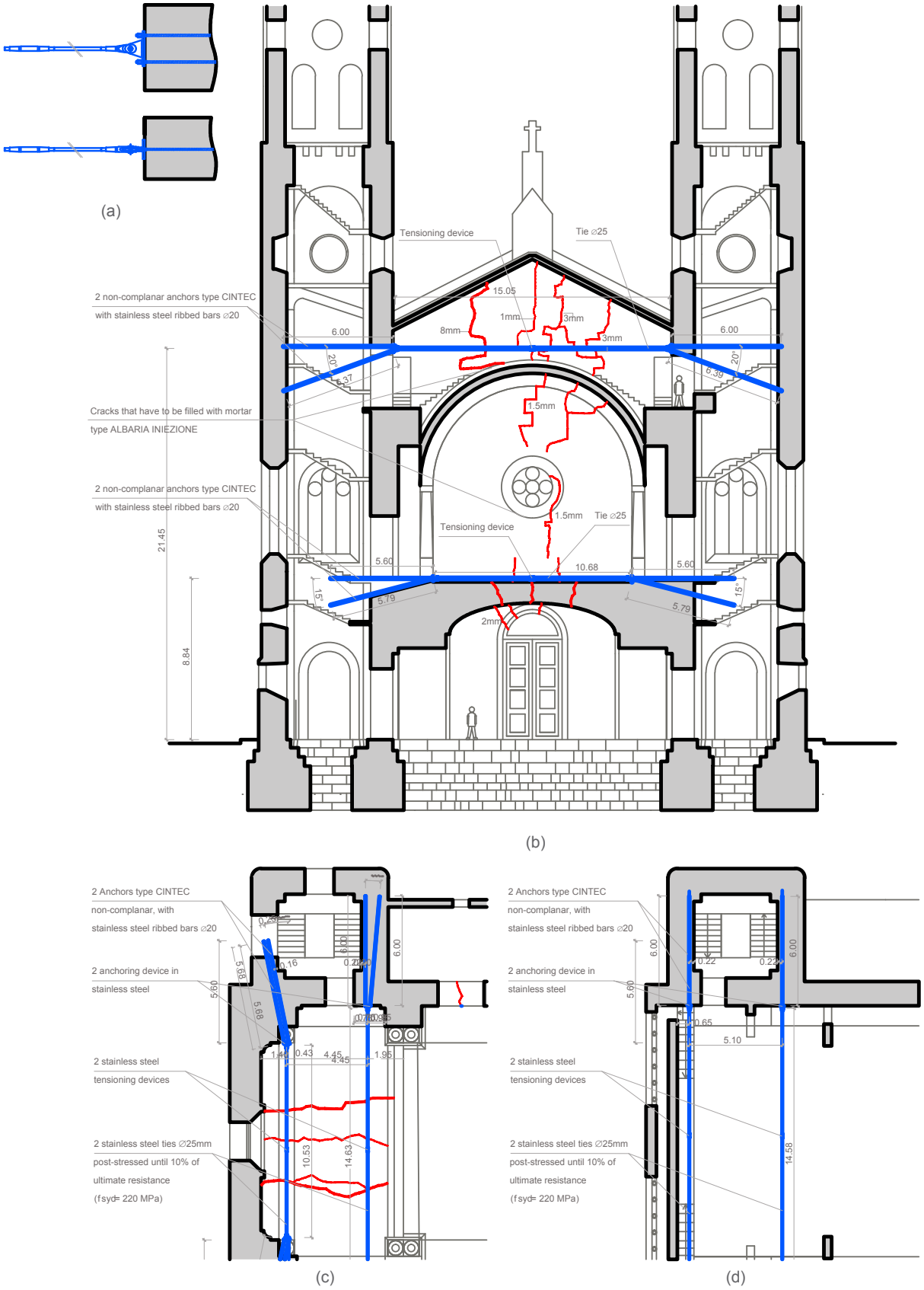

Figure 4.3: The system of anchoring designed by professor Ramos: (a) detail of the connection (b) section (c) plant at the choir level (d) plant at the vault level

its volume and guaranteeing the monolithic behavior of the system

- The anchoring of the interior micro-piles will be achieved paying attention to reach the same level of the beam bottom

- The rods will be activated by a post-tensioning device once the concrete have reached a suitable resistance

The system will be operative and fully operational since the anchors are active.

4.2.2 Anchoring design

The monolithic behavior of the façade will be recovered whit the union of the towers with proper steel ties. If the design of this system took into account the development of differential settlement of the structure, it would be necessary to increase excessively the intervention impact. Thus, Considering that the root causes of the soil settlement will be eliminated with the micro-piles intervention, this system will provide tensile resistance against unlikely further openings of the cracks. Four post-stressed ties will be placed in a suitable position to achieve a good constrain of the towers and in the same hide the intervention from the sight of the building users. Two couples of ties will be installed at the choir level, just on top of the floor. Other two couples of ties will be placed in the attic on top of the vault extrados (Figure 4.3).

The ties will be placed in the most symmetrical position as possible with respect to the towers axes, in order to avoid the transmission of torsional effects in case of relative tilting of the towers. For the evaluation of the force that will be applied on the ties it was considered the investigation performed by the SAHC student in 2013. By means of an FE analysis, they considered that the maximal tension that will arise due to the presence of ties is 68 kN (Merluzzi et al., 2008). It was chosen a diameter of 25 mm and a per-stressed level equal to 10% of the yielding force (220 MPa) to face the relative force. The ties are secured to steel plates with a hinge that permits the relative rotation of the structural parts. The plates are fixed to the structure by means of two ties anchored inside the tower walls for a length of six meters. The anchoring system of the clamps is achieved by the CINTEC reinforcing method: a socket is inserted inside a hole drilled with diamond-cut technology, then a ribbed rod is

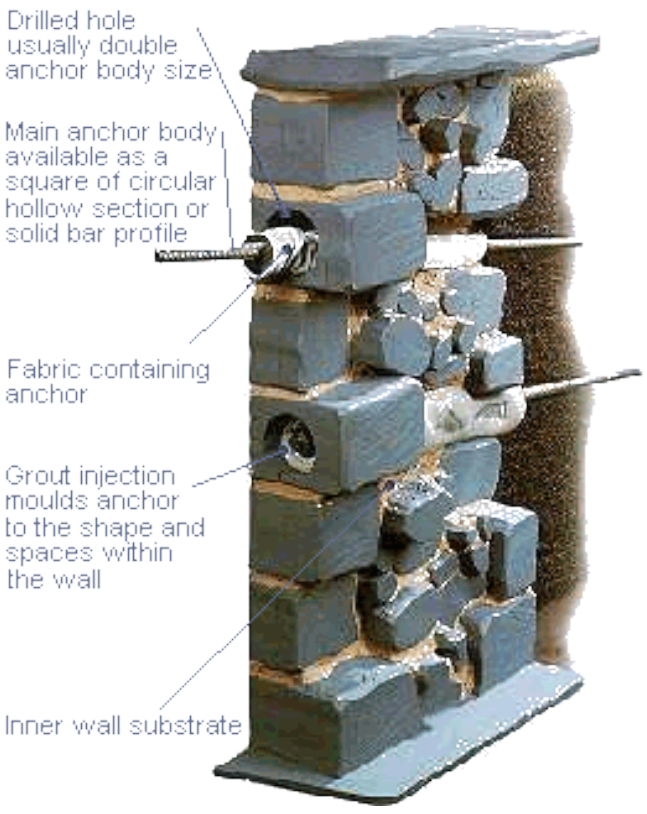

Figure 4.4: The system of anchoring developed by CINTEC, chosen for the intervention on the church (www.cintec.com)

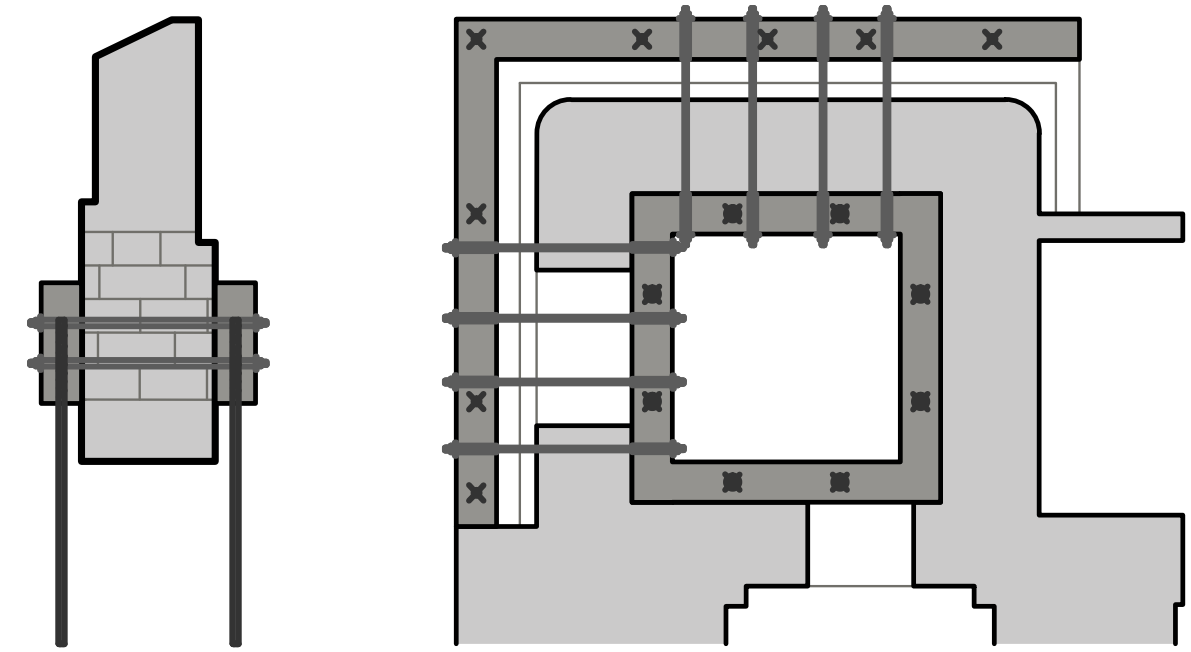

(a)

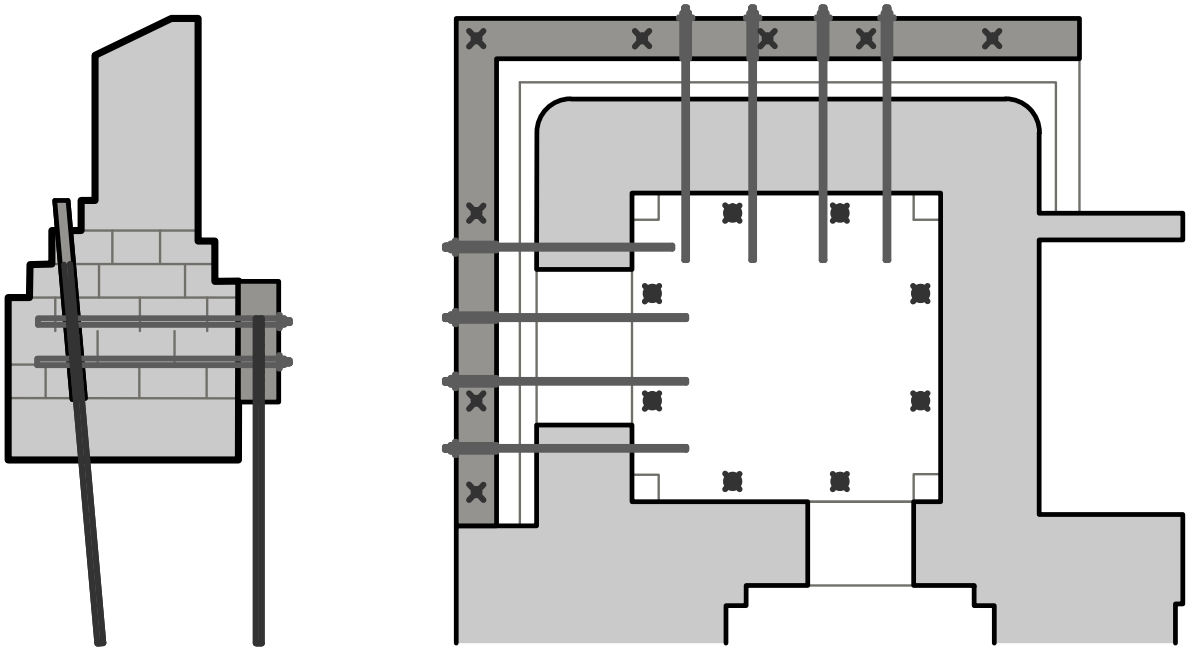

(b)

Figure 4.5: Changes of the design during the time: (a) first design, two concrete beam were placed in the tower and anchored with shear connector (b) last project, the internal beam disappear and the intervention takes into account the real shape of the foundation

inserted inside the sleeve and cement is grouted with high pressure, in this way the socket will expand guaranteeing a good anchoring with the surface of the hole (Figure 4.4). The two holes will be cut in diagonal way with a different inclination, in order to cross more bonds as possible and assure a perfect anchoring. The executive procedure will be the following:

- The holes will be drilled with diamond-core machine, with the help of water
- A CINTEC socket and a bar will be placed inside the hole
- The anchoring will be fixed to the tower by means of concrete injected with high pressure
- A steel plate will be fixed to the anchoring system with screws once the grout reaches a proper resistance
- The ties will be placed in the structures and pre-stressed until reach a 10% of ultimate load tension, by means of a specific tensioning device

The system will be operative and fully operational since the anchors are active.

4.2.3 Crack injections

Grout injection is an effective method of repair and strengthening masonry walls. This technique is able to restore the material continuity across the cracks allowing in the same time small movements without arm the structure.

A mortar type ALBARIA INIEZONE will be used for the intervention in S. Torcato. The injection is based on pozzolanic lime mortar and is especially designed for historic building. The method is useful to consolidate the building without alter the original structure neither physically nor chemically. Moreover, the hydraulic nature of the mortar does not affect the vapor and moisture permeability characteristics of the building.

4.3 Changes of the design

The strengthening works previously described represent the last step of a long process. The first design, in fact, was slightly different. In that case the concrete beam was coupled with a ring beam placed inside the tower. Subsequently, the shear connectors were passing through the whole system, assuring a perfect anchoring of the system. This design was based on wrong drawings that were reporting incorrectly the shape of the foundations. The update of the drawing and the subsequent change of the design were necessary after the visual inspection of the foundations (Figure 4.5).

4.4 Strengthening check

As mentioned in the introduction, the next step of the chapter is the cross-check of the design. This analysis will be focused on the foundation strengthening without knowing all the assumptions and hypothesis

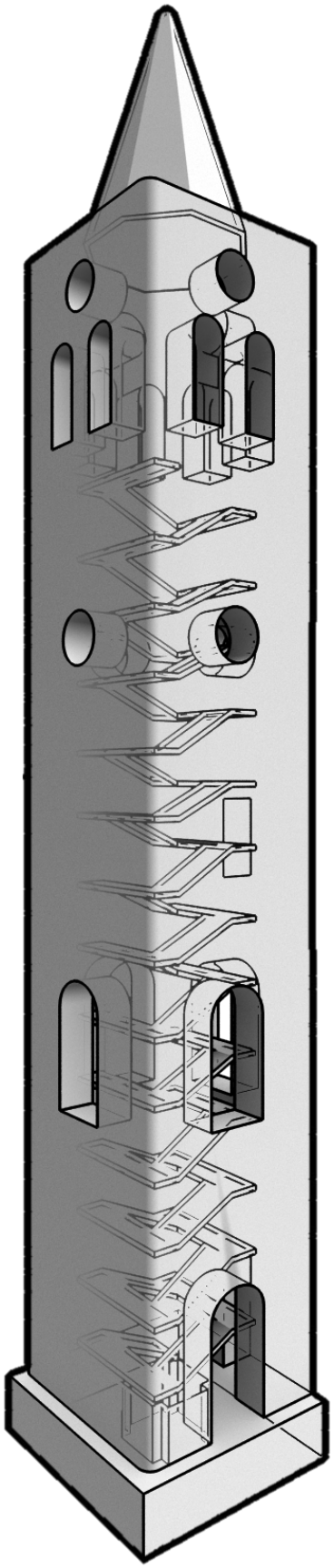

Figure 4.6: Model used for the evaluation of the volumes

of the Ramos' intervention. It would be too simple to examine the ties intervention because it was assumed a specific tension from previous FEM analysis. For this reason such verification was not performed.

The design will be divided in four parts, namely modeling of the problem, shear connectors verification, micro-piles design and beam verification. Personal assumption will be subsequently compared with those taken by professor Ramos and conclusion will be discussed. All the calculations necessary for the verification were performed with the help of a Mathcad sheet and are visible in Annex B.

4.4.1 Modeling of the problem

The first task of the intervention design was the reduction of the real problem into a suitable model that allowed developing the analysis in a reliable way. For this purpose, the tower was considered isolated, neglecting all the interaction with the rest of building. This simplification could be considered too strong in case of global analysis, but can be assumed in this case considering the aim of the design: transfer the weight of the towers to the bedrock. The general shape of the tower had been modeled in 3d Studio Max in order to evaluate easily its weight (Figure 4.6). Volume of walls, internal stairs, foundations and the spire were taken into account in the model. A specific weight of 26 kN/m^3, corresponding to pure granite stone, was assumed for the masonry walls. This statement do not considered that the building was constructed with three leaf walls with a probable lighter filling, but in this way the safety level can be increased. For the same reason, a partial factor of 1,2 was used to evaluate the total weight of the tower, estimated around 44,62 MN.

As discussed in Chapter 3, the cracks were detected at least since forty years and were attributed to differential settlement of the soil. It is very likely that such subsidence had been almost stabilized during this long period. Thus it was assumed to transfer just part of the towers weight, namely the 20%, reaching a design load of 8,9 MN. In this way it was possible to define an average design stress of 0,16 MPa at the base of the foundations. The following table shows the main data used for the problem.

Modeling of the problem	
Total volume of the tower	1430 m^3
Specific weight	26 kN/m^3
Total weight of the tower	37,18 MN
Partial security factor	1,2
Design weight of the tower	44,62 MN
Part of the weight considered for the analysis	20%
Design load at the foundation level	8,92 MN
Area of foundations	55,63 m^2
Average normal stress at the foundation level	0,16 MPa

Table 4.1: Results of the modeling of the problem

4.4.2 Shear connectors design

The continuity between the tower and the piles is given by structural connectors that work basically below shear condition. The design of those elements is very delicate, because the success of the whole intervention is guaranteed by them. In fact, if one of the micro-piles failed the structure would be able to re-arrange the load, while the failure of shear connectors would lead to the disconnection of the intervention and the relative collapse of the whole system. The design was performed placing the connectors in the same position as in the intervention drawings (Figure 4.2), so that would be possible to compare the results.

The main simplification of the design considers that the stress flow of the tower's weight will be split in two parts: the load directly applied on the exterior area, bounded by the middle plane of the foundations,

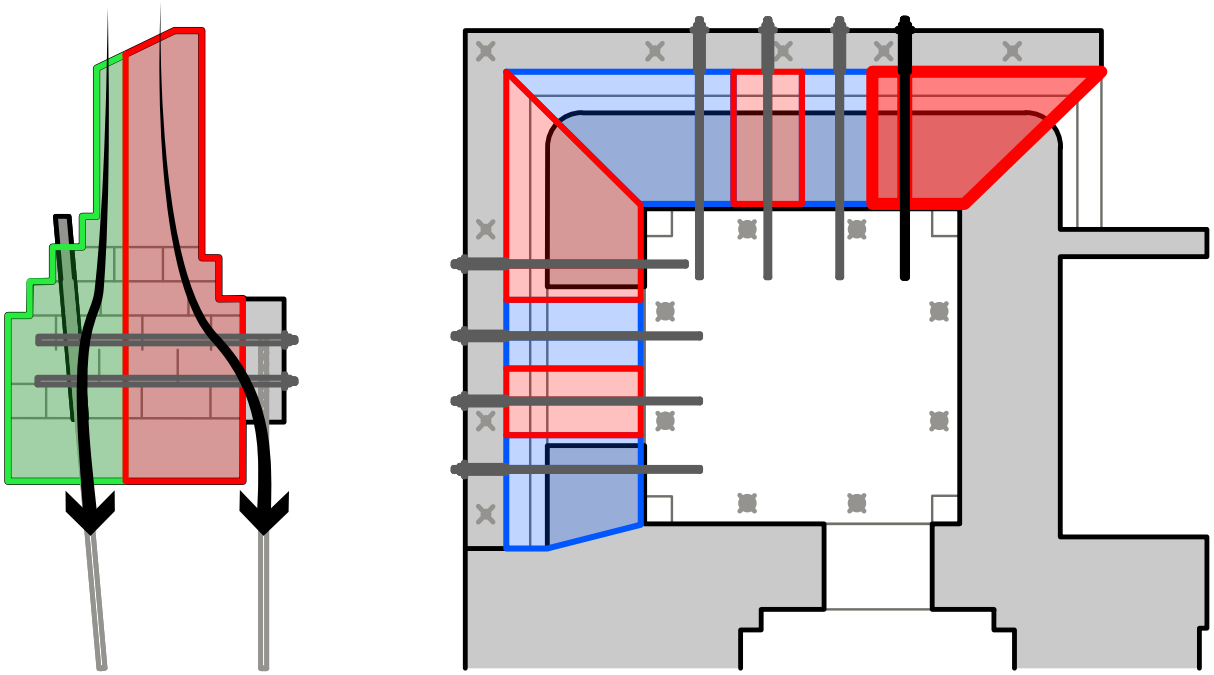

Figure 4.7: Flow stress considered for the design and area of influence relative to each shear connector. The element in condition more unfavorable is marked on the plant

will be discharged directly on the shear connectors, while the force applied of the remaining area will not affect them (Figure 4.7). The first approach of the analysis tried to evaluate the design shear for each connector (resulting in 250 kN) considering the total shear force applied on the area of influence (3,9 MN) and dividing it for the number of elements. In this way, however, the relative disposition of the ancillary structure and the subsequent change of load distribution are not taken into account. Thus, it was decided to calculate the shear load considering a proper area of influence, bearing in mind that they are coupled (Figure 4.2). The relative force applied on the connector with the highest area of influence (350 kN) was used to calculate the minimal diameter necessary to resist to the applied force, equal to 44,8 mm. This result fits perfectly with the dimensions adopted by professor Ramos for his design (45 mm). It is important to notice that the whole system will be able to resist 30% more than its capacity using such diameter for all connectors. This condition, however, guarantees a higher safety level. A resume of the results is visible in Table 4.2.

Shear connectors design	
Total area of influence of the connectors	24,49 m^2
Total shear applied on the connectors	3,93 MN
Shear per connector (per simple division of tot shear on them)	245,54 kN
Area of influence of the connector in less favorable conditions	4,44 m^2
Shear per connector (per area of influence of the worse case)	356,12 kN
Minimum resistant diameter for the bars	44,8 mm
Design diameter for the bars	45,0 mm
Total resistance of the connectors system	5,75 MN
Residual resistance capacity, using the same rod for all connectors	31,67 %

Table 4.2: Results of shear connectors design

4.4.3 Micro-piles design

The relative normal stress analyzed at the foundation level will be transferred directly to a proper soil, without consider the friction with it, by means of M-80 micro-piles. A minimum number of sixteen micro-piles was identified considering their maximal resistance (590 kN) and the design load applied on them (8,9 MN); it is important to notice that this number coincide with the number of piles of Ramos' intervention. The micro-piles were placed in the same way as shown in Figure 4.2, so as to compare the results with Ramos' design.

4.4.4 Beam verification

The concrete beam designed in the intervention assures the anchoring of micro-piles, the anchoring of shear connectors and their structural continuity, so that the vertical load can be transferred from the tower to the resistant soil. This structural member has to be designed to face the solicitations induced by the system.

The beam can be considered as an element simply supported, where the supports are represented by the heads of the micro-piles. The dimensions of the structure are considerable, 1,8 m height and 0,6 m

width (Figure 4.8). Such values, however, are attributable to anchoring requirements: the piles precise a minimum of 1 m of anchoring while the shear connectors need a minimum of 30 cm. The average normal stress at the base of the foundation (0,16 MPa) was used to define the force applied on the beam. For simplification, the load transferred by the connectors was considered as a distributed force, and the same stress flow described in the previous paragraph was used (Figure 4.7). The beam was divided in two elements and the stress was transformed in linear distributed force (respectively 250 kN and 290 kN) considering the depth of the relative area of influence (Figure 4.9). Once the diagram of shear and moment were evaluated by means of Ftool, their maximum values were chosen to verify the beam under ultimate limit state for bending and shear (respectively 170 kNm and 730 kN). The heterogeneous distribution of the moments brought, however, to a redesign of the piles that will be discussed in Section 4.6.

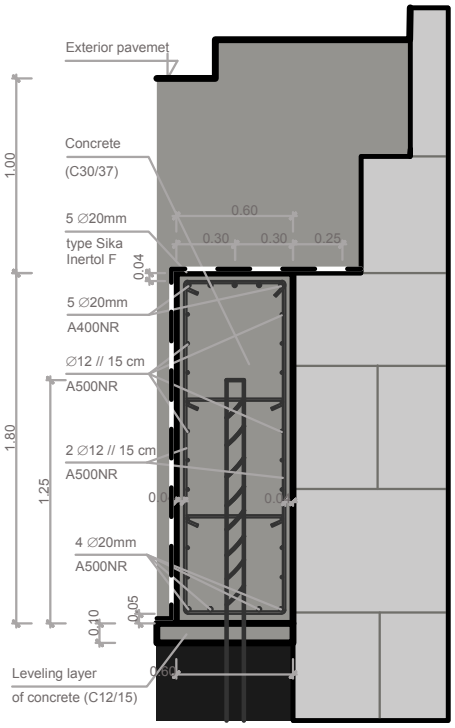

Figure 4.8: The beam designed for the intervention of Professor Ramos

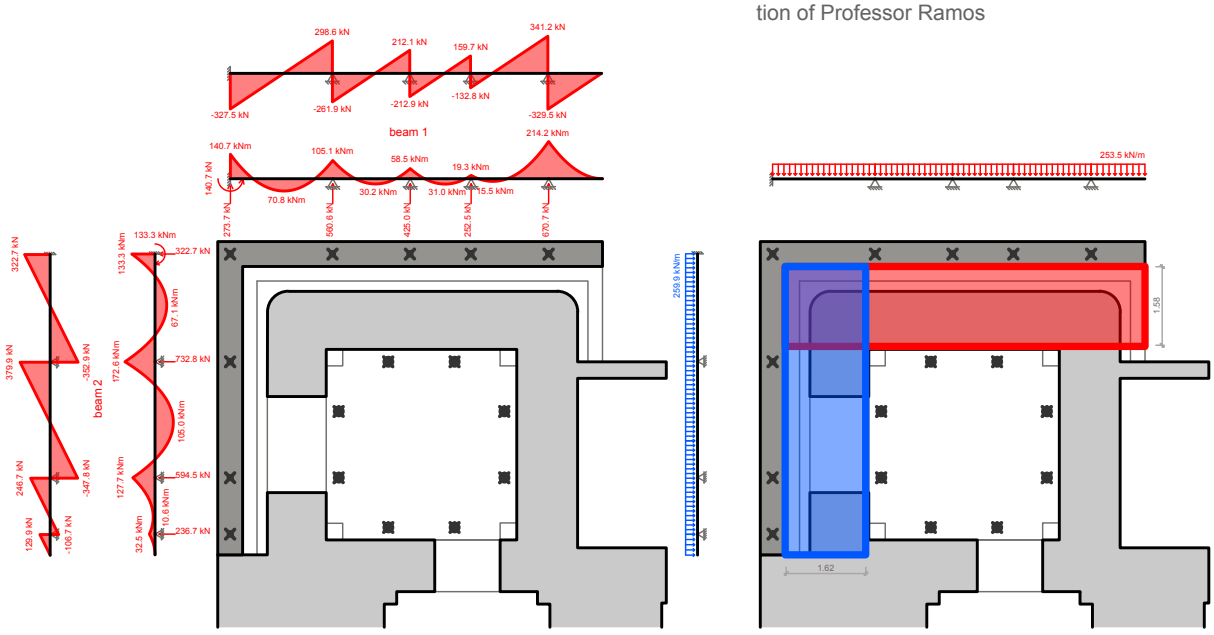

Figure 4.9: Verification of the beam: (a) diagrams of shear and bending moment (b) definition of beam loads

The verification was performed considering the parameters defined by Eurocode 2 (Design of concrete structures), together with the material characteristics assumed in the project (cement CEM I 42,5 R and steel R400NR). The results are completely satisfying as expectable for a beam of such dimensions and with such level of reinforcement. Just the 20% of its capacity would be used under bending design actions. It is important to remark, however, that theoretically the beam should be able to resist in buried condition for centuries: this means that the steel have to be big enough to face possible chemical

attacks, creep or fatigue problems. The check on shear resistance was satisfied as well, even consider ing the beam as not reinforced with specific shear bars (the stirrups for example). For this reasons the verification at torsion was neglected. The main results of the analysis are reported in Table 4.3.

Beam verification	
Cross section dimensions (height x width)	1,8 x 0,6 m^2
Distributed load on beam 1	253,5 kN/m
Distributed load on beam 2	259,9 kN/m
Bending moment affecting the beam (maximal)	214,2 kNm
Shear force affecting the beam (maximal)	379,9 kN
Shear resistance of the beam (considering the beam w/o reinforc.)	448,9 Kn
Resistance capacity used below shear load on the beam	84,6 %
Area of steel in upper part of the beam	15,7 cm^2
Area of steel in upper part of the beam	12,6 cm^2
Bending resistance of the beam	1,1 MNm
Resistance capacity used below bending load on the beam	19,9 %

Table 4.3: Results of beam verification

4.5 Comparison of the design

The differences between the main assumptions taken during the personal design and the Ramos' intervention will be discussed in this paragraph. Being the number of micro-piles identical, the design of them will not be considered.

4.5.1 Modeling of the problem

Professor Ramos divided the structure in tower and foundations. The weight of the bells was also added for the calculation of the total weight. Considering even the foundation, the total weight of the structure was estimated around 26 MN, more or less 30% less than the value calculated in the personal design (around 37 MN). This difference can be attributed to a slight difference of the chosen volumes (Ramos' calculi were done by hand while I used 3D software) and, more important, the difference of the specific weight assumed. In fact, he decided to use a value of 22 kN/m^3 instead of 26, probably taking into account the presence of void or light infill in the masonry walls. The relative number of micro-piles, however, is the same in both designs. This is because a safety factor of 1,4 was used to increase the safety level of his intervention, instead a value pf 1,2 was used in the personal design (1,2).

4.5.2 Shear connectors design

This part of the analysis was carried out in a simpler and more efficient way by professor Ramos. In his design it was considered the total way equally distributed on the shear connectors. Several minor connectors were also added in the calculations to reduce the effective load per rod on those parts where the influence area per element was significantly higher. More over, the friction developed by the pre-

stress of the elements was take into account in order to evaluate the effectiveness of shear reduction of the solution. In this way the diameter of the structure could be reduced (45 mm was used just for safety reasons) without have any problem of collapse for the connectors. An higher safety level guarantees a better durability of the intervention below fatigue and creep problems.

4.5.3 Beam design

The beam was designed by the professor accordingly to the first intervention project described in Paragraph. For this reason a direct comparison between the beam designs is almost impossible. It is possible, however, to compare the main assumption on the load distribution on the beam. Ramos decided to use the maximal load of the piles and transform it as a linear distributed load applied on the beam. The relative value of 500 kN/m was used to define the maximal bending and shear value, respectively 330 kNm and 750 kN. Even with this difference in value, the relative capacity of the beam is used just partially as in the personal design.

4.5.4 Summary of the differences

In the following tables it is possible to see the numerical differences of the main assumptions of both projects.

Modeling of the problem	Puliga	Ramos	Diff.
Total volume of the tower	1430 m^3	1349 m^3	3,85%
Specific weight	26 kN/m^3	22 kN/m^3	15,4%
Total weight of the tower	37,18 MN	29,68 MN	20,2%
Partial security factor	1,2	1,4	16,7%
Design weight of the tower	44,62 MN	41,55 MN	6,87%
Part of the weight considered for the analysis	20%	20%	-
Design load at the foundation level	8,92 MN	8,31 MN	6,87%
Area of the foundations	55,63 m^2	-	-
Average normal stress at the foundation level	0,16 MPa	0,15 MPa	6,64%

Table 4.4: Comparison of the modeling of the problem on both designs

Beam verification	Puliga	Ramos	Diff.
Distributed load on beam 1	253,5 kN/m	522,5kN/m	106%
Distributed load on beam 2	259,9 kN/m	522,5 kN/m	101%
Bending moment affecting the beam (maximal)	214,2 kNm	331,1kNm	54,6%
Shear force affecting the beam (maximal)	379,9 kN	756,0 kNm	99,0%
Resistance capacity used below bending load	19,9 %	30,7%	54,3%

Table 4.5: Comparison of beam verification on both designs

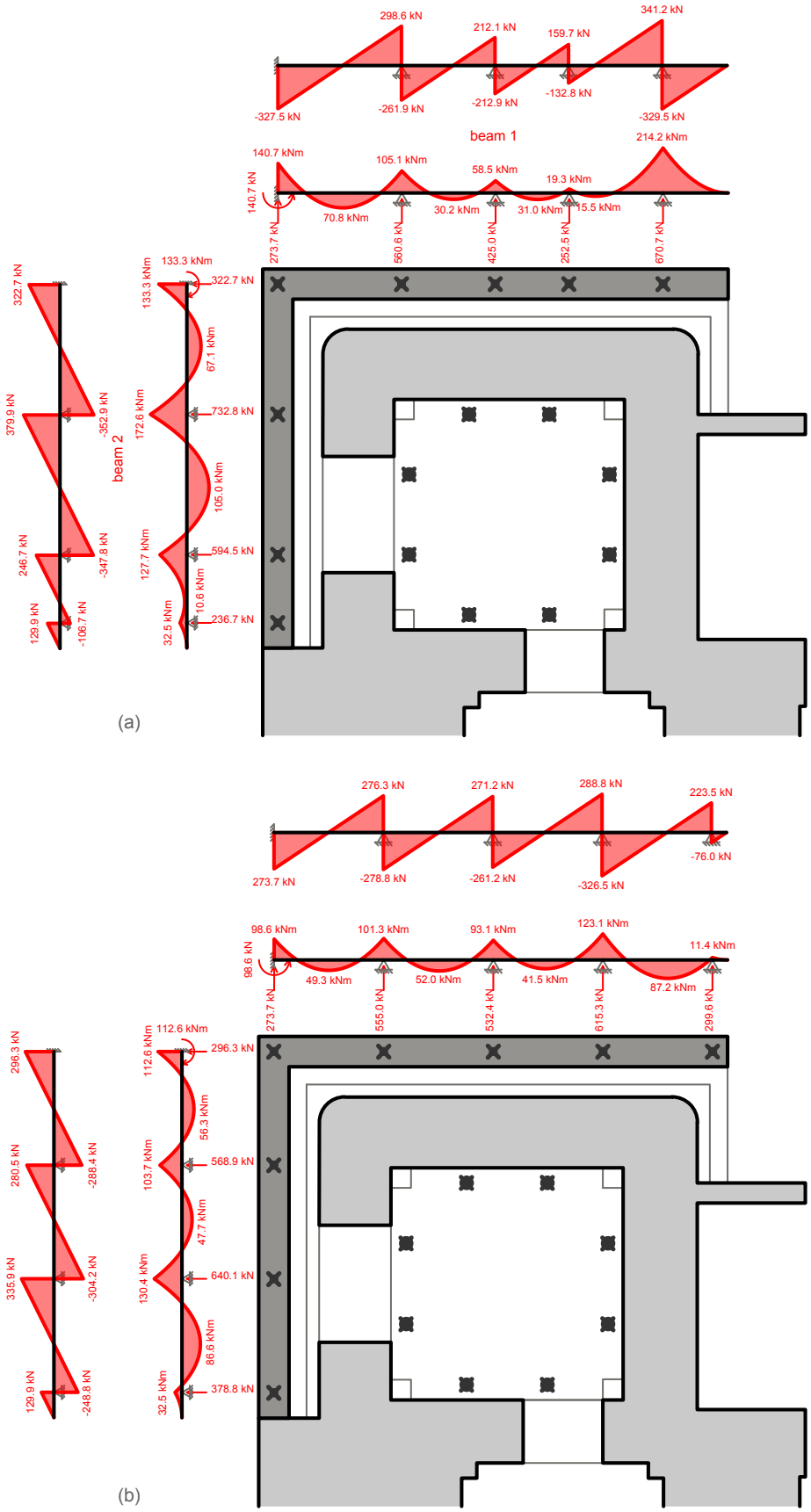

Figure 4.10: Comparison of the updated drawings, with the remarkable reduction of bending and shear solicitations: (a) the design defined by Ramos (b) The personal updating

4.6 Update of the design

As mentioned in Paragraph, the bending and shear distribution through the beam was not homogeneous. This is basically due to the variable spacing among the micro-piles. For this reason, it was considered to change the position of the micro-piles in a more rigorous scheme, without affect the position of shear connectors (Figure 4.10). In this way it was possible to rearrange the distribution of the actions in a more appropriate way, reducing bending moment until 40% and shear force until 12% without changing the number of micro-piles (Figure 4.11). The value of maximal shear force analyzed in the beam should not be plausible with the micro-piles resistance, because this limit would be overpassed. It is necessary to take into account, however, that part of the load will be transmitted by the piles to the soil for friction, some of the weight will be transferred directly from the beam to underlying soil and the system of piles will activate a group effect, a beneficial consequence not considered in the previous analysis. For this reason, it is likely that the load will be rearranged by the structure without reach the limit capacity of the micro-piles. The comparison of the other diagrams diagram developed in the analysis are visible in Annex B.

As a result of this last analysis, the previous project was discarded and the updated version was instead chosen for proceed with the executive works.

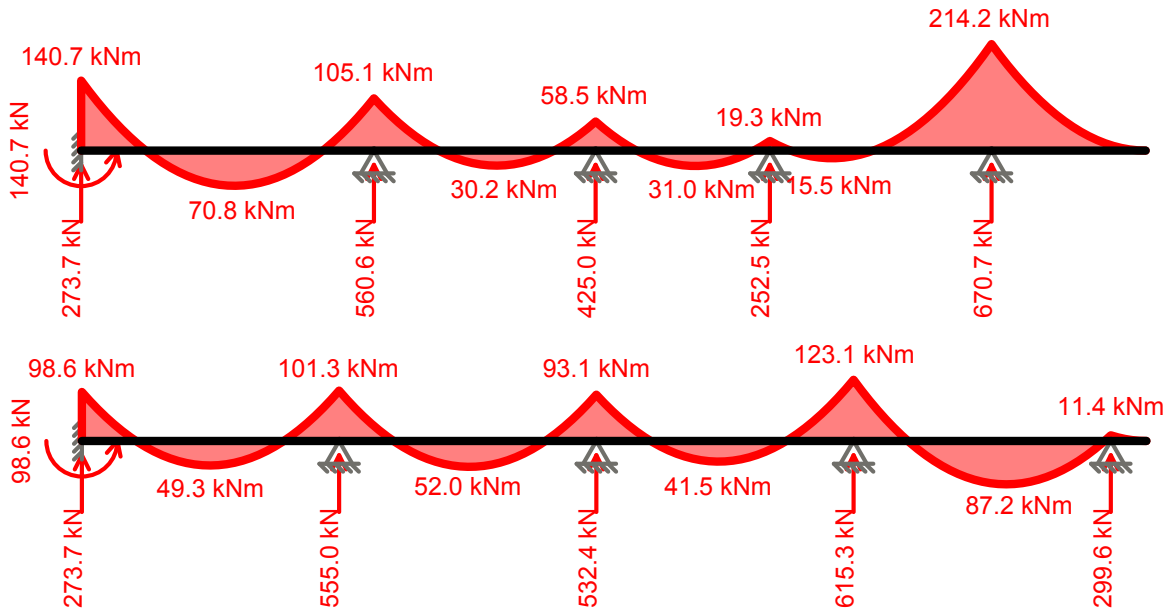

Figure 4.11: Difference in bending moment diagram between Ramos' design (on top) and the personal design updating (in the bottom). The enhancement of the system is visible both in the decrease of the maximal bending than in the rearrangement of the support reactions

5. DESIGN OF THE CROSS

5.1 Introduction

Throughout the previous chapter it was discussed the strengthening design involving the façade anchoring and the soil stabilization. Further minor works have to be carried out in order to retrofit or repair some others valuable parts of the building. Among the others, the crosses on top of both towers spire need to be replaced. In this chapter, the actual state of the cross will be presented and accompanied with the design of the new one, personally performed.

5.2 Current status of the cross

The cross is an iron detail present on top of both towers spine, one of which works as lightning rod for the surrounding area (Figure 5.1). The shape of this roof element is simply defined by two perpendicular bars of rectangular section, with sharp corners. The crossing point of those arms represents the center for a detail superstructure, defined by two concentric circles. Moreover, a minor cross rotated 45° with respect to the main one adorns the element. A decorative element is fixed to the terminal part of each brace and in the middle point of the secondary cross. In one of those element is fixed the lightning rod (Figure 5.2).

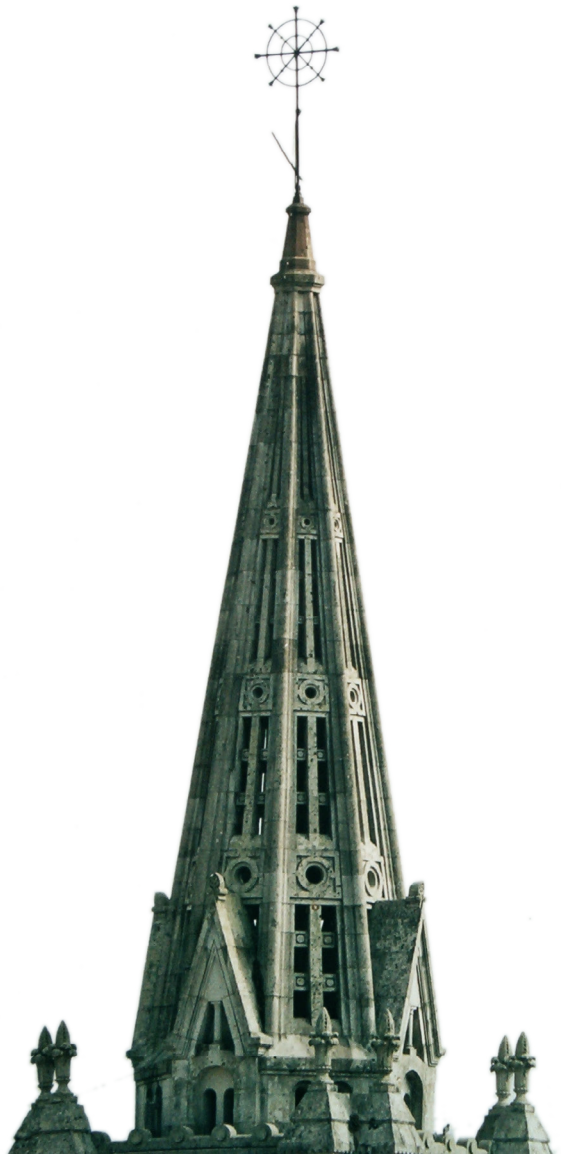

Figure 5.1: A panoramic view of the spire and the cross that decorates it

The dimensions of the cross were deducted thanks to previous drawings and photographic data archived in the Irmandade de S. Torcato and the museum (Figure 5.2 a). The problem on the element is induced by oxidation mechanisms that are severely damaging it, thus is required to replace the cross. However, several doubts and problems need to be solved before planning a strengthening design.

First of all, it was necessary to perform a geometrical survey and check if the assumed measures were precise enough. It was also necessary to evaluate directly on site the oxidation level of the cross, even if by means of a simple visual survey. This was necessary because the damage could be detected just by pictures or point views

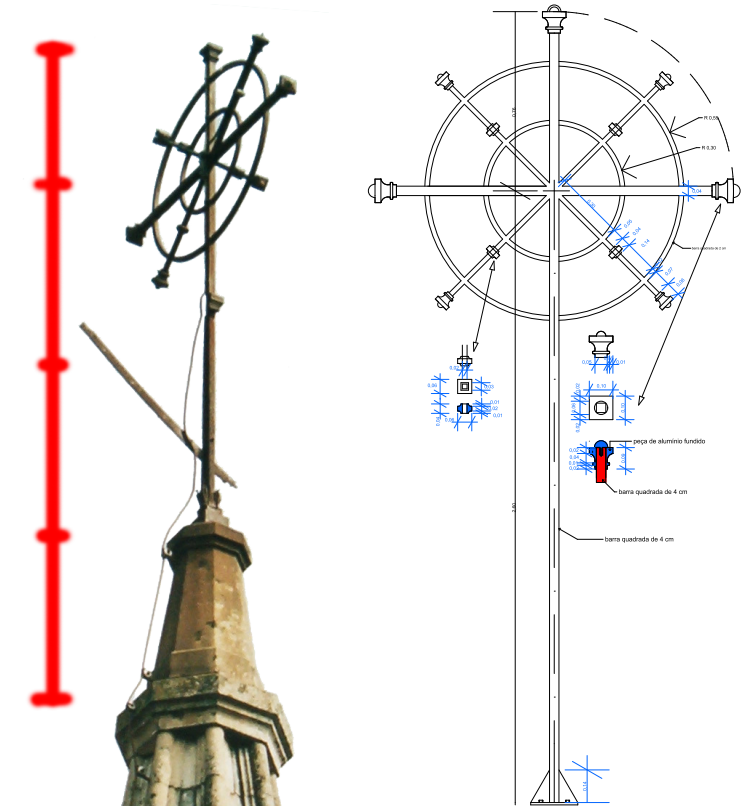

(a) (b)

Figure 5.2: A closed view of the cross: (a) a real picture with the highlight of the proportions between the cross and the base stone (b) the first AutoCAD drawing developed before the visual inspection

(a) (b)

Figure 5.3: The visual inspection on the crane: (a) the base of the cross was severely affected by corrosion (b) the measuring of the cross

too far away from the element, due to the inaccessibility on the top of the towers. Even the real height of the towers was uncertain and had to checked. Finally, it was not possible to establish how the cross is clamped to the underlying stone on the spire terminal. For all this reasons, it was planned a direct inspection of the cross by means of a telescopic crane.

5.3 Visual inspection

It is important to remark that, due to lack of a prompt notification from the construction enterprise, it was not possible to plan an effective inspection and diagnosis campaigns during the first visit. For this reason it was carried out just a visual inspection and a geometrical survey of the cross. A telescopic crane allowed to pull a small team in a cabin up to the height of sixty meters. From that position it was possible to get close to the cross and check its state. The element presented an advanced state of oxidation that had brought to a partial reduction of the cross section during the years. Such phenomenon was affecting mostly the base of the rod, a dangerous position due to the stress concentration induced by bending (Figure 5.3).

It was also possible to measure the cross system: basically, its thickness and the height of the base stone. All the other dimensions were calculated proportionally to those ones using pictures and historical data. An evident formal mistake was found in the technical drawings: the iron base

considered for the cross was not fitting with the real one (Figure 5.3 and 4.4).

It was not possible to measure the effective height of the cross due to the strong winds and the relative difficulties to move the crane cabin in safety without arming the cross and to place properly the metallic ruler. However, thanks to the pictures thanks to pictures, previous data and few measurements, it was possible to conclude that the technical drawings presented a good approximation.

From the first visit, however, a big lack remained. It was not possible to understand the clamping system between the cross and the base stone by visual inspection. Several hypothesis were considered: the base could be hollow and base of the cross may be inserted on it for example. However, without any indirect test (by means of geo-radar for example) or a direct test (dismounting the cross), them are just speculations without documented bases. Few weeks after the visit, it was discovered a system used to lift the stones during the construction phases that could probably been used to clamp the cross. The system included the carving of a trapezoidal niche on the top of the base stone, 5 to 10 centimeters deep. Three iron parts would be hosted in the hole and connected by them with a transversal bar. The shape of those parts was such as once the bars were pulled up they were going to open and grab the stone from the inside (Figure 5.5).

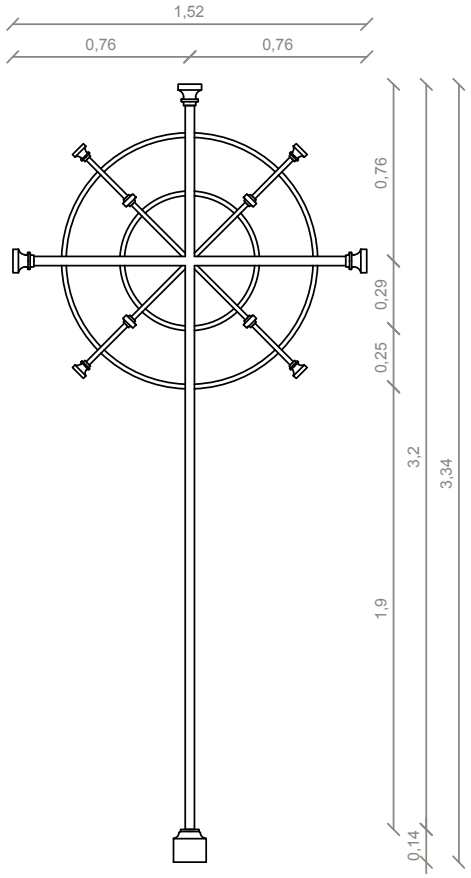

Figure 5.4: The update of the drawing after the visual inspection

Figure 5.5: Ancient clamp used to lift stones during construction phases

5.4 Static analysis

Taking into account all the information and discoveries in the previous paragraphs, it was developed a static analysis of the cross. The main of such study is checking if a replaced elements in stainless steel, made with the same shape and dimensions of the old one, should be able to satisfy the requirements of the current codes. Unknowing the clamping system of the cross, it was chosen to perform three different studies (Figure 5.6):

- A limit state analysis of the cross itself, considering the cross section most affected by wind actions: the base one

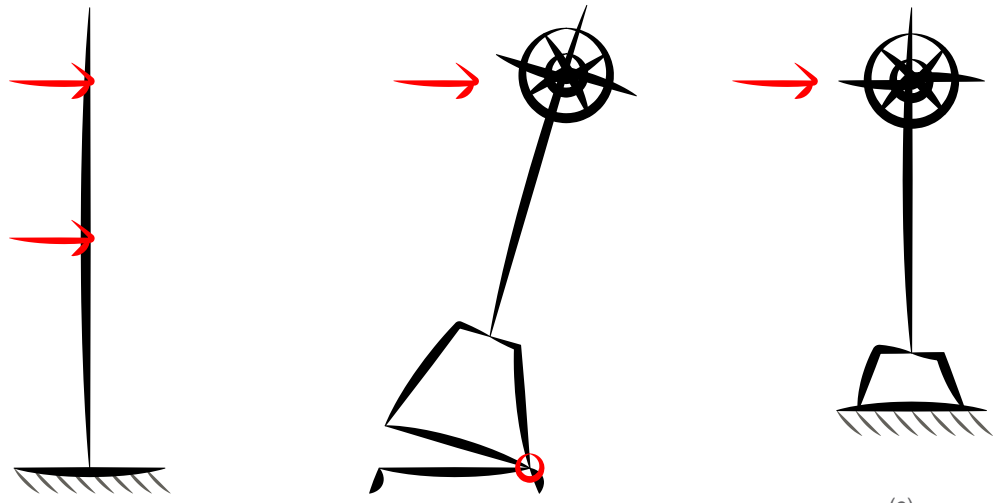

Figure 5.6: The schemes of the static analysis performed: (a) limit analysis of the cross (b) kinematic analysis of the system (c) limit analysis of the system

• A limit state analysis of the stone – cross system, considering the resistance of the stone at the cross section in the middle point

• A kinematic analysis of the whole system, considering the rotation pole at the base of the stone, assumed unclamped to the underlying structure

In the following chapter will the main assumptions and relative results of each scenario will be discussed. The details of the calculations can be seen in the annex. Such analysis was developed using Mathcad calculus sheets.

5.4.1 Verification of the cross

The first analysis was carried out in the bottom cross section of the main bar. It was analyzed following the limit state analysis steps prescribed by Eurocode 1-4 (General actions – Wind actions), Eurocode 3-1 (Design of steel structures - General rules) and Eurocode 3-3 (Design of steel structures - Towers, masts and chimneys).

The first task of the analysis was the creation of a suitable mathematical model available to describe the real cross behavior. It was decided to simplify the element in this way (Figure 5.7):

• The vertical bar that act as a main support was considered a cantilever perfectly fixed to the underlying stone

• The main horizontal arms and all the decorative structure was considered as an addiction. Its presence will be relevant just in terms of applied forces, transferred to the cantilever at the height of the decoration centroid.

The necessary dimensions were calculated by means of a CAD file and the material properties were de-

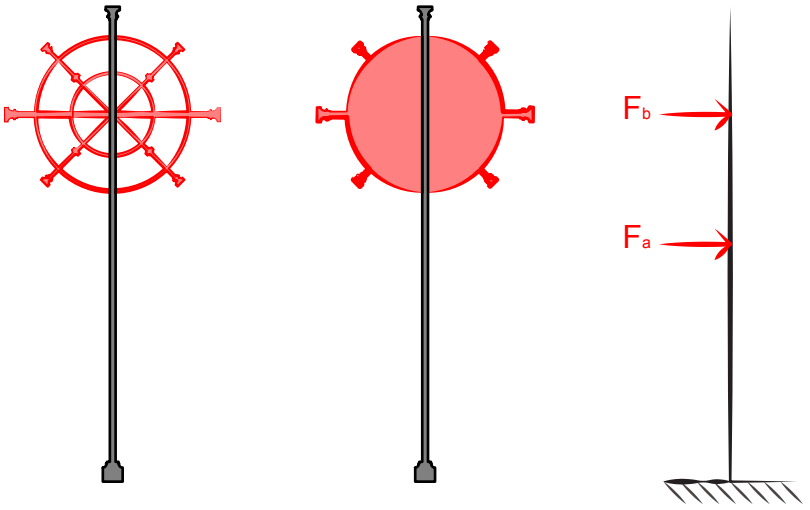

Figure 5.7: The mathematical simplification of the real geometry: (a) the drawing of the real cross (b) definition of two different systems, the rod and the detail (c) transformation of the rod into a cantilever and relative applied forces

fined by Eurocode. The wind actions were analyzed considering a basic wind value of 28 m/s, because of the considered site. The mean wind was analyzed considering the difference in height between the top of the cross and the ground level. The wind force was initially calculated considering the cantilever and the superstructure separately. In fact, due to the shape and the low solidity ratio of the detail with respect to main cantilever, the two parts should have different force coefficients that could bring to a different behavior below wind conditions. Anyway, the numerical values were not too much different from each other, so that their difference were neglected in the end (see annex). The wind force for each element, applied on their relative centroids, was calculated applying the peak velocity pressure to the relative impact area of the two parts and increased by the force coefficient of the elements, following the formula:

$$F_w = c_f \cdot q_{p(z)} \cdot A$$

All the values used to define the wind action are and the relative actions applied on the cross are visible in the following table:

Parameter	Symbol	Value
Basic wind velocity	v_b	28,0 m/s
Maximal height above ground level	Z	61,1 m
Mean wind velocity	$v_{m(z)}$	32,1 m/s
Wind turbulence	$I_{v(z)}$	0,19
Peak velocity pressure	$q_{p(z)}$	1,49 kPa
Approximated force coefficient of structural element	c_f	1,9
Force on the cantilever	F_A	0,36 kN
Force on the superstructure	F_B	0,63 kN
Total moment applied at the cross base	M_{tot}	0,16 kNm

Table 5.1: Main parameters used during the limit state analysis of the cross with relative results

The verification of the base cross section was carried out analyzing the relative design bending moment, shear and axial forces induced by wind forces in combination with dead loads, considering relative partial factors, as defined by Eurocode:

Imperfections and torsional effects were introduced as suggested by Eurocode, as well as second order effects. It was established that the cross satisfies all the requirements of the code. It results even over-designed for all the conditions with except of the pure bending one. The percentage of utilization of maximal resistance below each of the conditions is reported in Figure 5.8.

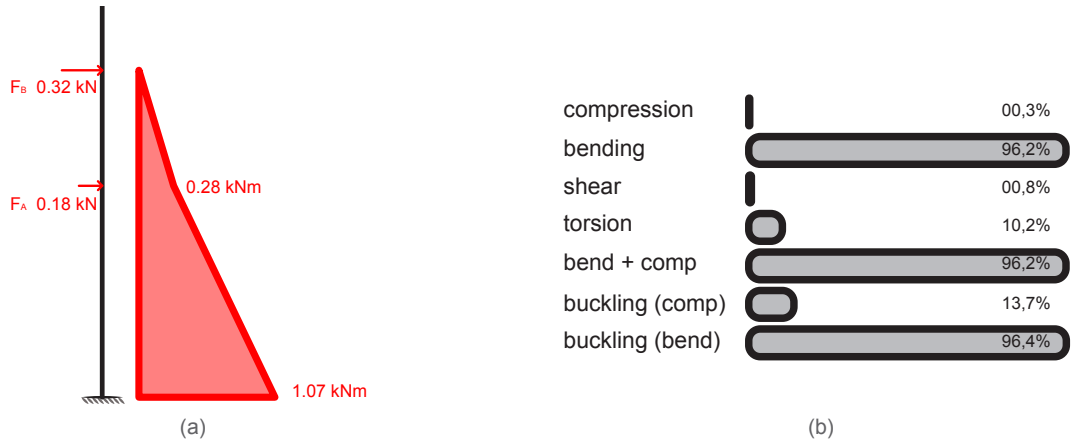

Figure 5.8: The results of the first analysis: (a) forces applied on the system and relative moment distribution (b) percentage of utilization of maximal resistance below each condition that affects the structure

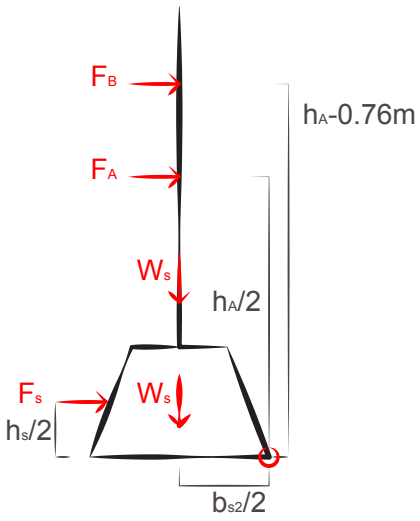

Figure 5.9: Simplified model used for develop the kinematic analysis

5.4.2 Kinematic analysis

The third analysis involved the 2d kinematic study of the cross and the base system. The cross was considered perfectly fixed to the underlying stone, which was assumed as simply supported by the spire. In this way the overturning of the model, calculated with respect to one side of the base, would be induced by wind forces and self-weight, combined with the same partial factors as the previous analysis.

Define the dimensions and the suitable shape of the base for the mathematical simplification was the hardest step of this analysis. In fact, recalling that the only available dimension checked during the first visit was the height of the stone, all the dimension had to be assumed proportionally with the help of pictures. The stone presents the shape of a truncated octagonal pyramid richly decorated both in the top as in the bottom sides. Such parts were

not taken into account in order to simplify the study (Figure 5.9). Cross and base were considered separately, considering the difference in shape that brought to a difference in force coefficients. The wind forces acting on the system were calculated taking into account, for simplification, the same peak velocity pressures of the previous analysis.

Those actions induce the overturning moment, counteracted by the resisting moment of the self-weight. The static equilibrium could not be reached with the made assumptions, so the analysis is failed. The acting design moment, in fact, is approximately four times higher than the other one. The problem cannot be due to an hypothetical bad approximation of the stone. Even if the shape or the weight of the stone should be tuned, it would be impossible to counteract the moment induced by the wind because of the big difference in force arms (Figure 5.9)

5.4.3 Verification of the stone base

As the previous analysis, it will be verified the cross sectional resistance of the base stone. In this case, the Eurocode did not present the same potentials in analysis as for the steel design. This is because Eurocode 6 is mainly focused on masonry constructions, considering them as composite structure of elements and mortar. Thus all parameters and coefficients assigned in Eurocode 6 are specific for masonry composite and do not take into account monolithic elements, as the one of the case study. The Italian code, instead, is much more suitable for the analysis of historic buildings. First of all, with the NTC-2008 it is possible to use test values, if in a sufficiently large number, and approximate them according to standard deviations. All the parameters take into account the uncertainty level of the materials, introducing a confidence factor that takes into account the level knowledge of the building. Such level is defined according to specific criteria of laboratory and site tests.

All the mechanical properties have been taken from the PHD thesis (Vasconcelos, 2005). The petrologic description of granite stones analyzed in the Guimarães area is " fine to medium-grained, with porphyritic trend, two mica granite". Fifteen saw-cut specimens of this region granite were successfully tested in laboratory, distinguish between dry and weathered type of granite. The results of the analysis was the definition of average values and their relative standard deviation of specific weight (26 kN/m3), compressive and tensile strengths those will be considered respectively 65,1 and 3,52 MPa, even it they represent "masonry" material and not the material it-self, for security reasons. The following table shows the main results of the tests.

Parameter	E (MPa)	ν	f_c (MPa)
GA	52244	0,23	135,7
	(2,3%)	(13,1%)	(5,0%)
GA*	35088	0,30	89,5
	(3,3%)	(17,1%)	(2,5%)
GA^*_s			65,1

Table 5.2: Masonry properties made of Guimarães granite, tested under axial compressive loading. The asterisk is referred to weathered granite, the values inside the brackets represent the coefficient of variation of each value (Vasconcelos G., 2005)

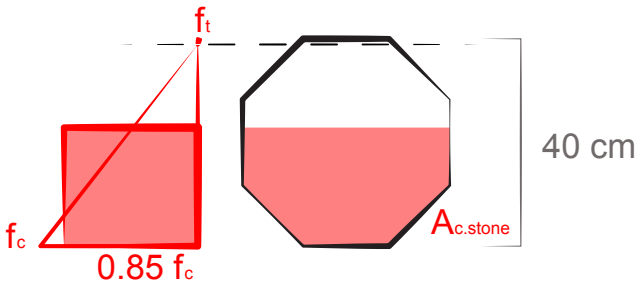

Figure 5.10: Distribution of the stresses in collapse situation with the relative stress block assumption

The system will be analyzed at the middle level of the stone base, considering the cross perfectly fixed to it and capable to transfer forces and moments without dissipations. The base is a truncated octagonal pyramid, as described in the previous paragraph. The acting design moments, shear and axial forces are induced by the same load combinations as in the previous elastic analysis. The collapse mechanism will be activated when it will be reached the maximal compressive strength of the stone, determining the crushing of the over-compressed area. The tensile resistance is neglected because too low compared to the compressive strength. The linear distribution of the stress has been transformed to a corresponding stress block with compressive resistance equal to the 85% of the granite one, so that the position of the force will not change with respect to the elastic distribution. The stress block is then multiplied for the relative compressed area, resulting in the maximal axial force that the section can bear. The relative moment, induced by the force eccentricity, will be the ultimate resisting moment of the cross section (Figure 5.10).

The analysis of the stone is fully satisfied. The stone is in fact too massive to have any problem of shear or moment failure because of the wind.

5.5 Conclusions

Both the designed cross and the stone are fully satisfy the codes requirements. The cross would be fully safe in the whole scenarios. It results well designed against the bending load induced by the wind, the worst load case.

It is different the situation of the kinematic analysis. The requirements are, in fact, not satisfied. The problem may be due to wrong mechanical assumptions: the assumption of not fixity of the base stone respect to the underlying structure, a wrong consideration of the load distribution or a coarse simplification of the system. On the other end, some of the factors prescribed by the Eurocode could be excessively restrictive in reality: it is important to recall that, even if the base would be unclamped and just supported, the element is standing on the tower approximately a century without suffer any previous collapse.

The easiest solution for the system will be, once the real supports will be checked, design a proper clamp of the cross to the base and of the base to the spire. The cross and the stone themselves are, however, well design and fully satisfy the code requirements.

6. ASSESSMENT OF DAMAGE INDUCED BY THE INTERVENTION

6.1 Introduction

The analysis of the monitoring data and their correlation with the ongoing works is crucial to understand if the intervention is interfering somehow with the structure. The aim of this chapter is report and describe the development of the data until the beginning of the strengthening, considering the trend of both crack developing and towers tilting. After that, the daily works will be reported and briefly described. Finally, the data involving the executive period will be analyzed in order to check the presence of harming of the structure.

6.2 Analysis of the monitoring data until the works

As described in Chapter 3, a monitoring campaign of the building has been ongoing since April 2009. The building has been analyzed below both static and dynamic conditions. This paragraph is focused on the analysis of the static system, namely the crack meter and the tilt meter devices, until the beginning of the executive works in May 2014. Thanks to the huge amount data, taken since five years, it is possible to determine and filter noise and seasonal fluctuations, in order to determine the significant structural movements recorded.

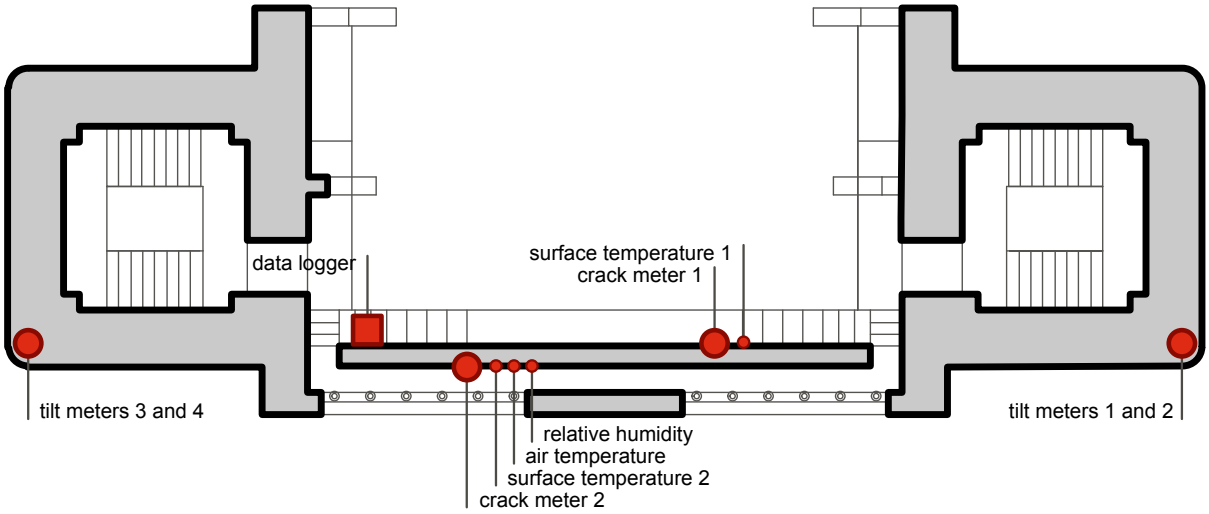

Figure 6.1: Position of the device used for the monitoring of S. Torcato

Two crack meters, four tilt meters, and various thermometers have been placed in the building (Figure 6.1). The instrument collected data in Volts, that can be translated in physical values by means of specific calibration factors (Table 6.1). The starting value of the raws data has been placed to zero, in order to evaluate relative displacements. A strong reduction of the noise of the output has been achieved considering a moving average of seven days in the recorded data.

	Factor
Crack meter 1	-25,7271
Crack meter 2	25,7759
Tilt meter 1	-5,8808
Tilt meter 2	-5,9353
Tilt meter 3	-5,5615
Tilt meter 4	-5,7176

Table 3.1: Factors used for the calibration of the devices

6.2.1 The crack data

Crack 1 and 2 are both at the vault extrados level: the first is in the interior side of the façade wall while the second is on the exterior balcony. Such values have been compared with relative humidity and exterior temperature. These last two values are, however, strictly related whereas the crack behavior could be compared just with temperature. The comparison with the surface temperature and the crack behavior has been neglected because the difference with the exterior temperature graph is practically null, with the exception of an imperceptible phase shift induced by the thermal capacity of the masonry.

Considering the graph of the crack behavior (Figure 6.2), it can be inferred that a period of strong drop of temperature values trigs a rushed development of crack width. On the contrary a long period of warmer temperature affects less the behavior of the crack, resulting in a more continuous and ruched part of the graph. These evaluation are of course more noticeable on the second crack: being the device on the exterior, its behavior is much more affected by environmental conditions than the interior one, protected by the building envelope.

It is possible to infer that the cracks reflect perfectly the temperature trend with a small phase shift, probably do to the thermal characteristics of the structure. The crack width behavior is, however, inverse to the temperature development: when the temperature drops the width increases, while it decreases when the exterior temperature goes up. The behavior of the slits is not perfectly cyclic, that means that there is always a residual value of width not recovered after a warm-cold cycle. This difference demonstrates the presence of a damage, still in development. The global trend is the increasing of width for both cracks, equal to 0,0590 mm/year mm/year for Crack 1 ad 0,0574 mm/year mm/year for Crack 2. This value has been calculated considering the average trend of the five years of monitoring. The first crack results less active even if the graph shows a higher amplitude with respect to the other. This could be induced by the sensible change of the very last period of the recorded data: the important drop, however, cannot be attributed systematically to a stabilization of the crack, a longer period should be analyzed in order to evaluate this possibility precisely. More discussion on this topic will be carried out in the last paragraph of the present chapter.

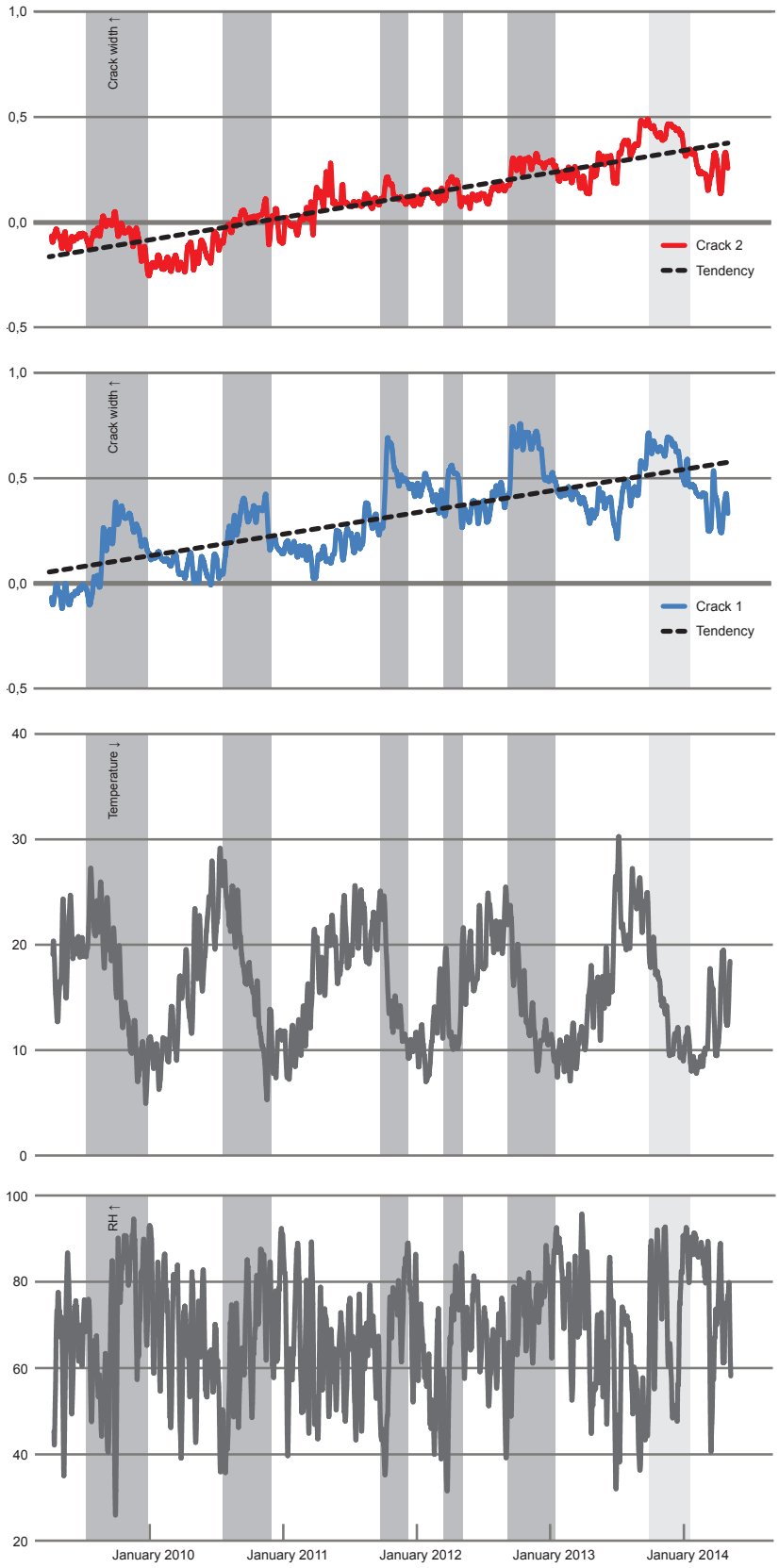

Figure 6.2: Analysis of the crack monitoring data. The gray pattern shows the behavior of the slits: both cracks width increase when the temperatures drop down and the humidity increases, whit the exception of the area marked with a lighter gray

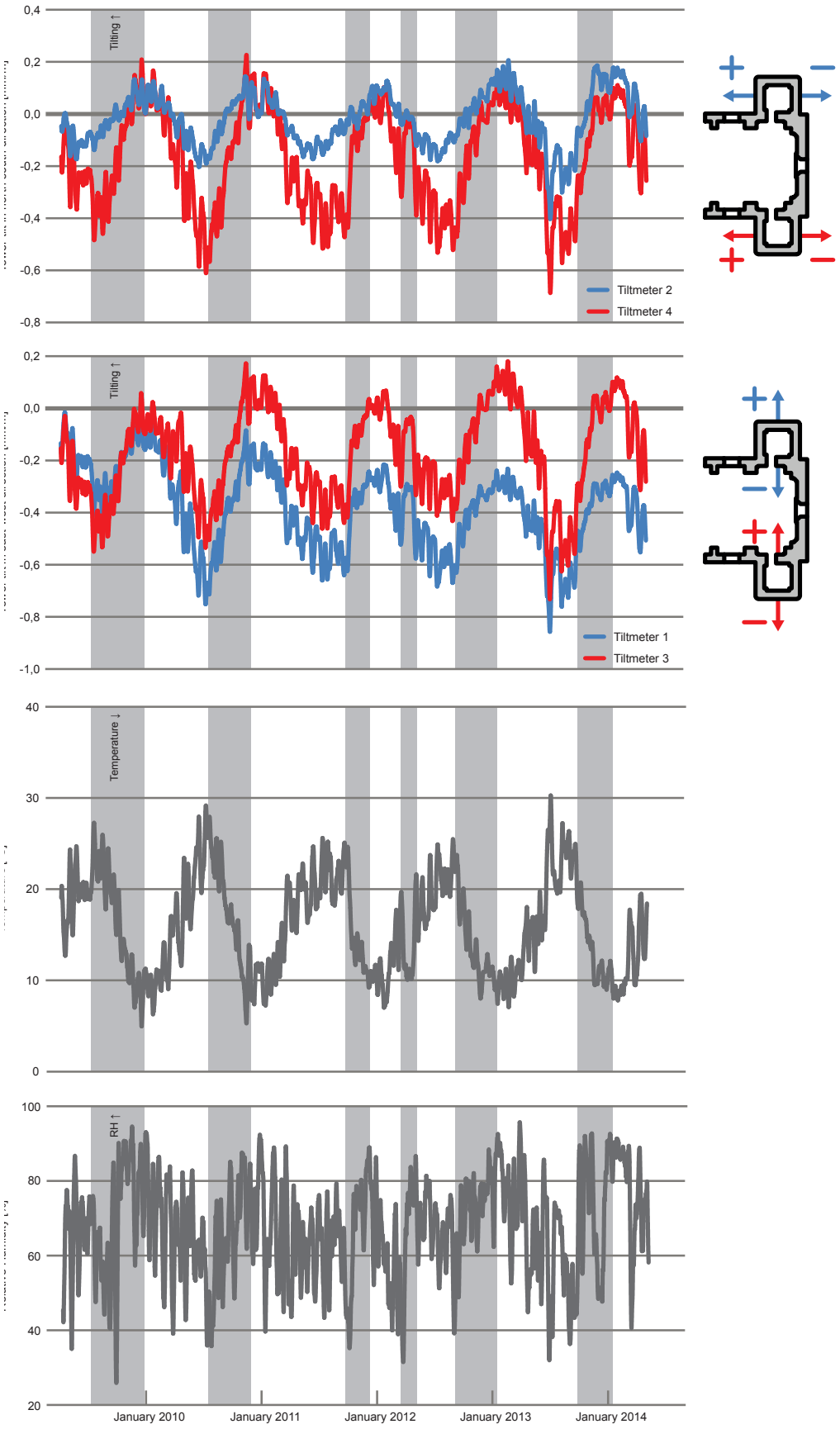

Figure 6.3: Analysis of the tilting monitoring data. The gray pattern shows the behavior of the towers with respect to the environmental conditions

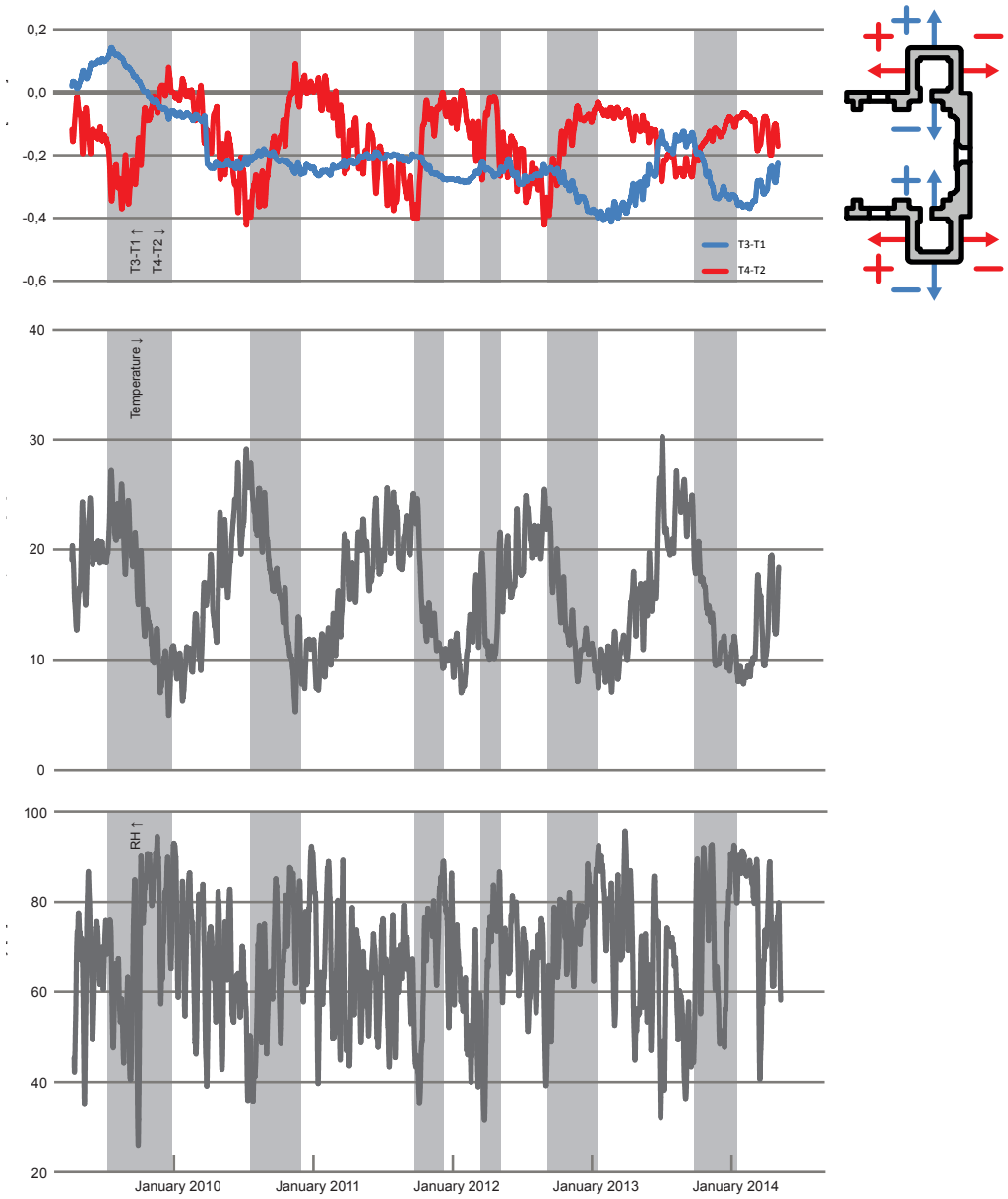

Figure 6.4: Differential behavior of the towers shown by the tilting monitoring data. The gray pattern shows the behavior of the towers with respect to the environmental conditions.

6.2.2 The tilt data

Two tilt meters have been placed at the bells level of each tower, in order to collect the horizontal rotations of such structures. As shown in Figure 6.3, Tilt meter 1 and 2 have been placed on the right tower in order to analyze the rotations in east-west direction (Tilt meter 1) and north-south direction (Tilt meter 2). The others two sensors have been placed in the left tower for the same purpose: analyzing the movement in east-west direction (Tilt meter 3) and north-south direction (Tilt meter 4).

Even in this case it is possible to consider the strict relation with the structures trend and the exterior temperature. It can inferred from the graph that the towers move basically in the same direction (Figure 6.4). The pattern of the displacements fits perfectly with seasonal fluctuation: a decrease of tempera-

Figure 6.5: The removal of the granite stones: (a) marking of the exterior stones (b) the external foundations exposed (c) first phase of the intervention (d) removal of important details (e) the internal foundations exposed

tures induces a movement of the towers to the eastern and southern sides, while higher temperatures lead to a rotation toward the western and northern sides. Moreover, the amplitude of tilting of the left tower results more prominent than the other one. This fact could invigorate the idea of differential settlements inferred from geotechnical analysis and confirms the conclusion of previous surveys and monitoring discussed in Chapter 3. The main results of the monitoring campaign are visible in Table 6.3.

	Tilt 1	Tilt 2	Tilt 3	Tilt 4
Trend [mm/m]/[year]	-0,0239	0,0025	0,0114	0,0041

Table 3.2: Trend of the towers behavior in terms of tilting

It is really interesting to compare the relative tilting of the towers (Figure 6.4). The difference is much more marked for tilting out of the façade plane (Tilt meter 4 and 2) than for the in-plane movements. This difference could be induced by the structural scheme of the church and the relative rigidity of the walls: the movement out of plane could be less restricted than the in-plane movement. Moreover a step drop of the difference between Tilt meter 1 and 3 is visible around February 2010: the reason of this phenomenon are unknown, but could represent a change induced by an intervention on the church.

6.3 Analysis of the design execution

The works on the building started the in the middle of May 2014 and are still ongoing while this thesis is being written. Unfortunately, the part of works that could be more invasive for the structure will be carried out in the future. It could be interesting, however, to report the development of the works and make a crosscheck with the data to identify a possible interference on the building induced by the intervention.

The execution carried out on the building until now are the basic step of the two main interventions. The holes for the anchoring of the ties system has been completed in the beginning of June 2014. The drilling and the grouting of the micro-piles on the exterior of the tower have been completed in the second week of July 2014, date in which the interior coring started.

6.3.1 Preparation of the works

A visual inspection was performed approximately one month before the effective beginning of the works. It was necessary to verify the real shape of the foundation both in the exterior side of the towers than in the interior one. For this purpose, the external pavement of both towers have been removed, taking care of mark and catalogue each stone, and the exposed soil has been dug until a suitable depth. The interior side of the towers has been worked in the same way, paying attention to important decorative elements stocked there (Figure 6.5).

6.3.2 Anchoring system execution

The works regarding the installation of the anchoring system of the towers started on the foundation strengthening started on 6^{h} of May 2014. On that day the coring of the walls started on the perimetric walls of the choir level. A special drill with diamond-cut technology was used to perform the holes neces-

Figure 6.6: The anchoring system installation on S. Torcato: (a) coring procedure at choir level (b) coring procedure at attic level (c) the collected and cataloged specimens (d) the holes performed in the structure (e) scheme of the specimen cataloging

sary for the further anchoring system. It was not necessary to remove any stone of the pavement during the drilling, which took a couple of days to be completed.

On 19h of May the same operation was carried out at the attic level, on the walls on top of the extrados. That time was necessary to built a specific scaffolding to reach the necessary height imposed by the design. Even this time a couple of days were necessary to finish the work (Figure 6.6).

The execution of the anchoring system is still stationary since the conclusion of the coring. The works will proceed soon after the completion of the whole foundation strengthening process.

The cores of the towers, wastes of the drilling operation, are valuable items that could be used to improve the knowledge of the mechanical properties of the church. For this reason, four specimen per drill have been collected and cataloged, using the logical scheme that is visible in Figure 6.6. Those samples could be analyzed in the future, for instance by means of uniaxial compressive tests performed in laboratory. The characteristic of the material could be, in this way, effectively compared with the ND tests previously performed (Chapter 3), in order to update the granite parameters and calibrate further analysis.

6.3.3 Micro-piles execution

The works on the foundation strengthening started on 20th of July 2014. On that day the perforation of the micro-piles started in the perimeter of the left tower. The foundation were exposed until 1,8 m in order to check the reliability with the drawings. The accuracy was good, even if the foundation were less regular. A problem, however, was found: the constructive technique used for build the foundation of the right tower was coarse. Instead of the regular blocks used for the other tower, various small cut stones were used and bonded with mortar. This could lead to the needed of strengthen such part.

All the holes of the same side had been completed before move to the other tower. The perforation until 21 meters was achieved by means of a special auger mounted on a drilling-machine controlled by an operator. Once the holes had been completed, micro-piles would be inserted on the holes and filled with cement (Figure 6.8).

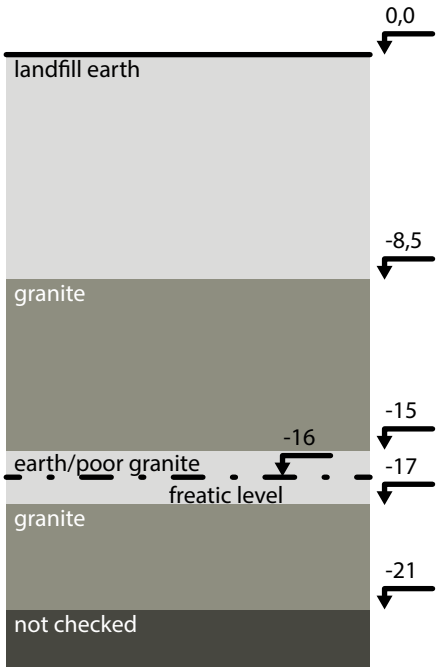

Figure 6.7: section inferred by the different soil resistance discovered during the perforations

The micro-piles used for the design had to be of 8,5 cm of diameter and 8,5 mm of thickness. However, the pipes used for the operation that were found in the yard were recycled from different stocks of the oil industry. Thus, it was possible to identify three groups of piles, depending on their condition: there were piles in good status, piles with average level of rust and piles completely rusted. Moreover, the thicknesses of the piles were variable.

(a)

(b)

(c)

(d)

(e)

Figure 6.8: The strengthening of the foundation: (a) perforation of the soil until 21m (b) installation of the micro-piles (c) coring of the interior of the towers (d) the block resulting of the coring procedure (e) marking of useless micro-piles

For this reason a check of the effective dimension was performed on 23th of June 2014. There were no problem with the requirements, because the minimal dimension discovered was 9,3 mm and maximal 11,6 mm, higher than the value prescribed. On the same day the third hole was being completed.

On 25th of June 2014 all the holes of the left tower were completed and the intervention on the right tower started. Pipes in a too bad conditions were marked in order to replace them. A new cross section of the soil could be drawn thanks to perforation (Figure 6.8).

On 30th of June 2014 the perforation works were complete and the placement of the holes started.

On 4th of July 2014 the intervention on the interior of the right tower started, even if four piles had still to be filled with concrete on the exterior side. Eight cores were extracted with a special device in order to preserve the historic pavement and replace it once the works would be finished. A new stock of brand-new piles arrived on site for the interior micro-piles.

On 10th of July 2014 the micro-piles still unfinished were filled with concrete. The coring of the left tower interior pavement started that day. The perforation of both towers will begin in the near future.

6.4 Monitoring during the construction and conclusions

The static monitoring data was checked during the construction process. The analysis of the data do not show any relevant arouse of interference on the structure induced by the intervention. Both crack meters and tilt meters seem to follow the regular trend conditioned by the environmental conditions. It is true that the graph is much more ruched and noisy respect to the previous periods. This condition, however, can be induced by the irregular variation of the weather in the last period. The data are plotted in Figure 6.7 (for simplicity are shown just two tilt meters and the crack meters).

The global behavior defined by the monitoring data is the following: the cracks are still active and the towers move each time in the same direction. Their trend is strictly correlated with environmental factors. The cracks grow and the towers move relatively towards each other during temperature drops and the

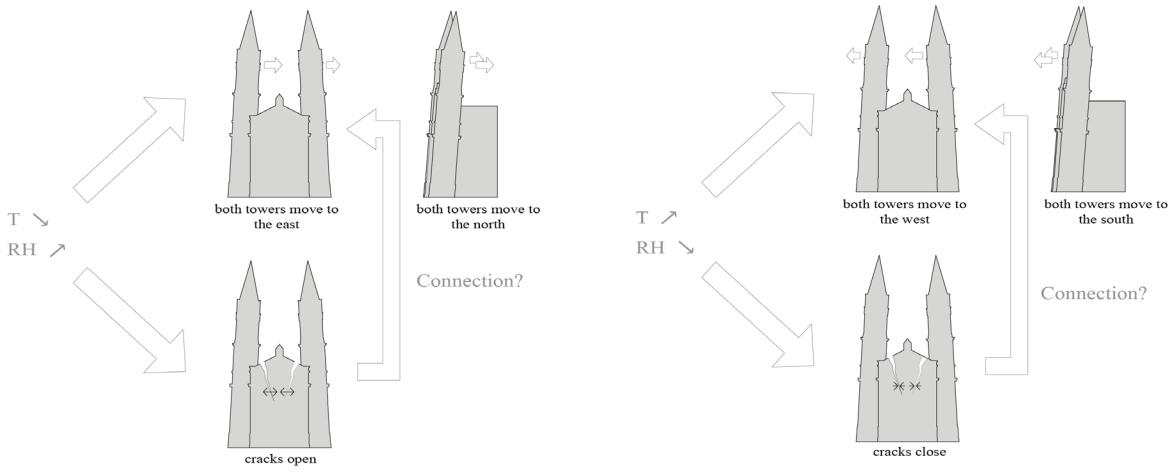

Figure 6.9: Global behavior of the structure in relation with environmental effects (Gutscoven, 2014)

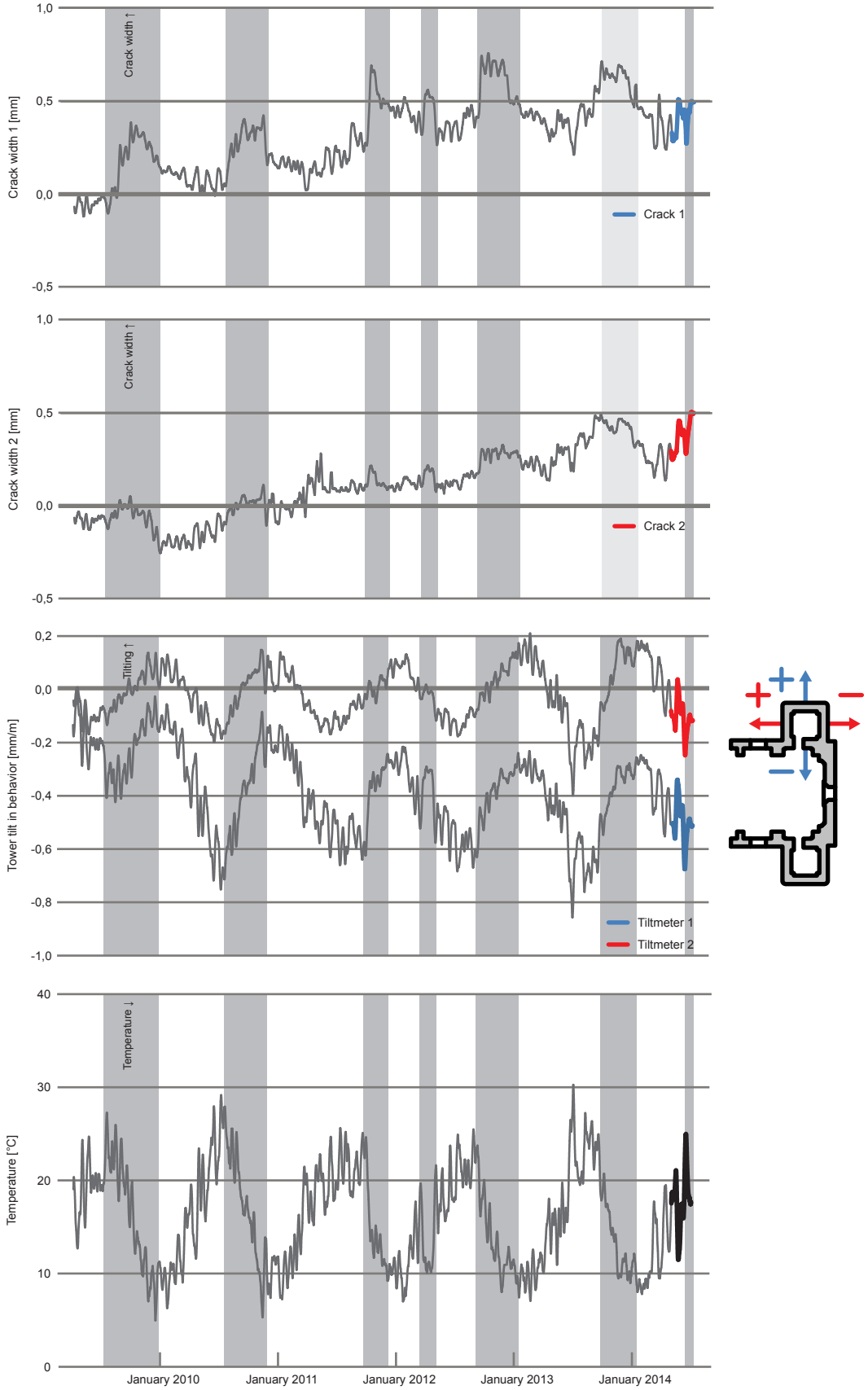

Figure 6.9: Analysis of the tilting and cracking monitoring data during the executions. The colored part shows the effective period of work. The gray pattern shows the behavior of the towers with respect to the environmental conditions

relative humidity incrementation: jumps on the cracks appear for rushed decrement of temperature and fast increase of the relative humidity. The opposite behavior is verified in case of increment of temperature and drop of relative humidity (Fig 6.9).

The lack of information regarding the interference induced by the works was expected. In fact, as previously discussed, the execution of the works with should involve more invasive operations have not being carried out yet. Moreover, the intensity of the work have been pretty low and have been spread in a too wide period. This means that possible interference will be visible in longer terms, probably with the order of magnitude of a monitoring cycle.

The comparison of the trends discovered in the previous analysis is an hard task. First of all because both position and system of analysis were changed since the first monitoring. Secondly because the relative range of time used for such comparison is different. The results, however, seems to show a reduction of the crack and tilting activity. The last period of the graph seems to show a reduction of the trends of each sensor. This condition, however, could be induced by the irregular variation of the weather of the beginning of summertime. For the same reason, the damage cannot be considered in phase of stabilization. Conclusion about this last hypotheses could be inferred once the seasonal fluctuation will finish its cycle (most likely next Autumn).

A resume of the data is visible in the following table.

Trend	Ramos (1999)	Ramos (2012)	Gutscoven (‘14)	Personal
Crack meter 1 [mm/year]	0,05 - 0,09	0,1 - 0,15	0,0809	0,0590
Crack meter 2 [mm/year]	-	0,1 - 0,15	0,0959	0,0574
Tilt meter 1 [mm/m/year]	$8,2 \times 10^{-5}$	$15 - 25 \times 10^{-3}$	-0,0497	-0,0239
Tilt meter 2 [mm/m/year]	$8,2 \times 10^{-5}$	$15 - 25 \times 10^{-3}$	0,0036	0,0025
Tilt meter 3 [mm/m/year]	$8,2 \times 10^{-5}$	$15 - 25 \times 10^{-3}$	0,0262	0,0114
Tilt meter 4 [mm/m/year]	$8,2 \times 10^{-5}$	$15 - 25 \times 10^{-3}$	0,0072	0,0041
T3-T1 [mm/m/year]	-	-	not comparable	-0,0345
T4-T2 [mm/m/year]	-	-	not comparable	$-9,5 \times 10^{-3}$

Table 3.3: Comparison of the different trends discovered during previous analyses

7. CONCLUSIONS AND REMARKS

The church of São Torcato, completed in 2008, was investigated considering its historical framework, which passed through various project managers and suffered lots of changes, nowadays reflected in its wide range of materials and constructive techniques. During the construction, the appearance of several structural anomalies of medium and high intensity, identified since 1976, prompted the beginning of a careful examination of the building.

Detailed investigation campaigns were able to build a complete picture of the mechanical characteristics of the temple and the causes which trigged the existent damage phenomena. All the studies and monitoring have been listed and reported chronologically in order to understand the actual level of knowledge of the church and offer a strong support for further investigation on it. The last ten years of investigations, enhanced both by a technological and by cognitive improvements, were able to circumscribe the most likely sources of the problems. The crack pattern is mainly caused by a differential soil settlement: the entrance part and the towers are basically sinking according to the heterogeneous distribution of mechanical resistance of the different soil layers. Besides defining the causes of the damages, it was possible to determine the mechanical properties of the structure, as well as its dynamical characteristic.

An effective system of interventions was design in order to face the problems on the church. Firstly, it was decided to directly transfer part of the tower weight to the resistant bedrock, by means of micro-piles, in order to solve or at least reduce the effect of the soil settlements. Secondly, a systems of steel ties anchored to the towers would be able to solve the differential leaning of the towers and the subsequent splitting of the façade in different macro-blocks, ensuring the monolithic behavior of the church. Finally, the cracks would be fixed with a suitable grouting system. A cross-check was carried out on such intervention to confirm its reliability and check the parts which could be enhanced: thanks to these changes, it was possible to rearrange the distribution of the actions in a more appropriate way, reducing maximum bending moment and shear action applied on the structural reinforcement without increase the number of its elements.

Furthermore, several minor works have to be carried out to retrofit or repair some valuable parts of the building. Among others, the design of the crosses on top of both spires has been addressed in the present thesis, in order to evaluate the real possibility to replace them accordingly with the actual requirements. Three different models were considered and analyzed: two limit state analyses satisfied the restrictions imposed by Eurocode while the kinematic one did not. The problem of this last model may be due to wrong mechanical assumptions or to the presence of too restrictive factors prescribed by the Eurocode: it is important to recall, however, that the element is standing on the tower approximately a century without suffering any previous collapse.

A deep analysis on the static monitoring data was carried out to know the specific trend of the building behavior: the towers move in the same direction accordingly to the temperature cycle, as well as for the crack opening. It was possible to infer that such phenomena indicate a damage of the building still in development. Afterwards, an attempt to evaluate the damage induced by the execution of the intervention was made. Unfortunately, the works on the building, which started the 6th of May 2014, are still

ongoing while this thesis is being written and the part that could be more invasive for the structure will be carried out in the future. The analysis of the works in progress did not show any relevant detail about the interference of the structure. The intensity of the work has been pretty low and has been spread in a too wide period. This means that possible interference will be visible in longer terms, probably with the order of magnitude of a monitoring cycle. Moreover, Conclusion about the possible stabilization of the crack could be inferred once the seasonal fluctuation will finish its cycle

The future tasks will have to take into account the effective development of the intervention works and the comparison with static and dynamic monitoring data. Moreover, an analysis with the dynamic data should be performed, because such devices are able to record structural variations in a more precise way. It is also necessary to perform more specific computational analysis regarding the mechanical behavior of the building considering cracked models and FEM that contemplate both settlement and thermal condition at the same time. Furthermore, several direct tests should be carried on the intervention wastes (such as coring samples) in order to evaluate the reliability of the non-destructive tests performed on the structure. The effective clamping system of the cross have to be studied, in order to define a more suitable and reliable kinematic model of the element-stone system. Finally, the real efficacy of the designed intervention should be considered: if the problems of the building persisted, it would be necessary to perform a more invasive and expensive intervention.

8. REFERENCES

• Alaboz M., Dynamic Identification and Modal Updating of S. Torcato Church, SAHC Master Thesis, University of Minho, Guimarães, 2009

• Baptista T. A. Maria Regina D., Arquitectura neomedieval portuguesa 1780-1924, vol. I and II, Fundação Calouste Gulbenkian, Lisbon, 1997

• Betzer R., Guzman A., Mordanova A., Vanin F., Inspection and diagnosis of S. Torcato church, SAHC Master, 1st SA4 assignment, Guimarães, 2013

• Binda, L., Drdácký, M. and Kasal, B., In-situ evaluation and non-destructive testing of historic wood and masonry structures, ITAM, Prague, 2006

• Consiglio Superiore dei Lavori Pubblici, Nuove Norme Tecnica dper le Costruzioni, NTC-2008, 2008

• EU, Eurocode 1: Actions on structures - General actions, UNI EN 1991-1-1, 2004

• EU, Eurocode 2: Design of concrete structures - Part 1-2: General rules, UNI EN 1992-1-1, 2005

• EU,Eurocode 3: Design of steel structures - Part 1-2: General rules, UNI EN 1992-1-1, 2005, UNI EN 1991-1-1, 2004

• Faccelli G., Gowda C., Meignen F., Mouyiannou A, Inspection and diagnosis of S. Torcato church, SAHC Master, 1st SA4 assignment, Guimarães, 2013

• Faccelli G., Meignen F., Toesca M, Vanin F., Non-destructive tests on S. Torcato, SAHC Master, 3rd SA4 assignment, Guimarães, 2013

• Farmanara A., Greco F., Guimarães H., Sengun R., Inspection and diagnosis of S. Torcato church, SAHC Master, 1st SA4 assignment, Guimarães, 2013

• Greco F., Gowda C., Ogrizovic J., Betzer R., Non-destructive tests on S. Torcato, SAHC Master, 3rd SA4 assignment, Guimarães, 2013

• Guimarães H., Farmanara A., Mouyiannou A., Inspection and diagnosis of S. Torcato church, SAHC Master, 1st SA4 assignment, Guimarães, 2013

• Gutscoven E., Structural Anlysis of an Historic Building: S. Torcato church in Portugal, Master Thesis, University of Leuven, 2014

• Guzmán-Corredor A., Mordanova A., Roldan-Zamarron E., Sengun R., Non-destructive tests on

S. Torcato, SAHC Master, 3rd SA4 assignment, Guimarães, 2013

• J.C. Tavares, Dicionário dos Santos, Lello & Irmão Editores, 1990

• Lourenço P. B., Ramos L. F., Investigação sobre as patologias do Santuário de São Torcato. Relatório Final, Final report on investigation of S. Torcato church, University of Minho, Guimarães, 1999

• Manning E., Ramos L. F., Fernandes F., Verstringe E., Ferreira J., Mendes P., Assessment of S. Torcato Church: nondestructive survey and proposed measures, Report, Programa Operacional Factores de Competitividade, 2013

• Mayank M., A Bayesian approach to NDT Data Fusion for St. Torcato Church, SAHC Master Thesis, University of Minho, Guimarães, 2013

• Merluzzi N., Lee H., Suganya K., Wan I., M., Integrated project - St. Torcato Church, SAHC Master, SA7 integrated project, Guimarães, 2008

• Multiple Authors, SAHC lectures, various courses, 2014

• Ogrizovic J., Roldan-Zamarron E., Toesca M., Yavari A., Damage assessment and diagnosis of S. Torcato church, SAHC Master, 1st SA4 assignment, Guimarães, 2013

• Ramos L. F., Aguilar Rafael, Lourenço P. B., Moreira S., Dynamic structural health monitoring of Saint Torcato church, paper published in Mechanical Systems & Signal Processing, vol. II n°1-2, Elsevier, 2012

• Sánchez-Aparicio L. J., Estudio de patologías con carácter estructural mediante la hibridación de sensores, PHD Thesis (Still in progress), University of Salamanca

• Sánchez-Aparicio L. J., Riveiro B., Gonzalez-Aguilera D., Ramos Luís F., The combination of geomatic approaches and operational modal analysis to prove calibration of Finite Element Models: a case study in San Torcato (Guimarães, Portugal), Journal: Construction and Building Materials, 2014

• Vasconcelos G. F. M., Experimental investigations on the mechanics of stone masonry: Characterization of granites and behavior of ancient masonry shear walls, PHD Thesis, Universidade do Minho, 2005

A. ANNEX A: PHOTOGRAPHIC SURVEY

A.1 Historic plans and photos

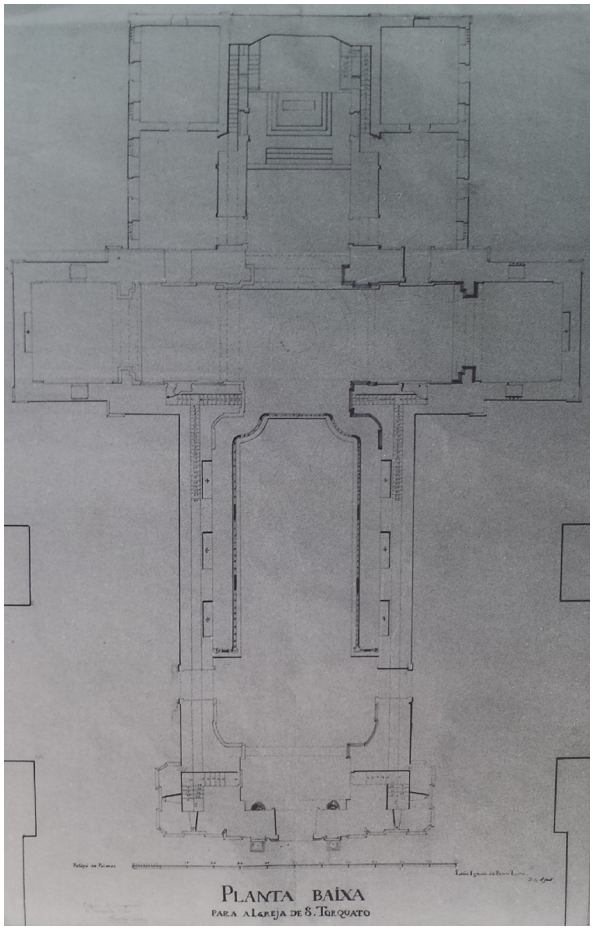

(a)

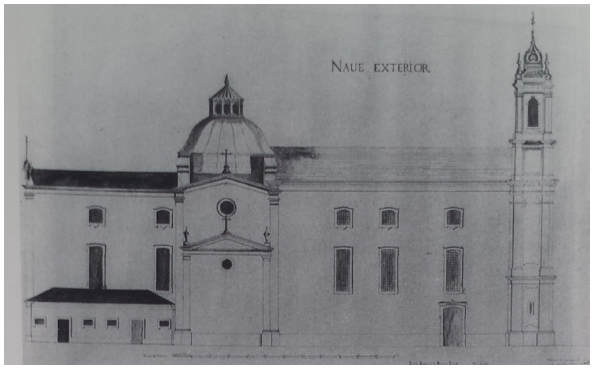

(b)

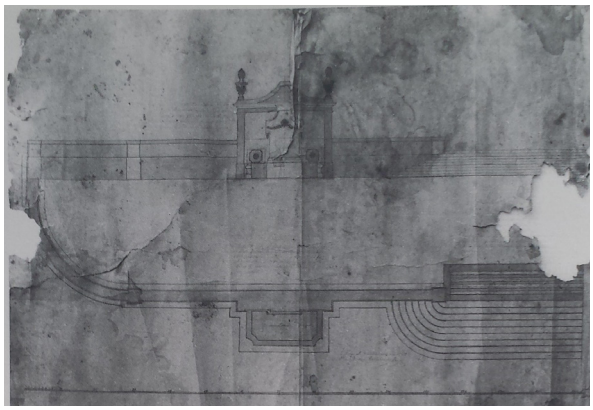

(c)

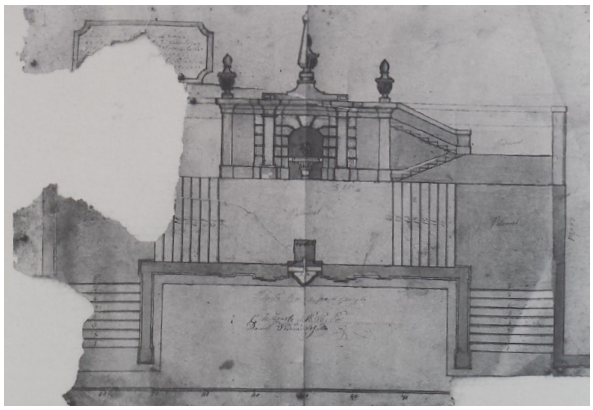

(d)

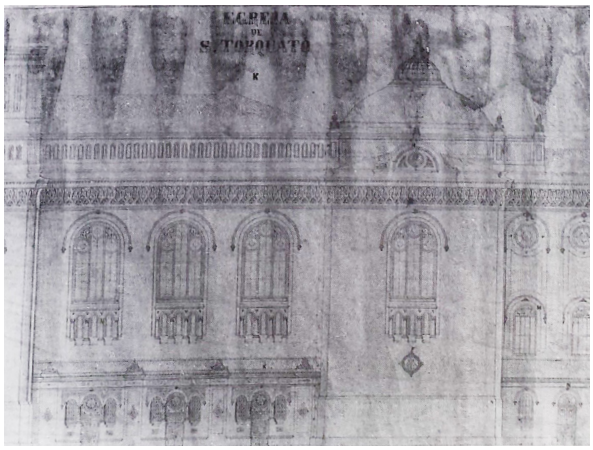

(e)

Figure A.1: (a) plan of S. Torcato made by the architect Barros Lima, 1824 (b) “Naue exterior” from Barros Lima, 1824 (c) first project for the fountain and the entrance staircase made by Daniel Fernandes, 1857 (d) second project made by Daniel Fernandes, 1857 (e) façade of S. Torcato designed by Ludwig Bohnstedt (Baptista, 1997)

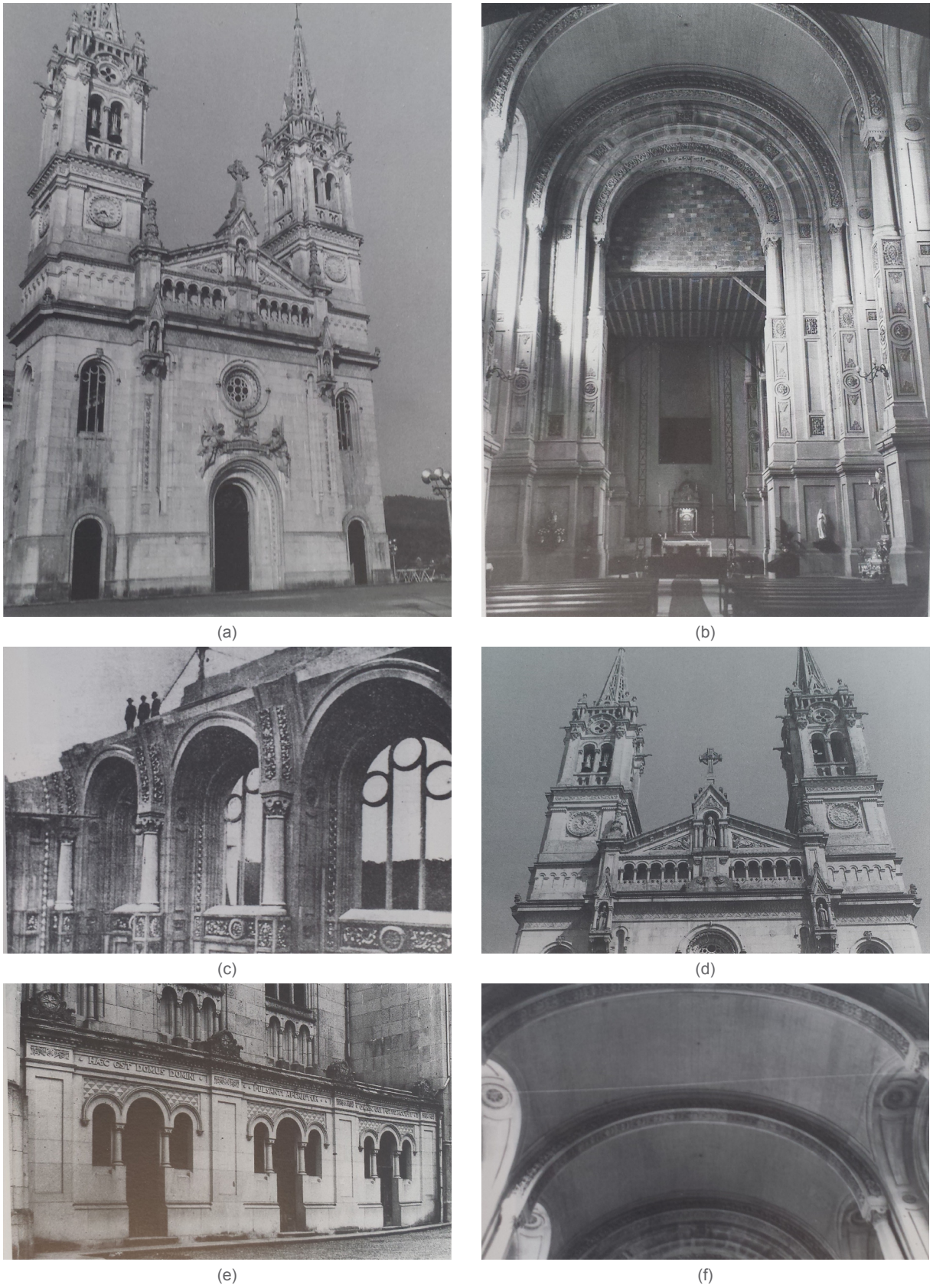

Figure A.2: (a) historical picture of the façade (b) the interior of the church during the construction of the dome (c) the church during the construction of lateral walls (d) a detail of the balustrade in a historical picture (e) lateral chapels added by Ludwig Bohnstedt (f) historical picture of the barrel vault (Baptista, 1997)

Figure A.3: (a) historical picture of tone of the towers (b) the statue of S. Damaso that adorn the façade (c) a picture of the entrance (d) the detail of the angels that decorate the entrance (e) intervention proposal of Moreira da Silva, 1954 (f) historical panoramic view of the church (Baptista, 1997)

(a)

(b)

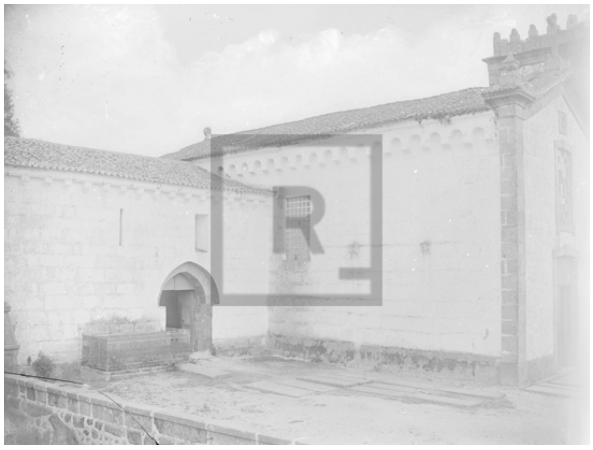

(c)

(d)

(e)

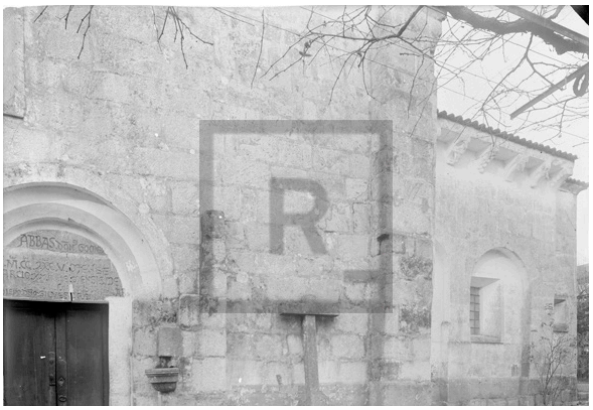

(f)

Figure A.4: (a) blazoned house close to the church of S. Torcato, middle of XX century (b) lateral view of S. Torcato,1912 (c) church of S.Torcato monastery, middle of XX century (d) the church with the right tower unfinished, between 1912 and 1928 (e) church of S.Torcato monastery, middle of XX century (f) church of S.Torcato monastery, middle of XX century (http://reimaginar.webprodz.com/)

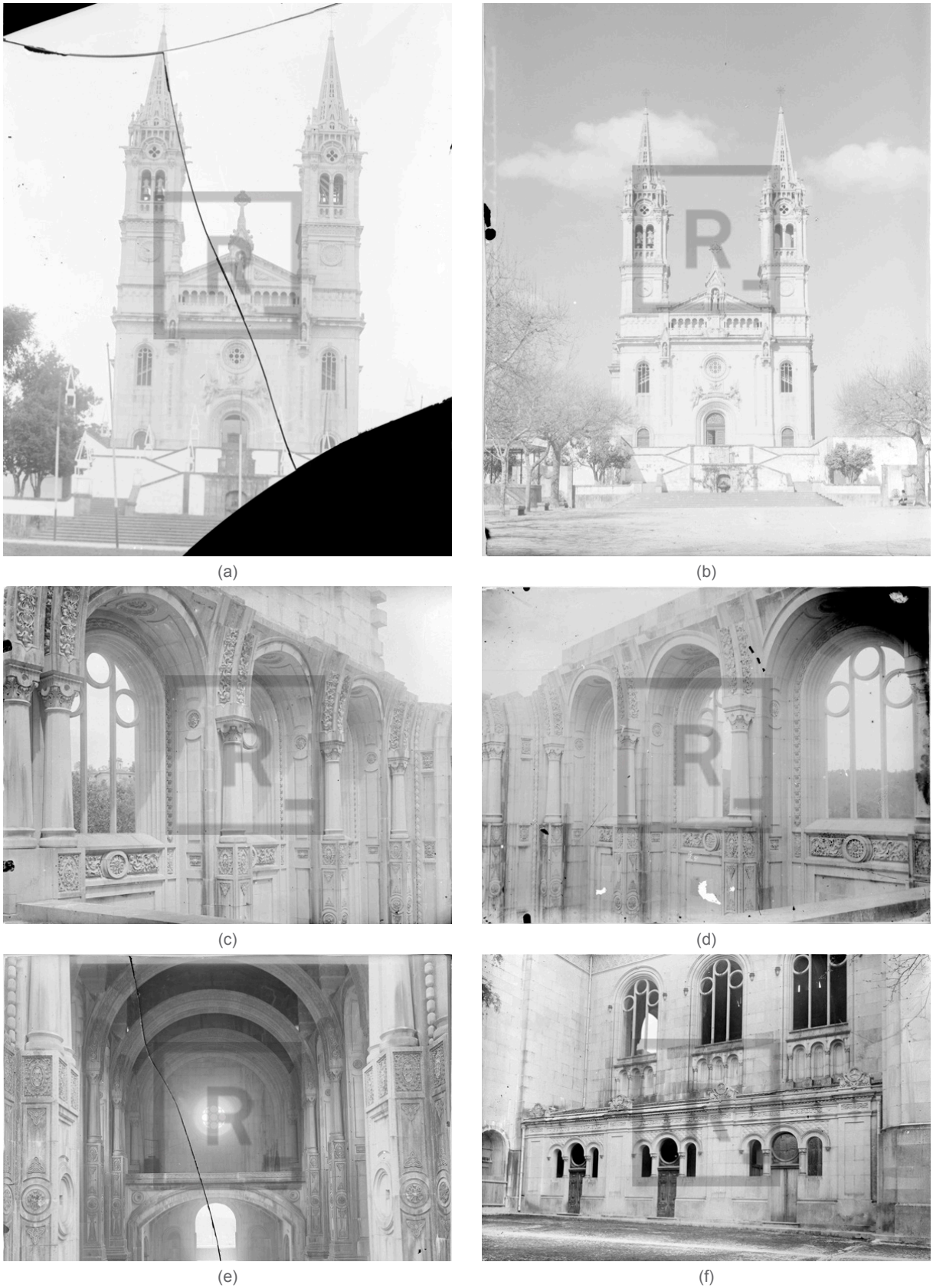

(a) (b)

(c) (d)

(e) (f)

Figure A.5: (a) front view of S. Torcato, between 1928 and 1946 (b) front view of S. Torcato, between 1928 and 1946 (c) interior of the church not completed, end of XIX century (d) interior of the church not completed, end of XIX century (e) interior of the church not completed, end of XIX century (f) exterior of the church not completed, end of XIX century (http://reimaginar.webprodz.com/)

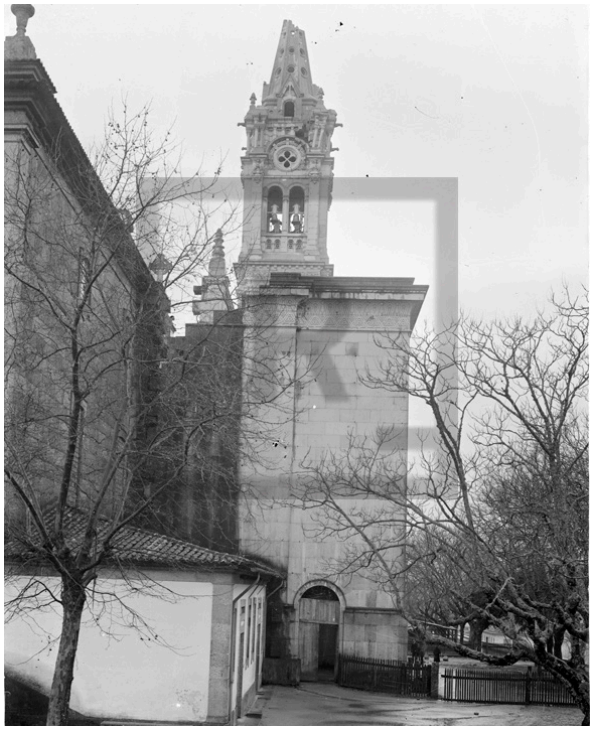

(a)

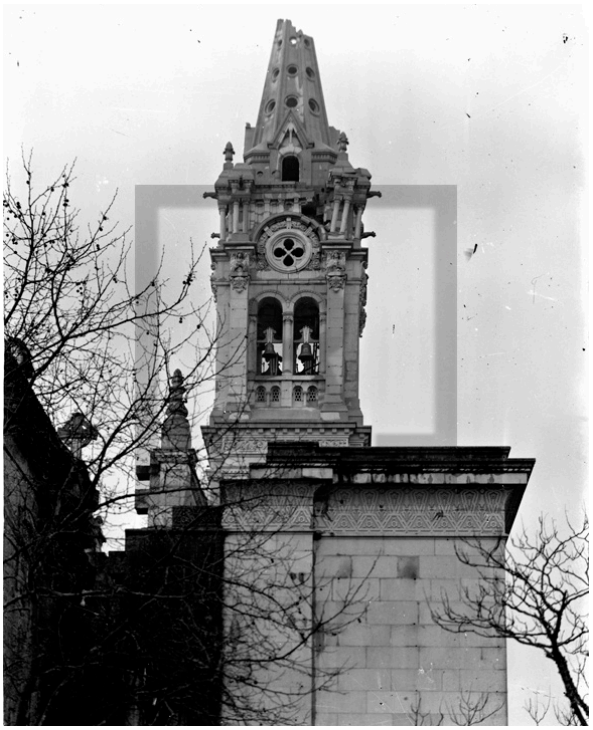

(b)

(c)

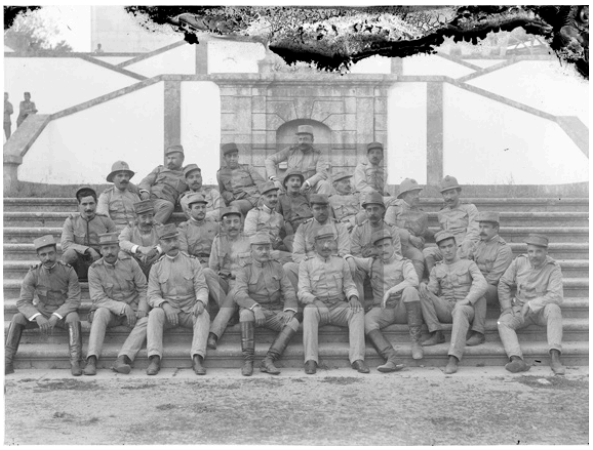

(d)

(e)

(f)

Figure A.6: (a) lateral side of S. Torcato, 1912 (b) lateral side of S. Torcato, 1912 (c) the church during visit of the arch-bishop of Braga, between 1915 and 1935 (d) Soldiers (20th infantry regiment) on the stairs of the curch, between 1910 and 1920(e) Soldiers (20th infantry regiment) Soldiers (20th and 16th regiment) on the stairs of the curch, between 1885 and 1911 (f) Soldiers (20th and 16th regiment) on the stairs of the church, between 1885 and 1911 (http://reimaginar.webprodz.com/)

(a) (b)

(c) (d)

(e) (f)

Figure A.7: (a) S. Torcato, between 1912 and 1948 (b) the church during the construction of the right tower, 1912 (c) the church during the construction of the right tower, 1912 (d) the church during the construction of the right tower, 1912 (e) pilgrimage on the church, between 1920 and 1940 (f) panoramic view of the church, between 1912 and 1928 (http://reimaginar.webprodz.com/)

A.2 Actual state

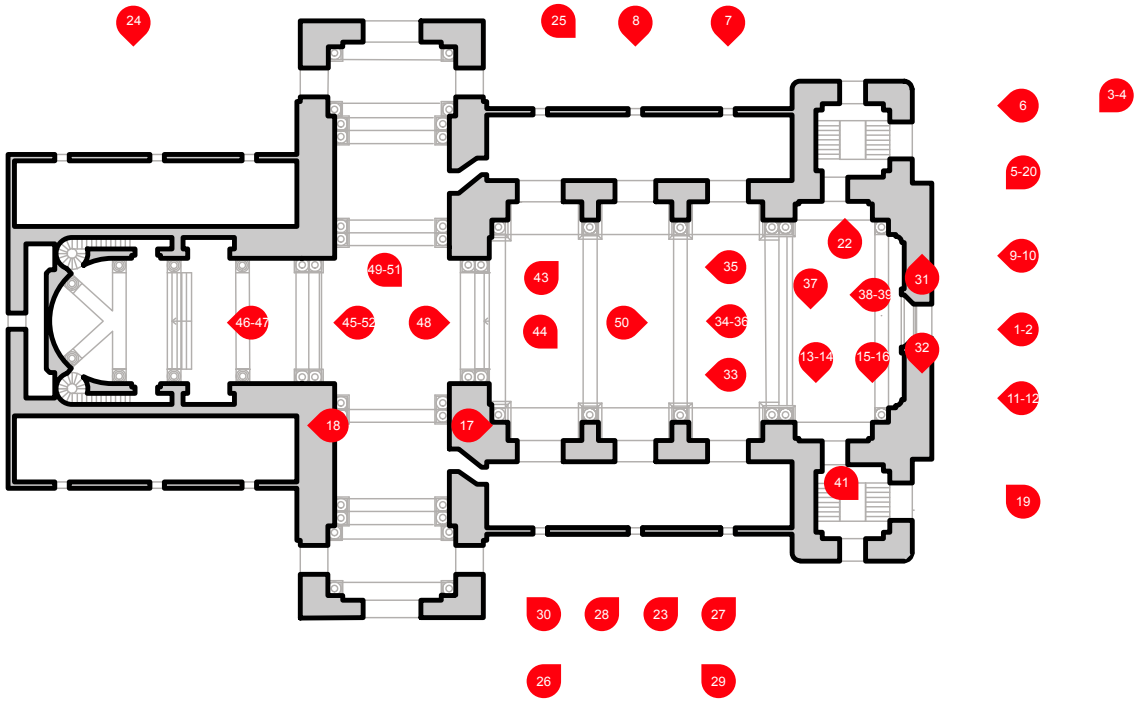

Figure A.8: Scheme of the photographic survey (personal work)

(1)

(2)

(3)

(4)

(5)

(6)

(7)

(8)

(9)

(10)


OVID VETRA
ADDENS
POTEST...
CVM ITA
GLORIFICA-
VERIS
SERVVM
TVVM

(11)

(12)

(13)

(14)

(15)

(16)

(17)

(18)

(19)

(20)

(21)

(22)

(23)

(24)

(25)

(26)

(27)

(28)

(29)

(30)

(31)

(32)

(33)

(34)

(35)

(36)

(37)

(38)

(39)

(40)

(41)

(42)

(43)

(44)

(45)

(46)

(47)

(48)

(49)

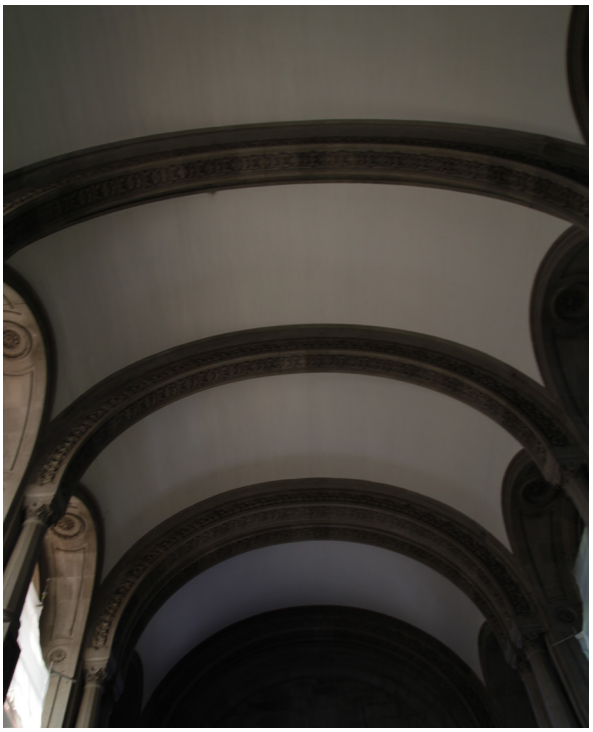

(50)

(51)

(52)

B. ANNEX B: CALCULATIONS

B.1 Strengthening cross-check

B.1.1 Geometry

$A_{base} := (60.83 - 5.20)\cdot m^2 = 55.63\,m^2$ Area of the foundation (without the central core)

$V_1 := 1249.62\cdot m^3$ Tower volume

$V_2 := 47.97\cdot m^3$ Stairs volume

$V_3 := 16.53\cdot m^3$ Spire volume

$V_4 := 116.00\cdot m^3$ Foundations volume

$V_{tot} := V_1 + V_2 + V_3 + V_4 = 1.43 \times 10^3\cdot m^3$ Total volume

B.1.2 Design Force

$\rho := 26\cdot\frac{kN}{m^3}$ specific weight of the granite

$\psi_P := 1.2$ partial factor of dead load

$P := \psi_P\cdot\rho\cdot V_{tot} = 44.62\cdot MN$ Total dead load

$\alpha := 20\%$ Transferred load percentage

$N_\alpha := P\cdot\alpha = 8.924\cdot MN$ Total design force

$\sigma_\alpha := \frac{N_\alpha}{A_{base}} = 0.16\cdot MPa$ Average normal stress at the tower base

B.1.3 Connectors Design

$A_{conn.tot} := 24.49m^2$ Area of influence for all connectors

$V_{\alpha.conn.tot} := \sigma_\alpha\cdot A_{conn.tot} = 3.929\cdot MN$ Total shear applyed to area of influence

$n_{conn} := 16$ Number of connectors

$V_{\alpha.conn.simply} := \frac{V_{\alpha.conn.tot}}{16} = 245.537\cdot kN$ Approximated value per connector

$A_{conn} := (3.57 + 0.87)m^2 = 4.44\,m^2$ Area of influence for the connector, worst case

$V_{\alpha.conn.Ed} := \frac{\sigma_\alpha}{2}\cdot A_{conn} = 356.124\cdot kN$ Design shear applyed to the connector

$V_{\alpha.conn.tot.Ed} := V_{\alpha.conn.Ed}\cdot 16 = 5.698\cdot MN$ Total shear considering the same load per connector

$i_{conn} := \frac{V_{\alpha.conn.tot.Ed} - V_{\alpha.conn.tot}}{V_{\alpha.conn.tot.Ed}} = 31.053 \cdot \%$ increase of the shear

$V_{\alpha.conn.Ed} = V_{\alpha.conn.Rd}$

$f_{yk.conn} := 450 \cdot MPa$ characteristic strenght of connector steel

$f_{yd.conn} := \frac{f_{yk.conn}}{1.15} = 391.304 \cdot MPa$ design strenght of connector steel

$d_{conn.min} := \sqrt{\frac{\sqrt{3} \cdot 4}{\pi \cdot f_{yd.conn}} \cdot V_{\alpha.conn.Ed}} = 44.8 \cdot mm$ minimum diameter of the connector

$d_{conn} := 45mm$

$V_{\alpha.conn.Rd} := \frac{\pi \cdot f_{yd.conn}}{\sqrt{3}} \cdot \frac{d_{conn}^{2}}{4} = 359.31 \cdot kN$

B.1.4 Piles Design

$N_{pile} := 60000 \cdot kg \cdot g = 588.399 \cdot kN$ Maximal normal force resistance per pile

$n_{pile.min} := \frac{N_{\alpha}}{N_{pile}} = 15.166$ Minimun number of piles for the problem

$n_{pile} := 16$ Number of piles for predimensioning

B.1.5 Beam 1 loads

$l_1 := 1.62 \cdot m$ distance from the beam 1 to the middle of the foundations

$q_1 := \sigma_{\alpha} \cdot l_1 = 259.874 \cdot \frac{kN}{m}$ distributed load on the beam 1

$M_1 := 172.6 \cdot kN \cdot m$ Maximal moment applyed in beam 1

$S_1 := 379.9 \cdot kN$ Maximal shear applyed in beam 1

B.1.6 Beam 2 loads

$l_2 := 1.58 \cdot m$ distance from the beam 1 to the middle of the foundations

$q_2 := \sigma_{\alpha} \cdot l_2 = 253.457 \cdot \frac{kN}{m}$ distributed load on the beam 1

$M_2 := 214.2 \cdot kN \cdot m$ Maximal moment applyed in beam 1

$S_2 := 341.2 \cdot kN$ Maximal shear applyed in beam 1

B.1.7 Design Values

$M_{Ed} := M_2 = 214.2\,m\cdot kN$ Design moment

$V_{Ed} := S_1 = 379.9\cdot kN$ Design shear

B.1.8 Beam verification

B.1.8.1 Geometry

$b := 600\cdot mm \quad h := 1800\cdot mm \quad d_1 := 30\cdot mm \quad d := h - d_1 = 1.77\times 10^3\cdot mm$

B.1.8.2 Concrete CEM I 45,2 R

$f_{ck} := 45\cdot MPa$

$f_{cd} := \frac{f_{ck}}{1.5} = 30\cdot MPa$

B.1.8.3 Steel

$f_{vk} := 450\cdot MPa \qquad E_s := 200000\cdot MPa$

$f_{yd} := \frac{f_{yk}}{1.15} = 391.304\cdot MPa$

$A_{s.\beta} := 5\cdot\left(\frac{20\cdot mm}{2}\right)^2\cdot\pi = 15.708\cdot cm^2$ Area of steel on the upper part (yielded)

$A_{s2.\beta} := 4\cdot\left(\frac{20\cdot mm}{2}\right)^2\cdot\pi = 12.566\cdot cm^2$ Area of steel on the bottom (not yielded)

B.1.8.4 Verification (Bending)

Given

$$-0.8\cdot b\cdot x_\beta\cdot f_{cd} + A_{s.\beta}\cdot f_{yd} - A_{s2.\beta}\cdot\left[\frac{0.35\%}{x_\beta}\cdot\left(x_\beta - d_1\right)\right]\cdot E_s = 0$$

$\mathrm{Find}(X_\beta) \qquad X_\beta := 0.035\ m$

$\varepsilon_{s2.\beta} := \frac{0.35\%}{X_\beta}\cdot\left(X_\beta - d_1\right)$

$M_{Rd.\beta} := A_{s.\beta}\cdot f_{yd}\cdot\left(d - 0.4\cdot X_\beta\right) + A_{s2.\beta}\cdot\varepsilon_{s2.\beta}\cdot E_s\cdot\left(0.4\cdot X_\beta - d_1\right) = 1.077\times 10^3\cdot kN\cdot m$

$\frac{M_{Ed}}{M_{Rd.\beta}} = 19.882\cdot\%$ the beam is verified

B.1.8.4 Verification (Shear)

Verification of the beam neglecting the shear reinforcement

$b_w := b = 0.6\,m$ thickness of the beam (without consider the steel covering)

$d = 1.77 \times 10^{3}\,mm$

$$\kappa := 1 + \sqrt{\frac{200}{\left(1.77 \times 10^{3}\right)}} = 1.336$$

$$A_{s.lateral.\beta} := 2 \cdot 10 \cdot \left(\frac{10 \cdot mm}{2}\right)^{2} \cdot \pi = 15.708 \cdot cm^{2}$$

$$\rho_1 := \frac{A_{s.\beta} + A_{s2.\beta} + A_{s.lateral.\beta}}{h \cdot b} = 4.072 \times 10^{-3}$$

$f_{ck.l} := 45 \quad MPa$

$$\nu := 0.035 \cdot \kappa^{\frac{3}{2}} \cdot f_{ck.l}^{\frac{1}{2}} = 0.363$$

$\nu_{min} := \nu \cdot MPa = 3.626 \times 10^{5}\,Pa$

$$V_{Rd} := \left[\frac{0.18 \cdot \kappa \cdot \left(100 \cdot \rho_1 \cdot f_{ck.l}\right)^{\frac{1}{3}}}{1.5}\right] \cdot d \cdot b_w \cdot MPa = 448.933\,kN \quad > \quad \nu_{min} \cdot b \cdot h = 391.633\,kN \text{ ok}$$

$$i_V := \frac{V_{Ed}}{V_{Rd}} = 84.623\,\%$$

8the beam is verified even without considering the shear reinforcement (stirrup)

B.2 Shear and bending moment diagrams on the beam

B.2.1 Ramos' design

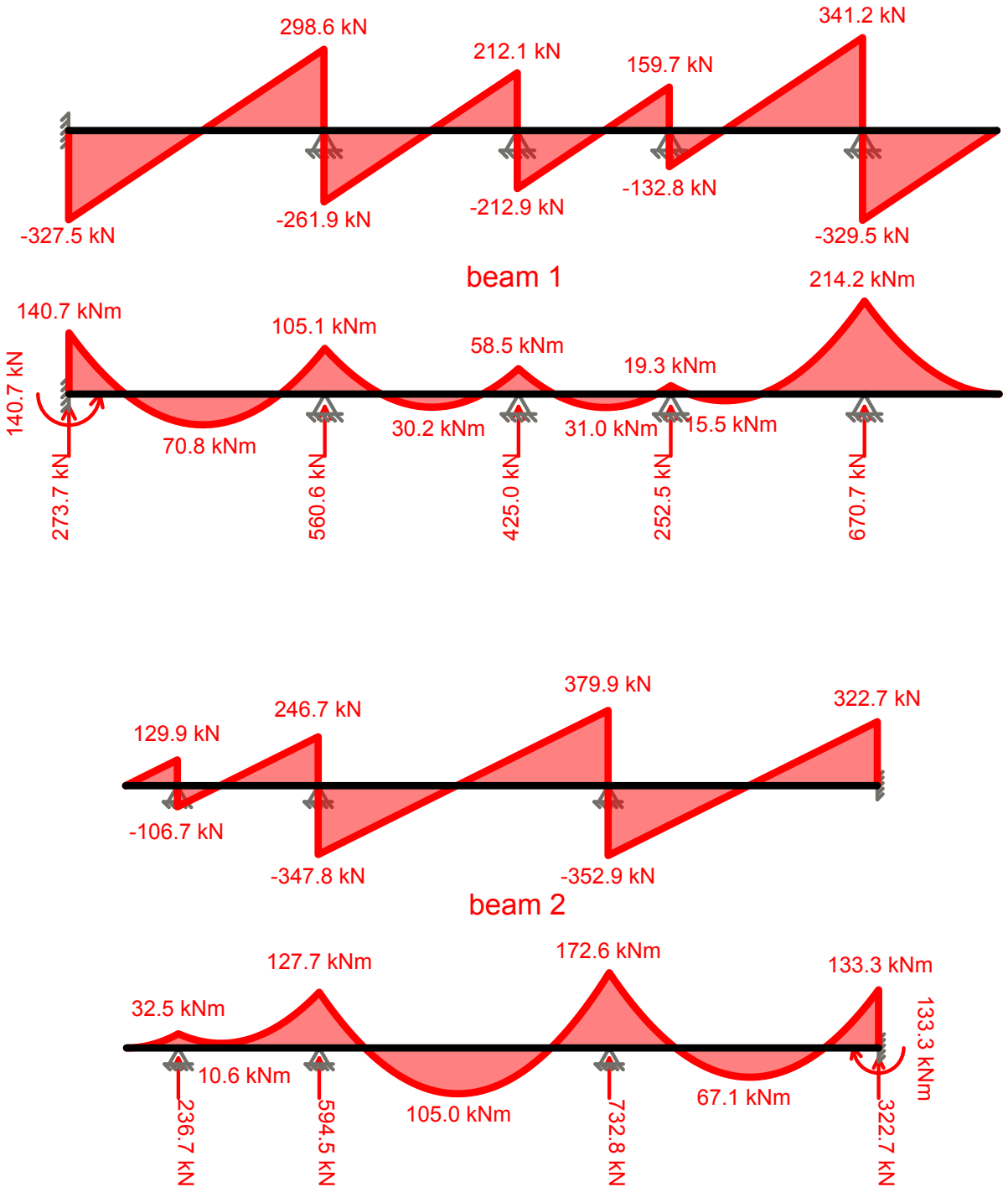

Figure B.1: Shear and bending moment diagrams on the beam 1 (on top) and beam 2 (on the bottom) for the project of Professor Ramos (personal work)

B.2.2 Updated design

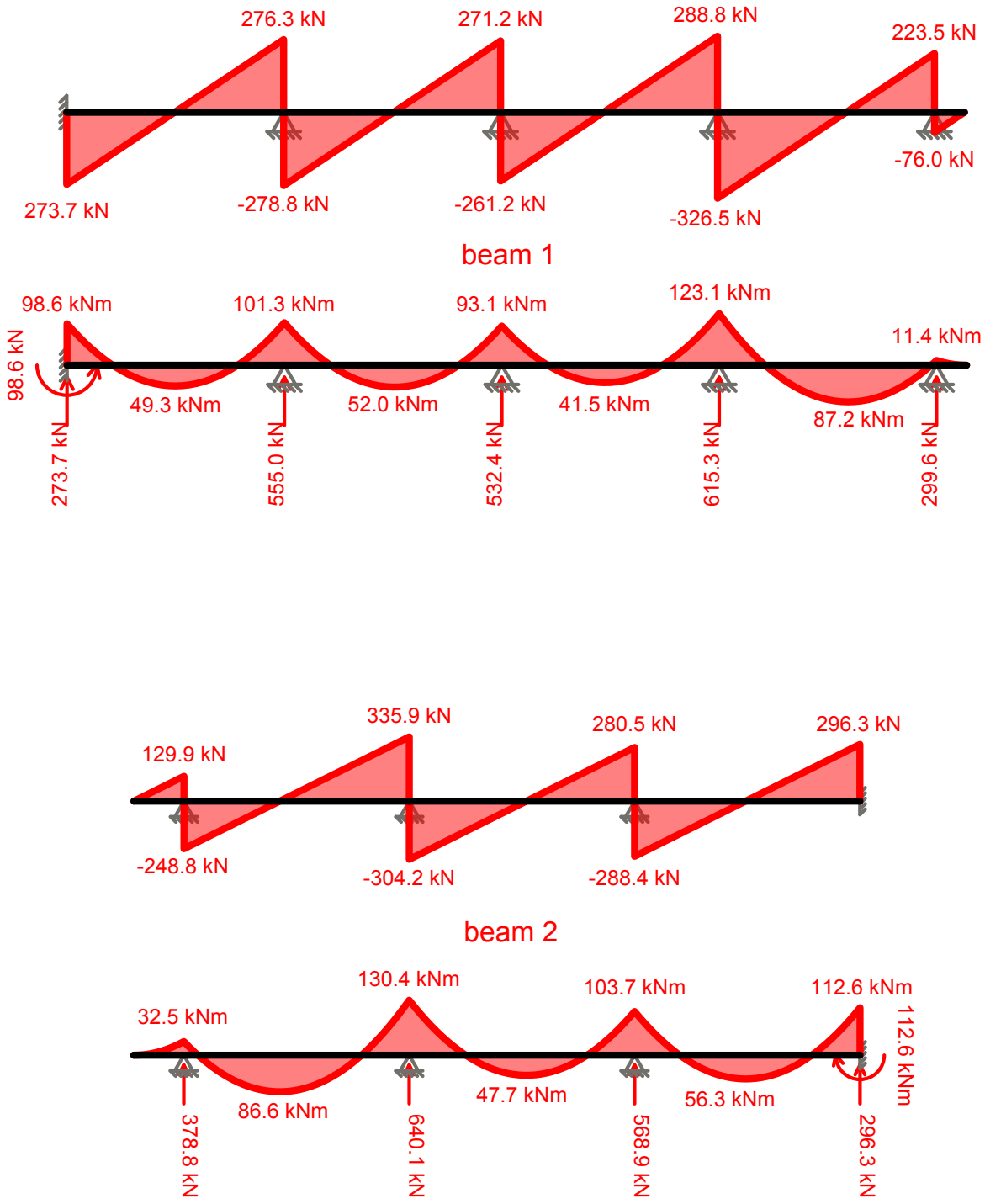

Figure B.1: Shear and bending moment diagrams on the beam 1 (on top) and beam 2 (on the bottom) for the update of the project (personal work)

B.2.3 Cross design

Introduction (all the calculation follow the steps suggested by chapter 1-4 of EN-2005)

The following analysis have to show the stability of three different structural system represented by the final part of the spire and the cross on top of it. The analysis will considered for the following models:

- ultimate state analysis of the cross considering it as a perfect cantilever
- kinematic analysis of the whole system defined by the cross and the upper stone of the spire
- ultimate state analysis of the upper ston at the hypotetic clamping level of the cross

Problem 1: ultimate analysis of the cross

Introduction

The cross will be analyzed as a perfect cantilever affected by the wind perpendicularly to the upper detail. The model will be converted in a two dimensional problem, with the forces applyed on the plane of the paper. The cross has been divided in two parts, for an easier calculation. The main rod correspond to the cantilever shape, the upper decoration, instead, will be considered just in terms of torces. The resultant force will be applyed in the centroid of the decoration and transmitted to the rod at the same height.

Cross data

Rod (all the terms with A are related to the rod)

$h_A := 3.2 \cdot m$ height of the element

$b_A := 4 \cdot cm$ width of the element

$A_{eff.A} := h_A \cdot b_A = 0.128\, m^2$ impact area for the wind

Crown detail (all the terms with B are related to upper crown detail)

$A_B := 2 \cdot 0.111 \cdot m^2$ sum of the projected area of the members (7.13)

$A_{c.B} := 2 \cdot 0.4729 \cdot m^2$ overall envelope area (7.13)

$h_B := (3.2 - 0.76) \cdot m$ height of the detail centroid

Overall element

$A_{tot} := A_{eff.A} + A_B = 0.35\, m^2$ overall projected area of the cross

$V_{tot} := A_{tot} \cdot b_A = 0.014 \cdot m^3$ total volume of the cross

$w_s := 77110 \cdot \frac{N}{m^3}$ specific weight of the steel

$W_{cross} := V_{tot} \cdot w_s = 1.08 \cdot kN$ total weight of the cross

4 Wind velocity and velocity pressure

All the following analysis steps will follow the logical process of the Chapter 1-4 of the Eurocode 1993-2005

4.2 Basic values

$v_b := 28 \cdot \frac{m}{s}$ basic wind velocity (value for zone A, exteme wind classification II) (formula 4.1 and national annex)

4.3 Mean wind

$v_{m.z} = c_{r.z} \cdot c_{0.z} \cdot v_b$ mean wind velocity (formula 4.3)

$z_0 := 0.3 \cdot m$ roughness lenght, III terrain category was assumed for the case study (table 4.1)

$z_{0II} := 0.05 \cdot m$ roughness lenght for terrain category II (table 4.1)

$k_r := 0.19 \cdot \left(\frac{z_0}{z_{0II}} \right)^{0.07} = 0.215$ terrain factor (formula 4.5)

$z := 61.14 \cdot m$ maximal height above ground level (tower height + cross + cross base) (4.3.2)

$c_{r.z} := k_r \cdot ln\left(\frac{z}{z_0} \right) = 1.145$ roughness factor (first formula 4.4)

$c_{0.z} := 1$ orography factor (first formula 4.3.1)

Terrain orography irrelevant (4.3.3 and annex A.3)

Larger or higher neighbouring structures not present (4.3.4 and annex A.4)

Close buildings and obstacle structures not present (4.3.5 and annex A.5)

$v_{m.z} := c_{r.z} \cdot c_{0.z} \cdot v_b = 32.067 \frac{m}{s}$ mean wind velocity (formula 4.3)

4.4 Wind turbolence

$k_I := 1$ turbulence factor (4.4)

$\sigma_v := k_r \cdot v_b \cdot k_I = 6.031 \frac{m}{s}$ standard deviation of the turbulence (formula 4.6)

$I_{v.z} := \frac{\sigma_v}{v_{m.z}} = 0.188$ turbulence intensity (first formula 4.7)

4.5 Peak velocity pressure

$q_{p.z} = \left(1 + 7 \cdot I_{v.z}\right) \cdot \frac{1}{2} \cdot \rho \cdot {v_{m.z}}^2 = c_{e.z} \cdot q_b$ peak velocity pressure (formula 4.8)

$\rho := 1.25 \cdot \frac{kg}{m^3}$ air pressure (value chosen following the note 2 of chapter 4.5)

$q_{p.z} := \left(1 + 7 \cdot I_{v.z}\right) \cdot \frac{1}{2} \cdot \rho \cdot {v_{m.z}}^2 = 1.489 \cdot kPa$ peak velocity pressure (formula 4.8)

$q_b := \frac{1}{2} \cdot \rho \cdot v_b^2 = 490\,Pa$ basic velocity pressure (formula 4.10)

$c_{e.z} := \frac{q_{p.z}}{q_b} = 3.038$ exposure factor (formula 4.9)

5 Wind actions

5.3 Wind forces

The following formula will be used because the analyzed body is a roof element

$F_w = c_s \cdot c_d \cdot c_f \cdot q_{p.z} \cdot A_{ref}$ wind force acting on the element (formula 5.3)

7 Pressure and force coefficients

In the case study, force coefficients should be determined for solve the problem, taking into account the note 4 in chapter 7.1. More precisely, due to the nature of the cross, such roof element will be considered a square cross-section with sharp edges (7.6).

Torsional effects due to force eccentricity will be considered (7.1.2)

Combination of wind with snow and ice will not be considered (7.1.3)

7.6 Structural elements with rectangular sections

$c_f = c_{f.0} \cdot \psi_r \cdot \psi_\lambda$ force coefficient of structural element (formula 7.9)

$c_{f.0} := 2$ force coefficient of rectangular sections with sharp corner (figure 7.23)

$\psi_r := 1$ reduction factor for sections with rounded corners (figure 7.23)

because of the difference in shape of the church, two differents end-effect factors will be considered. As stated above, the cross will be divided in two parts, the pole and the upper crown detail. Due to the difference of solidity ratio (ϕ) of those elements they have to be analyzed separately

7.13 Effective slenderness and end-effect factor

$\lambda_A := \frac{h_A}{b_A} = 80$ effective slenderness of the rod (table 7.19)

$\lambda_B := 1$ effective slenderness of the upper crown detail (table 7.19)

$\phi_A := 1$ solidity ratio of the rod (formula 7.37)

$\phi_B := \frac{A_B}{A_{c.B}} = 0.235$ solidity ratio of the upper crown detail (formula 7.37)

$\psi_{\lambda A} := 0.93$ end-effect reduction factor of the rod (figure 7.39)

$\psi_{\lambda B} := 0.95$ end-effect reduction factor of the upper crown detail (figure 7.39)

The reduction factors are very similar thus just one of them (the worst one) will be taken into account during the calculation

$\psi_\lambda := 0.95$

7.6 Structural elements with rectangular sections

$c_f := c_{f.0} \cdot \psi_r \cdot \psi_\lambda = 1.9$ force coefficient of structural element (formula 7.9)

5 Wind actions

5.3 Wind forces

The structural factor will be consider equal to one, because the natural frequency of the roof element is higher than 5 Hz. The element have been considered a cantilever with punctual force applyed on it.

$f = \sqrt{\frac{k}{m}} = \sqrt{12 \cdot \frac{E \cdot I}{h_A^3 \cdot m}} = 17.68 \cdot Hz \quad \rightarrow \quad c_s \cdot c_d = 1 \quad c_{s.d} := 1$

$F_{w.A} := c_{s.d} \cdot c_f \cdot q_{p.z} \cdot A_{eff.A} = 0.362 \cdot kN$ wind force acting directly on the rod (formula 5.3)

$F_{w.B} := c_{s.d} \cdot c_f \cdot q_{p.z} \cdot A_B = 0.628 \cdot kN$ wind force acting directly on the detail (formula 5.3)

$M_{w.base} := F_{w.A} \cdot \frac{h_A}{2} + F_{w.B} \cdot h_B = 2.112 \cdot kN \cdot m$ moment acting on the cross base induced by the wind forces

$V_{w.base} := F_{w.A} + F_{w.B} = 0.99 \cdot kN$ shear acting on the cross base induced by the wind forces

Verification of the cross

All the calculation and criteria depend on the Eurocode 3 EN 1993-2005, concerning the design of steel structure (that will be most likely the material used for the intervention). All the analysis steps will follow the logical process adopted by the above mentioned code. Where specified, the part 3-1 of the eurocode 3 (concerning masts, pole and chimneys) will be used.

3 Material

3.2 Structural steel

Recalling the the cross will be formed by hot rolled bars (without hollow sections), and considering a stainless steel AISI 316, the resistance of the material can be assumed as:

$f_y := 220 \cdot MPa$	yelding strenght (for thickness < 40 mm)	(table 3.1)
$f_u := 360 \cdot MPa$	ultimate tensile strenght (for thickness > 40 mm)	(table 3.1)
$E := 200 \cdot GPa$	modulus of elasticity	(3.2.6)
$G_s := 81 \cdot GPa$	shear modulus	(3.2.6)
$v := 0.3$	Poisson's ratio	(3.2.6)

$I := \frac{1}{12} \cdot b_A^4 = 21.333 \cdot cm^4$ moment of inercia of the cross section

$A_c := b_A^{\,2} = 16 \cdot cm^2$ area of the cross section

$I_{t2} := \frac{1}{3} \cdot \left(h_A - 2 \cdot 0.3 \cdot b_A\right) \cdot b_A^{\,3} = 6.775 \times 10^3 \cdot cm^4$ approximated torsional inercia

$I_t := 4 \cdot I = 85.333 \cdot cm^4$ torsional inercia

cross section class 1 (5.5)

5 Structural analysis

5.3 Imperfections

In case of solid section, the relative buckling curve id defined as c (table 6.2)

$\frac{e_0}{h_A} = \frac{1}{200}$ design values for initial local bow imperfection (table 5.1)

$e_0 := \frac{h_A}{200} = 1.6 \cdot cm$ initial eccentricty of the cross upper point due to local imperfections

$e_{0.p} := \frac{h_A}{3 \cdot 200} = 0.533 \cdot cm$ eccentricity of the body force with respect to the middle plane of the rod. the load is cosidered linearly distributed from the top to the botton, thus the force is applyed at 1/3 of the height.

$M_p := W_{cross} \cdot e_{0.p} = 5.758 \cdot N \cdot m$ moment induced in the cross base by the selweight, in case of small imperfections of constructions.

Combination of loads and partial factors (from part 3-1 of Eurocode 3)

$\gamma_{M0} := 1$	partial factor, considering yelding resistance	(6.1)
$\gamma_{M1} := 1$	partial factor, considering instability resistance	(6.1)
$\gamma_{M2} := 1.2$	partial factor, considering fracture resistance	(6.1)

Considering that the structure has a reliability class 3 (annex A.1 from part 3-1 of Eurocode 3) because its failure could lead to loss of life. Fro this reason, the combination of load that will be considered is the unfavorable situation shown below:

$$\psi_P \cdot P + \psi_Q \cdot Q$$

where:

$\psi_P := 1.2$	partial factor for permanent actions	(table A.2 from part 3-1)
P	permanent actions (wind only)	
$\psi_Q := 1.6$	partial factor for variable actions	(table A.2 from part 3-1)
Q	variable actions	

Design actions

The analysis will be carried out at the base level of the cross element.

$V_{Ed} := \psi_Q \cdot V_{w.base} = 1.584 \cdot kN$ design shear acting on the cross base

$M_{Ed} := \psi_Q \cdot M_{w.base} + \psi_P \cdot M_p = 3.385 \cdot kN \cdot m$ design moment acting on the cross base

$N_{Ed} := \psi_P \cdot W_{cross} = 1.295 \cdot kN$ design axial force acting on the cross base

$M_{t.Ed} := F_{w.B} \cdot \frac{0.76}{3} \cdot m = 0.159 \cdot kN \cdot m$ design torsional force at the cross base

6 Ultimate limit states

6.2 Resistance of cross sections

6.2.4 Compression

$N_{c.Rd} := A_c \cdot \frac{f_y}{\gamma_{M0}} = 352 \cdot kN$ design resistance in compression (formula 6.10)

$i_c := \frac{N_{Ed}}{N_{c.Rd}} = 0.368 \cdot \%$ ▮ < 1 percentage of utilization of the resistant section in compression

The cross satisfies the requirements in compression.

6.2.5 Bending moment

$W_{pl} := \frac{b_A^3}{4} = 16 \cdot cm^3$ plastic resistance modulus in square cross section

$M_{c.Rd} := W_{pl} \cdot \frac{f_y}{\gamma_{M0}} = 3.52 \cdot kN \cdot m$ design resistance in bending (formula 6.13)

$i_m := \frac{M_{Ed}}{M_{c.Rd}} = 96.176 \cdot \%$ ▮ < 1 percentage of utilization of the resistant section in flexion

The cross satisfies the requirements below pure flexion

6.2.6 Shear

$V_{pl.Rd} := A_c \cdot \frac{f_y}{\gamma_{M0} \cdot \sqrt{3}} = 203.227 \cdot kN$ design resistance in bending (formula 6.18)

$i_s := \frac{V_{Ed}}{V_{pl.Rd}} = 0.779 \cdot \%$ ▮ < 1 percentage of utilization of the resistance below shear conditions

The cross satisfies the requirements below pure shear

6.2.7 Torsion

$\tau_{t.max} := 4.804 \cdot \frac{M_{t.Ed}}{b_A^3} = 11.941 \cdot MPa$ approximated value of shear force for closed cross sections

$i_t := \frac{\left(\frac{V_{Ed}}{A_c} + \tau_{t.max}\right) \cdot \sqrt{3}}{f_y} = 10.181 \cdot \%$ percentage of utilization of the resistance below torsional conditions

6.2.8 Bending and shear

This calculation can be neglected because the shear force il less than half the plastic shear resistence of the section (as specified in note 2 of 6.2.8)

6.2.8 Bending and axial force

$M_{n.Rd} := M_{c.Rd} \cdot \left[1 - \left(\frac{N_{Ed}}{N_{c.Rd}}\right)^2\right] = 3.52 \cdot kN \cdot m$ for rectangular solid section without fastener hoes (formula 6.32)

$i_{m.c} := \frac{M_{Ed}}{M_{n.Rd}} = 96.178 \cdot \% \blacksquare < 1$ percentage of utilization of the resistant below bending and axial force conditions

The cross satisfies the requirements below bending and axial force conditions

6.3 Buckling resistance of the members

6.3.4 Uniform members in compression

$N_{b.Rd} = \chi \cdot A_c \cdot \frac{f_y}{\gamma_{M1}}$ design buckling resistance (formula 6.47)

$N_{cr} := \frac{\pi^2}{4} \cdot \frac{E \cdot I}{h_A^2} = 10.281 \cdot kN$ Eulerian critical load

$\lambda_{eff} := \sqrt{\frac{A_c \cdot f_y}{N_{cr}}} = 5.851$ non dimensional slenderness (formula 6.49)

$\alpha := 0.49$ imperfection factor for bucling curves type c (table 6.1)

$\Phi_c := 0.5 \cdot \left[1 + \alpha \cdot \left(\lambda_{eff} - 0.2\right) + \lambda_{eff}^2\right] = 19.004$ (formula 6.49)

$\chi := \frac{1}{\Phi_c + \sqrt{\Phi_c^2 - \lambda_{eff}^2}} = 0.027$

$N_{b.Rd} := \chi \cdot A_c \cdot \frac{f_y}{\gamma_{M1}} = 9.492 \cdot kN$

$i_{B.c} := \frac{N_{Ed}}{N_{b.Rd}} = 13.648 \cdot \%$ percentage of utilization of the geometrical resistance in axial force conditions (considering all the load on top of the cross)

The cross satisfies the geometrical requirements below axial force conditions

6.3.4 Uniform members in bending

$M_{b.Rd} = \chi_{lt} \cdot W_{pl} \cdot \frac{f_y}{\gamma_{M1}}$ design buckling resistance moment (formula 6.55)

$M_{cr} := \pi^2 \cdot \frac{E \cdot I}{h_A^2} \cdot \sqrt{\frac{h_A^2 \cdot G_s \cdot I_t}{\pi^2 \cdot E \cdot I}} = 53.315 \cdot kN \cdot m$ Eulerian critical moment (formula F.1)

$\lambda_{lt} := \sqrt{\frac{W_{pl} \cdot f_y}{M_{cr}}} = 0.257$ non dimensional slenderness for lateral buckling (formula 6.56)

$\alpha_{lt} := 0.76$ imperfection factor for bucling curves type d (table 6.3)

$\Phi_{lt} := 0.5 \cdot \left[1 + \alpha_{lt} \cdot \left(\lambda_{lt} - 0.2\right) + \lambda_{lt}^2\right] = 0.555$ (formula 6.49)

$\chi_{lt} := \frac{1}{\Phi_{lt} + \sqrt{\Phi_{lt}^2 - \lambda_{lt}^2}} = 0.956$ not possible! it will be taken equal to one

$M_{b.Rd} := W_{pl} \cdot \frac{f_y}{\gamma_{M1}} = 3.52 \cdot kN \cdot m$

$i_{B.m} := \frac{M_{Ed}}{M_{b.Rd}} = 96.176 \cdot \% \blacksquare < 1$ percentage of utilization of the geometrical resistannce below bending conditions

The cross satisfies the geometrical requirements below bending conditions

Conclusions

The cross satisfies all the statical requirements given in the Eurocode, the cross resuslts overstrenghtened

Problem 2: kinematic analysis of the whole system

Introduction

For semplification, the previous values for wind velocity and wind pressure will be used. Moreover, such approach, in which the maximum high of the cross, is more conservative. The solving scheme or the problem can be seen below.

Cross data

The same as in the problem 1

Stone data

The stone will be solved as a perfect cone

$h_s := 1.08 \cdot m$ height of the stone

$b_{s.1} := 30 \cdot cm$ width of the upper part of the stone (approximated)

$b_{s.2} := 50 \cdot cm$ width of the lower part of the stone (approximated)

$V_s := 0.14666 \cdot m^3$ volume of the stone

$S_s := 1.72 \cdot m^2$ total surface of the element

$A_{s.w} := \frac{3}{8} \cdot \left[S_s - (0.2071 + 0.0746) \cdot m^2 \right] = 0.539\, m^2$ surface directly hit by the wind

$w_{stone} := 25 \cdot \frac{kN}{m^3}$ specific weight of the stone

$W_s := V_s \cdot w_{stone} = 3.667 \cdot kN$

5 Wind actions

5.3 Wind forces

The following formula will be used because the analyzed body is a roof element

$F_{w.s} = c_s \cdot c_d \cdot c_{f.s} \cdot q_{p.z} \cdot A_{s.w}$ wind force acting on the stone (formula 5.3)

$c_{f.s} := 1.45$ force coefficients for regular poligonal sections (table 7.11)

$F_{w.s} := c_{s.d} \cdot c_{f.s} \cdot q_{p.z} \cdot A_{s.w} = 1.164 \cdot kN$

Combination of loads and partial factors

In this analysis will be used the same combination of loads and partial factors for action used in the problem one. The formula is recall below:

$$\psi_P \cdot P + \psi_Q \cdot Q$$

Combination of loads and partial factors

In this analysis will be used the same combination of loads and partial factors for action used in the problem one. The formula is recall below:

$$\psi_P \cdot P + \psi_Q \cdot Q$$

Overturning condition

The structure could overturn in case the resisting moment (applyed by the dead load) will be overpassed by the external moment (due to the wind)

$$M_{O.Rd} := \psi_P \cdot \left[\left(W_s + W_{cross} \right) \cdot \frac{b_{s.2}}{2} \right] = 1.424 \cdot kN \cdot m$$

$$M_{O.Ed} := \psi_Q \cdot \left[F_{w.s} \cdot \frac{h_s}{2} + F_{w.A} \cdot \left(\frac{h_A}{2} + h_s \right) + F_{w.B} \cdot \left(h_B + h_s \right) \right] = 6.095 \cdot kN \cdot m$$

The analysis is failed. Moreover, it is visible that the structure may fail even without consider the wind applyed on the stone. The filure suggests a mistake in the mathematical conception or values of the code too much restrictive, because the whole system is stable there since centuries. More likely, the stone block is pinned to the underlying structure.

Problem 3: ultimate state of the stone

Introduction

For semplification, the previous values for wind velocity and wind pressure will be used. The end of the cross clamping will be hypothesized in the middle of the height of the stone. In this case the Eurocode 6 (Masonry structure) was used as reference

Cross data

The same as in the problem 1

Stone data

The same as in the problem 2 with the addiction of:

$h_{s.c} := \frac{h_s}{2}$ height of the cross clamping in the stone

$b_{s.c} := 40 \cdot cm$ width of the of the stone at the clamping level (approximated)

$A_{s.c} := 1325.48 \cdot cm^2$ area of the cross section at the clamping level

$f_m := 135.7 \cdot MPa$ mean compressive strenght of granite

$s_{fm} := 5\% \cdot f_m = 6.785 \cdot MPa$ coefficient of variation of the mean compressive strenght

$k_s := 2.1$ partial security coefficient in case of ten samples (11.10.3.1.1 NTC-2008)

$f_k := f_m - s_{fm} \cdot k_s = 121.451 \cdot MPa$ characteristic value of the masonry (11.10.3.1.1 NTC-2008)

$\gamma_{stone} := 1.35$ confidence factor, level of knowledge 1 (the lower one)(NTC-2008)

$f_{vk0} := 0.3 \cdot MPa$ characteristic initial shear strenght (table 3.4)

$\sigma_d := \frac{\frac{W_s}{3} + W_{cross}}{A_{s.c}} = 0.017 \cdot MPa$ for calculus semplicity it was considered just 1/3 of the toatl weight acting on the middle section

$f_{vk} := \frac{f_{vk0}}{2} + 0.4 \cdot \sigma_d = 0.157 \cdot MPa$ characteristic shear strenght of the masonry (formula 3.6)

$E_s := 52 \cdot GPa$ elastic modulus of stone

$G_{stone} := 0.4 \cdot E_s = 20.8 \cdot GPa$ shear modulus

$f_d := \frac{f_k}{\gamma_{stone}} = 89.964 \cdot MPa$ design compressive strenght of granite

$f_{vd} := \frac{f_{vk}}{\gamma_{stone}} = 0.116 \cdot MPa$ design shear strenght of granite

Combination of loads and partial factors

In this analysis will be used the same combination of loads and partial factors for action used in the problem one. The analysis for vertical loads will not be perfermed.

Design values

$$V_{Ed.stone} := \psi_Q \cdot \left(\frac{F_{w.s}}{2} + F_{w.A} + F_{w.B} \right) = 2.516 \cdot kN$$

$$M_{Ed.stone} := \psi_Q \cdot \left[\frac{F_{w.s}}{2} \cdot \frac{h_s}{4} + F_{w.A} \cdot \left(\frac{h_A}{2} + \frac{h_s}{2} \right) + F_{w.B} \cdot \left(h_B + \frac{h_s}{2} \right) \right] = 4.485 \cdot kN \cdot m$$

6 Ultimate state limit

6.2 Unreinforced masonry walls subjected to shear loading

$V_{Rd.stone} := f_{vd} \cdot A_{s.c} = 15.41 \cdot kN$

$i_{v.stone} := \frac{V_{Ed.stone}}{V_{Rd.stone}} = 16.325 \cdot \%$ percentage of utilization of the resistant below shear loading

The stone satisfies the requirements below shear compression

6.3 Unreinforced masonry walls subjected to lateral loading

The tensile strenght of the granite will be neglected because irrelevant with respect to the compressive one (the tensile is 3% of the compressive one)

$A_{c.stone} := 777.4085 \cdot cm^2$ area in compression of the relative stress block

$F_c := 0.85 f_d \cdot A_{c.stone} = 5.945 \cdot MN$ maximal compressive force beared by the section

$x_c := 27.44 \cdot cm = 0.274\, m$ distance between neutral axis and applyed force

$M_{Rd.stone} := F_c \cdot x_c = 1.631 \cdot MN \cdot m$ resisting moment of the section

$i_{m.stone} := \frac{M_{Ed.stone}}{M_{Rd.stone}} = 0.275 \cdot \%$ percentage of utilization of the resistant below shear loading

The stone satisfies the requirements below moment action